

RICE UNIVERSITY

Coupling Surface Flow with Porous Media Flow

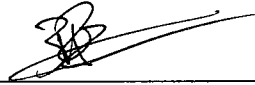
by

Prince Chidyagwai

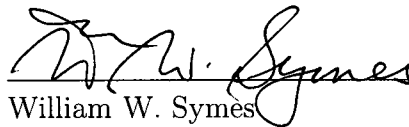
A THESIS SUBMITTED
IN PARTIAL FULFILLMENT OF THE
REQUIREMENTS FOR THE DEGREE

Doctor of Philosophy

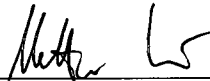
APPROVED, THESIS COMMITTEE:



Béatrice Rivière, Chair
Associate Professor of Computational and
Applied Mathematics, Rice University



William W. Symes
Noah G. Harding Professor of
Computational and Applied Mathematics,
Rice University



Matteo Pasquali
Professor of Chemical and Biomolecular
Engineering, Rice University

Houston, Texas

May, 2010

UMI Number: 3425207

All rights reserved

INFORMATION TO ALL USERS

The quality of this reproduction is dependent upon the quality of the copy submitted.

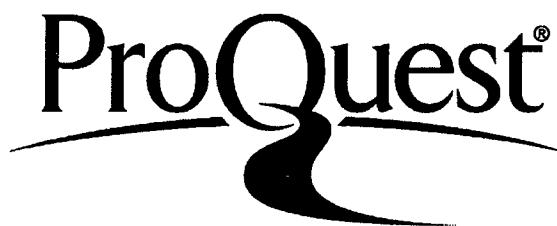
In the unlikely event that the author did not send a complete manuscript and there are missing pages, these will be noted. Also, if material had to be removed, a note will indicate the deletion.



UMI 3425207

Copyright 2010 by ProQuest LLC.

All rights reserved. This edition of the work is protected against unauthorized copying under Title 17, United States Code.



ProQuest LLC
789 East Eisenhower Parkway
P.O. Box 1346
Ann Arbor, MI 48106-1346

ABSTRACT

Coupling Surface Flow with Porous Media Flow

by

Prince Chidyagwai

This thesis proposes a model for the interaction between ground flow and surface flow using a coupled system of the Navier-Stokes and Darcy equations. The coupling of surface flow with porous media flow has important applications in science and engineering. This work is motivated by applications to geo-sciences.

This work couples the two flows using interface conditions that incorporate the continuity of the normal component, the balance of forces and the Beaver-Joseph-Saffman Law. The balance of forces condition can be written with or without inertial forces from the free fluid region. This thesis provides both theoretical and numerical analysis of the effect of the inertial forces on the model. Flow in porous media is often simulated over large domains in which the actual permeability is heterogeneous with discontinuities across the domain. The discontinuous Galerkin method is well suited to handle this problem. On the other hand, the continuous finite element is adequate for the free flow problems considered in this work. As a result this thesis proposes coupling the continuous finite element method in the free flow region with the discontinuous Galerkin method in the porous medium.

Existence and uniqueness results of a weak solution and numerical scheme are proved. This work also provides derivations of optimal a priori error estimates for the numerical scheme. A two-grid approach to solving the coupled problem is analyzed.

This method will decouple the problem naturally into two problems, one in the free flow domain and other in the porous medium. In applications for this model, it is often the case that the areas of interest (faults, kinks) in the porous medium are small compared to the rest of the domain. In view of this fact, the rest of the thesis is dedicated to a coupling of the Discontinuous Galerkin method in the problem areas with a cheaper method on the rest of the domain. The finite volume method will be coupled with the Discontinuous Galerkin method on parts of the domain on which the permeability field varies gradually to decrease the problem sizes and thus make the scheme more efficient.

Acknowledgments

I would like to thank my advisor Dr. Béatrice Rivière for her guidance and unwavering support throughout my graduate work. I also want to thank my committee members Dr. Symes, Dr. Pasquali and Dr. Warburton for helpful suggestions and discussions during the course of this work. I also owe my success over the years to my family who are a constant source of inspiration and support.

Contents

Abstract	ii
Acknowledgments	iv
List of Illustrations	viii
List of Tables	xi
1 Introduction	1
2 Coupled Navier-Stokes/Darcy Model	6
2.1 Numerical Schemes	6
2.2 The Navier-Stokes Equations	7
2.3 Darcy Equations	7
2.4 Interface Conditions	8
3 Mathematical Analysis	11
3.1 Preliminary Notation and Function Spaces	11
3.1.1 L^p Spaces	11
3.1.2 Sobolev Spaces	12
3.2 Variational Formulation	14
3.3 Existence of a weak solution	18
3.4 Uniqueness of weak solution	23
4 Numerical Analysis	26
4.1 Discrete Spaces for Navier-Stokes Equations	26
4.2 Discrete Space for Darcy Problem	27

4.3	Numerical Scheme	28
4.4	Consistency	32
4.5	Existence of Numerical Solution	34
4.6	Uniqueness of Numerical Solution	37
4.7	A Priori Error Estimates	39
5	Numerical Results	45
5.1	Software	45
5.2	Numerical Schemes	45
5.2.1	Continuous finite element scheme (CG-CG)	47
5.2.2	Discontinuous Galerkin finite element scheme (DG-DG)	49
5.2.3	Coupled continuous finite element with discontinuous Galerkin method scheme (CG-DG)	51
5.3	Numerical Convergence	51
5.4	Effect of Physical Parameters	56
5.4.1	Permeability	56
5.4.2	Kinematic Fluid Viscosity	65
5.5	Local Mass Conservation: An Application to Filtration Systems	67
5.6	Comparison of Interface conditions	70
6	Two Grid Method	90
6.1	Coupled Stokes/Darcy Model	90
6.1.1	Variational Formulation for Stokes/Darcy Coupling	92
6.1.2	Numerical Scheme: Stokes/Darcy coupling	93
6.1.3	L_2 error estimate for Stokes/Darcy problem	94
6.1.4	Regularity for the Coupled Stokes/Darcy problem	96
6.1.5	Error estimates in L_2	96
6.1.6	Two Grid Algorithm: Coupled Stokes/Darcy Model	99
6.1.7	Error Analysis: Two Grid Stokes/Darcy Algorithm	100

6.1.8	Numerical Results: Two Grid Stokes/Darcy problem	104
6.2	Coupled Navier-Stokes/Darcy Model	109
6.2.1	Two Grid Algorithm: Coupled Navier-Stokes/Darcy	109
6.2.2	Error Analysis: Two-grid Navier-Stokes/Darcy Model	111
6.2.3	Convergence Study: Two-grid Navier-Stokes/Darcy Model	111
6.2.4	CPU Times: Two-grid Coupled Navier-Stokes/Darcy Model	117
6.3	Conclusion	118

7	Coupled Discontinuous Galerkin Method with Finite Volume Method	119
7.1	Introduction	119
7.2	Model Problem And Scheme	119
7.3	Error Analysis	124
7.4	Numerical Examples	129
7.5	Conclusions	137
8	Conclusion	139
8.1	Coupled Navier-Stokes/Darcy Model	139
8.2	Computational Efficiency	140
8.3	Future Work	141

Illustrations

2.1	Computational domain of surface and subsurface	6
5.1	Computational domain and numerical results	58
5.2	Computational domain adapted from [30]	59
5.3	CG-CG: velocity and pressure	60
5.4	CG-DG: velocity and pressure	61
5.5	CG-CG on refined mesh: velocity and pressure	62
5.6	DG-DG scheme of order two: velocity and pressure	63
5.7	CG-CG: streamlines and norm of velocity at fracture intersection	64
5.8	CG-DG: Computational domain on random permeability field	65
5.9	CG-DG: Random permeability (a) Norm velocity and (b) Pressure	66
5.10	Filter: Computational domain	68
5.11	Dead-end filter: CG-DG norm velocity and pressure	69
5.12	Streamlines for the numerical velocity for the model without inertial forces (a) and with inertial forces (b) for viscosity equal to 1.	73
5.13	Difference between the solutions obtained from the two models for viscosity equal to 1: (a) x -component of velocity, (b) y -component of velocity and (c) pressure.	74
5.14	Streamlines for the numerical velocity for the model without inertial forces (a) and with inertial forces for viscosity equal to 0.005.	75

5.15	Difference between the solutions obtained from the two models for viscosity equal to 0.005: (a) x -component of velocity, (b) y -component of velocity and (c) pressure.	76
5.16	Inertial forces (κ) for model W_A^h and W_B^h for $\nu = 1.0$ and $\mathbf{K} = \mathbf{I}$	77
5.17	Norm of velocity for model W_A^h (a) and W_B^h (b) for $\nu = 1.0$ and $\mathbf{K} = \mathbf{I}$	78
5.18	Inertial forces (κ) for solution W_A^h and W_B^h for $\nu = 0.1$ and $\mathbf{K} = \mathbf{I}$	79
5.19	Inertial forces (κ) for model W_A^h and W_B^h for $\nu = 0.01$ and $\mathbf{K} = \mathbf{I}$	80
5.20	Streamlines and norm velocity for the models W_A^h (a) and W_B^h (b) for $\nu = 0.01$ and $\mathbf{K} = \mathbf{I}$	81
5.21	Inertial forces κ (a) and flux (b) for model W_A^h for different values of \mathbf{K} and $\nu = 1.0$	82
5.22	Inertial forces (a) and flux (b) for model W_B^h for different values of \mathbf{K} and $\nu = 1.0$	82
5.23	Norm velocity for models W_A^h (a) and W_B^h (b) for $\mathbf{K} = 10^{-8}\mathbf{I}$ and $\nu = 1.0$	83
5.24	Inertial forces on NSE (a) and Darcy (b) sides of interface for W_A^h and W_B^h for $\mathbf{K} = 10^{-8}\mathbf{I}$ and $\nu = 0.01$	84
5.25	Norm of velocity for models W_A^h (a) and W_B^h (b) for $\mathbf{K} = 10^{-8}\mathbf{I}$ and $\nu = 0.01$	85
5.26	Computational domain with polygonal interface	85
5.27	Norm of velocity profiles along $y = 0.60$ for schemes W_A^h , W_B^h and W_C^h	86
5.28	Norm of velocity profiles along $y = 0.75$ for schemes W_A^h , W_B^h and W_C^h	86
5.29	Norm of velocity profiles along $y = 0.60$ for schemes W_A^h and W_C^h for $\nu = 0.01$	87
5.30	Norm of velocity profiles along $y = 0.6$ for schemes W_A^h and W_C^h for $\mathbf{K} = \mathbf{I}$	87
6.1	Computational meshes $H = 0.5, h = 0.25$	105

6.2	x- component of velocity $H = 0.5, h = 0.25, NIPG, k_2 = 2, \sigma = 0$. . .	113
6.3	y- component of velocity $H = 0.5, h = 0.25, NIPG, k_2 = 2, \sigma = 0$. . .	114
7.1	Computational mesh with 340 Voronoi cells: Ω_F is the white region and Ω_D is the grey region.	130
7.2	Contours of exact and numerical solutions for example 1.	131
7.3	Computational meshes in the case of triangular inclusion (grey region in left figure). The DG region is a larger rectangular region that contains the triangular inclusion (grey region in right figure).	133
7.4	Contours of pressure solution for example 2	135
7.5	Computational mesh for example 3: $\delta = 10^{-3}$ in the triangulated grey region and $\delta = 1$ in region partitioned into Voronoi cells.	136
7.6	Contours of pressure solution for example 3. Streamlines are only shown in the DG region.	137

Tables

5.1	Errors and convergence rates: CG-CG scheme without inertial forces ($k_1 = 1, k_2 = 1$)	53
5.2	Errors and convergence rates: CG-CG scheme with inertial forces ($k_1 = 1, k_2 = 1$)	53
5.3	Errors and convergence rates: CG-DG scheme without inertial forces ($k_1 = 1, k_2 = 1$)	53
5.4	Errors and convergence rates: CG-DG scheme with inertial forces ($k_1 = 1, k_2 = 2$)	54
5.5	Errors and convergence rates: CG-CG scheme ($k_1 = 1, k_2 = 1$)	55
5.6	Errors and convergence rates: CG-DG ($k_1 = 1, k_2 = 1$)	55
5.7	Numerical errors and convergence rates: CG-DG ($k_1 = 1, k_2 = 2$)	56
5.8	Numerical errors and convergence rates for varying ν : CG-CG	67
5.9	Relative numerical errors and ratios for model W_A^h with choice $k_2 = 1$	71
5.10	Relative numerical errors and ratios for model W_B^h and the choice $k_2 = 1$	72
5.11	Relative numerical errors and ratios for model W_A^h and the choice $k_2 = 1$	75
5.12	Relative numerical errors and ratios for model W_B^h and the choice $k_2 = 1$	76
6.1	Errors and rates for (W^h) ($k_1 = 1$, NIPG $\sigma = 1, k_2 = 1$).	106
6.2	Errors and rates for $(W_{h,\alpha}, \alpha = S, D)$ ($k_1 = 1$, NIPG $\sigma = 1, k_2 = 1$).	107

6.3	Errors and rates for $(W_{h,\alpha}, \alpha = S, D)$ ($k_1 = 1$, SIPG $\sigma = 3, k_2 = 1$).	107
6.4	Errors and rates for $(W_{h,\alpha}, \alpha = S, D)$ ($k_1 = 1$, NIPG $\sigma = 0, k_2 = 2$).	108
6.5	Errors and rates for $(W_{h,\alpha}, \alpha = S, D)$ ($k_1 = 1$, SIPG $\sigma = 18, k_2 = 2$).	108
6.6	Errors and rates for $(W_{h,\alpha}, \alpha = S, D)$ ($k_1 = 1$, NIPG $\sigma = 0, k_2 = 3$).	109
6.7	Errors and rates for $(W_{h,NS})$ ($k_1 = 1$, NIPG $\sigma = 1, k_2 = 1$).	112
6.8	Errors and rates for $(W_{h,\alpha}, \alpha = NS, D)$ ($k_1 = 1$, NIPG $\sigma = 1, k_2 = 1$).	113
6.9	Errors and rates for $(W_{h,NS})$ ($k_1 = 1$, NIPG $\sigma = 0, k_2 = 2$).	114
6.10	Errors and rates for $(W_{h,\alpha}, \alpha = NS, D)$ ($k_1 = 1$, NIPG $\sigma = 0, k_2 = 2$).	115
6.11	Errors and rates for $(W_{h,NS})$ ($k_1 = 1$, SIPG $\sigma = 6, k_2 = 1$).	115
6.12	Errors and rates for $(W_{h,\alpha}, \alpha = NS, D)$ ($k_1 = 1$, SIPG $\sigma = 6, k_2 = 1$).	116
6.13	Errors and rates for $(W_{h,NS})$ ($k_1 = 1$, SIPG $\sigma = 18, k_2 = 2$).	116
6.14	Errors and rates for $(W_{h,\alpha}, \alpha = NS, D)$ ($k_1 = 1$, SIPG $\sigma = 18, k_2 = 2$).	116
6.15	Direct Solver CPU times (s): $W_{NS}^h, W_{h,NS}, W_{h,D}$, (NIPG $\sigma = 0, k_2 = 2$).	117
6.16	Assembly and Solve CPU times (s): $W_{NS}^h, W_{h,NS}, W_{h,D}$, (NIPG $\sigma = 0,$ $k_2 = 2$).	118
7.1	Numerical errors and convergence rates for DG scheme of order one coupled with FV.	132
7.2	Numerical errors and convergence rates for DG scheme of order two coupled with FV.	132

Chapter 1

Introduction

Coupling free flow and porous media flow is an important problem because of the wide ranging applications in science and engineering. This thesis develops efficient numerical techniques for solving coupled surface flow and porous media flow by coupling the continuous finite element, also referred to as the Continuous Galerkin method (CG) in the free flow domain with Discontinuous Galerkin (DG) method in the porous medium. The choice of the DG method is suitable because of the difficulties that arise due to the heterogeneities and discontinuities in porous media. As the algebraic systems from the coupled model are large and time-consuming to solve, this work also proposes a decoupling technique based on a two-grid method for more efficient computations.

Motivation for this work is driven by applications of this coupling phenomenon to modelling the interaction between groundwater flow and porous media flow. Other applications include modelling industrial filtration [17] and modelling filtration of blood flow. When coupled with a transport equation, this phenomenon can also be used to study the diffusion and propagation of pollutants in water [8]. In this work, the free fluid domain is modelled by the Navier-Stokes equations and the flow in the porous medium is modeled by Darcy's law. The choice of these models requires conditions to be specified on the interface to couple the velocity and pressure variables in the two computational domains. To address the issue of coupling the velocity variables, Beavers and Joseph [3] perform experiments measuring the mass efflux of

Poiseuille flow over a permeable block. They postulate that the difference between the slip velocity of the fluid and tangential component is proportional to the shear rate of the fluid. Saffman [50] provides a theoretical justification of the condition proposed by Beavers and Joseph [3, 29]. This interface condition is now a widely accepted interface condition known as the Beavers-Joseph-Saffman law. The interface conditions were later completed by Payne and Straughan [39] to include the continuity of the normal component of the velocity and the balance of forces.

Early numerical work on coupling Navier-Stokes and Darcy equations can be found in the work by Salinger et al. [51] where they couple the Navier-Stokes and Darcy equations to study combustion of coal being transported due to exothermic reactions with oxygen. Gartling et al. [20] have studied the coupling of viscous and porous media flow with applications to alloy solidification. In [51, 20] the porous medium is fairly homogeneous and the continuous finite element method is used for numerical simulations. However, in modelling the interaction between surface flow and groundwater, the permeability in the porous medium is in practice heterogeneous and discontinuous. Kaasschieter [30] has shown that the continuous finite element method produces unphysical flow in the case where the porous medium has highly discontinuous permeability coefficients.

This thesis builds upon these previous works by proposing a method that has proven capabilities in handling discontinuities that may arise in porous media applications. This will be achieved by a numerical scheme that couples the DG method for the porous media region and the CG method in the free flow region. The DG method is well suited for this application as it is locally mass conservative and allows for discontinuous basis elements which can easily capture the underlying discontinuous rock structure. However, DG methods are computationally expensive as they result

in larger linear systems compared to CG methods. The continuous finite element method is very effective for simulating surface flow. Therefore the coupling of DG for subsurface and CG for surface flow seems to be an efficient scheme.

Theoretical studies of models of coupling free flow and porous media flow were independently studied by Layton et al. [33] and Discacciati et al. [14]. Layton et al. [33] analyze a mixed finite element formulation for the coupling of the Stokes and Darcy equations. In [33] a domain decomposition approach is proposed that imposes the interface conditions using Lagrange multipliers. The Stokes equations are best suited for modelling laminar flow; however, free flow can be non-linear in a lot of applications. As a result this work proposes to model free flow using the Navier-Stokes model. Discacciati et al. [14] analyzed the coupled Navier-Stokes and Darcy models in the continuous finite element case. Discacciati et al. have proved well-posedness results and numerical simulations have been done for the Stokes/Darcy model. Cesmelioglu and Riviere [9, 10] have studied the time dependent coupled Navier-Stokes and Darcy equation using the DG method. In this work I prove existence and uniqueness results for a numerical solution for the coupled Navier-Stokes and Darcy equations, and derive a priori error estimates. The discontinuous Galerkin method provides robustness to the model to handle different conditions simulating a wide range of rock structures in the porous medium. In order to illustrate the effectiveness of coupling the continuous finite element method with the discontinuous Galerkin method, implementations of the coupled scheme using only the continuous finite element method will be compared to implementations with DG in the porous medium.

Obtaining a numerical scheme from the coupled Navier-Stokes/Darcy scheme is often time consuming. In particular for the applications that are considered in this work the computational domains are very large. It is therefore necessary to develop

faster and more efficient ways to solve the coupled problem. One approach that can be used is a two-grid approach. The application of two-grid methods was first applied to finite element methods by Xu [55, 53, 54]. The method has also been used for the linearization of nonlinear problems in [34, 21, 22]. The two-grid method involves solving the coupled problem on a coarse grid, then decoupling the problem on finer grids by using the coarse mesh solution for the interface in each region on the finer grid. This is a useful technique because it allows easy parallel implementation and results in solving two relatively smaller problems on the fine grid. Codes that have been optimized for solving the Navier-Stokes and Darcy equations separately may also be employed to solve the linear systems resulting from the decoupling. Girault and Lions [22] have applied a two-grid technique to the Navier-Stokes problem in polyhedra in three dimensions. The same technique has also been applied to the transient Navier-Stokes problem by Girault and Lions [21]. Xu and Mu [36] have solved the coupled Stokes/Darcy problem using the mixed finite element formulation using this two-grid approach. The two-grid method will be extended to solve the coupled Navier-Stokes/Darcy problem proposed in this thesis.

A closer look at the numerical examples solved in this work shows that in the porous medium it is often the case that the areas of interest (pinches, faults) are usually smaller in comparison to the rest of the domain. The finite volume method studied in for example [35, 42, 6, 5, 27, 19] is widely used in applications to flow in porous media. This method is capable of capturing the flow in parts of the domain in which the permeability is well behaved; however, it is not as accurate in fractures, faults or areas of high discontinuities. The advantage of the finite volume method is that it results in smaller linear systems to solve. With these facts in mind it seems that coupling the DG method with the finite volume method would be a natural

choice.

The outline of this thesis is as follows. In Chapter 2 I introduce the partial differential equations that model fluid flow in the Navier-Stokes and Darcy domains. To complete the model, interface conditions are also specified. Existence and uniqueness proofs of the weak solution are proved in Chapter 3. The coupled problem is discretized in Chapter 4 and a numerical scheme is proposed. Chapter 5 presents numerical results from simulations of the coupled problem under various parameters of the model. Chapter 6 introduces the two-grid decoupling techniques and presents the theoretical framework. The last chapter in this thesis is devoted to the coupling of the finite volume method with the DG method.

Chapter 2

Coupled Navier-Stokes/Darcy Model

Introduction

In this chapter the partial differential equations that model flow in the free flow domain and the porous media domain are introduced. In order to complete the model, coupling conditions on the interface are also specified.

2.1 Numerical Schemes

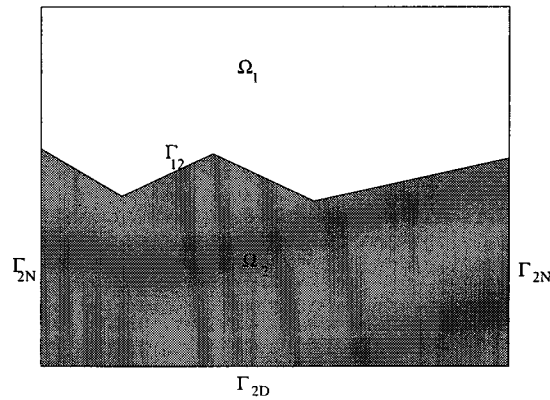


Figure 2.1 : Computational domain of surface and subsurface

The computational domain Ω is assumed to be a bounded domain in \mathbb{R}^n , $n = 2, 3$ composed of two disjoint subdomains Ω_1 and Ω_2 , the free flow and porous media domains respectively. The two domains are separated by a an interface $\Gamma_{12} = \partial\Omega_1 \cup$

$\partial\Omega_2$. The interface Γ_{12} is assumed to be a polygonal line. An example domain is shown in Figure (2.1). The fluid flow is described by the Navier-Stokes and Darcy equations in the free flow (Ω_1) and porous medium (Ω_2) domains respectively.

2.2 The Navier-Stokes Equations

The flow in Ω_1 is incompressible and is characterized by the Navier-Stokes equations. The Navier-Stokes equations are used to model fluid flow in which the non-linear effects are important but they are balanced by the viscous effects. The resulting flow problem will always achieve equilibrium.

$$-\nabla \cdot (2\nu \mathbf{D}(\mathbf{u}_1) - p_1 \mathbf{I}) + \mathbf{u}_1 \cdot \nabla \mathbf{u}_1 = \mathbf{f}_1, \quad \text{in } \Omega_1, \quad (2.1)$$

$$\nabla \cdot \mathbf{u}_1 = 0, \quad \text{in } \Omega_1, \quad (2.2)$$

$$\mathbf{u}_1 = 0, \quad \text{on } \partial\Omega_1 \setminus \Gamma_{12} = \Gamma_1. \quad (2.3)$$

The fluid velocity and pressure in Ω_1 are denoted by \mathbf{u}_1 and p_1 respectively. The coefficient $\nu > 0$ is the kinematic fluid viscosity, the function \mathbf{f}_1 is an external force acting on the fluid, \mathbf{I} is the identity tensor and $\mathbf{D}(\mathbf{u}_1)$ is the strain rate:

$$\mathbf{D}(\mathbf{u}_1) = \frac{1}{2}(\nabla \mathbf{u}_1 + \nabla \mathbf{u}_1^T). \quad (2.4)$$

2.3 Darcy Equations

The flow in Ω_2 is driven by pressure pushing the fluid through pores in the medium. The porous medium is assumed to be saturated by the fluid. This type of flow is characterized by Darcy's law. The porous medium boundary $\Gamma_2 = \partial\Omega_2 \setminus \Gamma_{12}$ is the union of two disjoint sets Γ_{2D} and Γ_{2N} on which Dirichlet and Neumann boundary

conditions are imposed respectively. The Dirichlet and Neumann boundary conditions correspond to a prescribed pressure and flux respectively.

$$-\nabla \cdot \mathbf{K} \nabla p_2 = f_2, \text{ in } \Omega_2, \quad (2.5)$$

$$-\mathbf{K} \nabla p_2 = \mathbf{u}_2, \text{ in } \Omega_2, \quad (2.6)$$

$$p_2 = g_D, \text{ on } \Gamma_{2D}, \quad (2.7)$$

$$\mathbf{K} \nabla p_2 \cdot \mathbf{n}_2 = g_N, \text{ on } \Gamma_{2N}. \quad (2.8)$$

The fluid velocity and pressure in Ω_2 are denoted by \mathbf{u}_2 and p_2 respectively. The function f_2 is an external force acting on the fluid, the functions g_D and g_N are the prescribed value and flux respectively, the vector \mathbf{n}_2 denotes the unit vector normal to Γ_2 and the coefficient \mathbf{K} is a symmetric positive definite tensor uniformly bounded from above and below. There exist constants $\lambda_{\min} > 0$ and $\lambda_{\max} > 0$ such that:

$$\text{a.e. } \mathbf{x} \in \Omega_2, \lambda_{\min} \mathbf{x} \cdot \mathbf{x} \leq \mathbf{K} \mathbf{x} \cdot \mathbf{x} \leq \lambda_{\max} \mathbf{x} \cdot \mathbf{x}. \quad (2.9)$$

The hydraulic conductivity may be expressed as

$$\mathbf{K} = \frac{\mathbf{k} \rho g}{\nu}$$

where \mathbf{k} is the intrinsic permeability of the medium, ρ is the density of the fluid and g is the acceleration due to gravity [38].

2.4 Interface Conditions

The model is completed by specifying coupling conditions on the interface Γ_{12} . The mathematical difficulty arises from the fact that the partial differential equations governing the flow in each domain are of different orders. The interface conditions incorporate three main properties listed below.

1. The continuity of the normal component of velocity arising from the incompressibility condition. Let \mathbf{n}_{12} be the unit normal vector to Γ_{12} directed from Ω_1 to Ω_2 :

$$\mathbf{u}_1 \cdot \mathbf{n}_{12} = K \nabla p_2 \cdot \mathbf{n}_{12}. \quad (2.10)$$

2. The second condition is on the tangential component of the velocity in the free flow region. Let $\boldsymbol{\tau}_{12}$ be the unit tangent vector on the interface Γ_{12} then the Beavers-Joseph-Saffman law [3, 28, 50] will be written as

$$\mathbf{u}_1 \cdot \boldsymbol{\tau}_{12} = -2\nu G(\mathbf{D}(\mathbf{u}_1)\mathbf{n}_{12}) \cdot \boldsymbol{\tau}_{12}. \quad (2.11)$$

The variable G is an experimentally determined constant that depends on the nature of the porous medium.

3. The last condition relates to the balance of forces on the interface, this can be achieved in two different ways:

(a) including inertial forces using one of the following conditions:

$$((-2\nu \mathbf{D}(\mathbf{u}_1) + p_1 \mathbf{I})\mathbf{n}_{12}) \cdot \mathbf{n}_{12} + \frac{1}{2}(\mathbf{u}_1 \cdot \mathbf{u}_1) = p_2 \quad (2.12)$$

Remark 1. *A dimensional analysis will show that:*

$$((-2\nu \mathbf{D}(\mathbf{u}_1) + p_1 \mathbf{I})\mathbf{n}_{12}) \cdot \mathbf{n}_{12} + \frac{1}{2}\rho(\mathbf{u}_1 \cdot \mathbf{n}_{12})^2 = p_2$$

might be the correct condition to use. In Chapter (5) we study the numerical solution resulting from this condition.

(b) without inertial forces

$$((-2\nu \mathbf{D}(\mathbf{u}_1) + p_1 \mathbf{I})\mathbf{n}_{12}) \cdot \mathbf{n}_{12} = p_2, \quad (2.13)$$

Conclusion

The partial differential equations of the coupled surface flow and porous media flow model have been presented. The Navier-Stokes equations will model free flow and Darcy's Law models flow in the porous media. The next chapter establishes the mathematical framework of this model.

Chapter 3

Mathematical Analysis

Introduction

A mathematical description of fluid flow requires the definition of functional spaces. This chapter introduces the function spaces required in order to define the weak problem for the coupled Navier-Stokes and Darcy problem. Furthermore, existence and uniqueness results for a weak solution will be proved. The work in this chapter has been published in [40].

3.1 Preliminary Notation and Function Spaces

The following is a short review of function and notation used in the rest of the chapter. A complete presentation of this material can be found for example in [1, 31].

3.1.1 L^p Spaces

Let \mathcal{O} denote an open set in \mathbb{R}^d in the Lebesgue measure. Let $1 \leq p \leq \infty$, recall the Banach space L^p of measurable functions v such that

$$\int_{\mathcal{O}} |v(x)|^p dx < \infty, 1 \leq p \leq \infty, \quad (3.1)$$

and in the case $p = \infty$,

$$\text{ess sup}\{|v(x)| | x \in \mathcal{O}\} < \infty. \quad (3.2)$$

In fact L^p is the space of equivalence of measurable functions, satisfying (3.1) or (3.2) with respect to the equivalence relation:

$$v \equiv w \text{ iff } \text{meas}(\{x \in \mathcal{O} \mid v(x) \neq w(x)\}) = 0 \quad (3.3)$$

In the case $p = 2$, L^2 is a Hilbert Space endowed with the following inner product

$$(u, v)_{L^2(\mathcal{O})} = \int_{\mathcal{O}} uv, \quad \|v\|_{L^2(\mathcal{O})} = \left(\int_{\mathcal{O}} v^2 \right)^{1/2}.$$

If $1 \leq p < \infty$, the dual space of $L^p(\mathcal{O})$ is L^q , where $\frac{1}{p} + \frac{1}{q} = 1$ and for $q = \infty$, $p = 1$. Recall that in $L^p(\mathcal{O})$ Hölder's inequality holds:

$$\left| \int_{\mathcal{O}} w(x)v(x) dx \right| \leq \|w\|_{L^p} \|v\|_{L^q}. \quad (3.4)$$

For the case $p = 2$ the Hölder inequality is the Cauchy Schwarz inequality:

$$\forall v, w \in L^2(\mathcal{O}), \quad |(v, w)_{\mathcal{O}}| \leq \|v\|_{L^2(\mathcal{O})} \|w\|_{L^2(\mathcal{O})}. \quad (3.5)$$

$$(3.6)$$

We also recall Young's inequality:

$$\forall a, b \in \mathbb{R}, \forall \delta > 0, \quad ab \leq \frac{\delta}{2} a^2 + \frac{1}{2\delta} b^2. \quad (3.7)$$

3.1.2 Sobolev Spaces

Let $\mathcal{D}(\mathcal{O})$ denote the space the space of infinitely differentiable functions with compact support in \mathcal{O} . The dual space $\mathcal{D}'(\mathcal{O})$ is a space of distributions. If $\alpha = (\alpha_1, \dots, \alpha_d)$, $\alpha_i \geq 0$, then the distributional derivative $\mathcal{D}^\alpha(\mathcal{O})$ is defined by

$$\forall \phi \in \mathcal{D}(\mathcal{O}), \quad D^\alpha v(\phi) = (-1)^{|\alpha|} \int_{\mathcal{O}} v(x) \frac{\partial^{|\alpha|} \phi}{\partial x_1^{\alpha_1} \dots \partial x_d^{\alpha_d}}.$$

The Sobolev space $H^k(\mathcal{O})$, with $k \geq 0$ is the space of functions $v \in L^2(\mathcal{O})$ such that the distributional derivatives of v up to order k are functions of $L^2(\mathcal{O})$.

$$H^k(\mathcal{O}) = \{v \in L^2(\mathcal{O}) : \forall 0 \leq |\alpha| \leq k, D^\alpha v \in L^2(\mathcal{O})\}.$$

$H^k(\mathcal{O})$ is a Hilbert space endowed with the norm

$$\|v\|_{H^k(\mathcal{O})} = \left(\sum_{0 \leq |\alpha| \leq k} \|D^\alpha v\|_{L^2(\mathcal{O})}^2 \right)^{1/2},$$

and scalar product

$$(w, v)_{H^k(\mathcal{O})} = \sum_{|\alpha| \leq k} (D^\alpha w, D^\alpha v)_{L^2(\mathcal{O})}$$

Further, the Sobolev seminorm associate with $H^k(\mathcal{O})$ is

$$|v|_{H^k(\mathcal{O})} = \|\nabla^k v\|_{L^2(\mathcal{O})} = \left(\sum_{|\alpha|=k} \|D^\alpha v\|_{L^2(\mathcal{O})}^2 \right)^{1/2}.$$

Other important inequalities to recall are Poincaré and Korn's inequalities and trace and Sobolev inequalities: there exists constants $\mathcal{P}_1, C_1, C_2, C_4$ and \mathcal{P}_4 that only depend on the Navier-Stokes domain Ω_1 and \mathcal{P}_2, C_3 depending on the Darcy domain Ω_2 such that

$$\|\mathbf{v}\|_{L^2(\Omega_1)} \leq \mathcal{P}_1 \|\nabla \mathbf{v}\|_{L^2(\Omega_1)}, \quad \|\mathbf{v}\|_{L^4(\Omega_1)} \leq \mathcal{P}_4 \|\nabla \mathbf{v}\|_{L^2(\Omega_1)}, \quad (3.8)$$

$$\|\nabla \mathbf{v}\|_{L^2(\Omega_1)} \leq C_1 \|\mathbf{D}(\mathbf{v})\|_{L^2(\Omega_1)}, \quad (3.9)$$

$$\|\mathbf{v}\|_{L^2(\Gamma_{12})} \leq C_2 \|\nabla \mathbf{v}\|_{L^2(\Omega_1)}, \quad \|\mathbf{v}\|_{L^4(\Gamma_{12})} \leq C_4 \|\nabla \mathbf{v}\|_{L^2(\Omega_1)}, \quad (3.10)$$

and for all $q \in M_2$,

$$\|q\|_{L^2(\Omega_2)} \leq \mathcal{P}_2 \|\nabla q\|_{L^2(\Omega_2)}, \quad (3.11)$$

$$\|q\|_{L^2(\Gamma_{2N})} \leq C_3 \|\nabla q\|_{L^2(\Omega_2)}; \quad (3.12)$$

moreover, owing to (2.9), for all $q \in H^1(\Omega_2)$:

$$\frac{1}{\sqrt{\lambda_{\max}}} \|\mathbf{K}^{1/2} \nabla q\|_{L^2(\Omega_2)} \leq \|\nabla q\|_{L^2(\Omega_2)} \leq \frac{1}{\sqrt{\lambda_{\min}}} \|\mathbf{K}^{1/2} \nabla q\|_{L^2(\Omega_2)}. \quad (3.13)$$

3.2 Variational Formulation

Let $H^s(\mathcal{O})$ be the usual Sobolev space of order s [1] with norm $\|\cdot\|_{H^s(\mathcal{O})}$. We first lift the Dirichlet boundary condition (2.7). If $g_D \in H^{1/2}(\Gamma_{2D})$, there exists a function $p_D \in H^1(\Omega_2)$ satisfying:

$$p_D = g_D, \text{ on } \Gamma_{2D}, \quad (3.14)$$

$$p_D = 0, \text{ on } \Gamma_{12}, \quad (3.15)$$

$$\|p_D\|_{H^1(\Omega_2)} \leq C_0 \|g_D\|_{H^{1/2}(\Gamma_{2D})}, \quad (3.16)$$

where C_0 is a constant that only depends on Ω_2 . The Navier-Stokes velocity and pressure belong to the space:

$$\mathbf{X}_1 = \{\mathbf{v}_1 \in (H^1(\Omega_1))^2 : \mathbf{v}_1 = 0 \text{ on } \Gamma_1\},$$

$$M_1 = L^2(\Omega_1),$$

respectively, and the Darcy pressure belongs to the space:

$$M_2 = \{q_2 \in H^1(\Omega_2) : q_2 = 0 \text{ on } \Gamma_{2D}\}.$$

The first variational form (W_A) includes the inertial forces in the balance of forces on the interface:

$$(W_A) \left\{ \begin{array}{l} \text{Find } \mathbf{u}_1 \in \mathbf{X}_1, p_1 \in M_1, p_2 = \varphi_2 + p_D, \text{ with } \varphi_2 \in M_2, \text{ s.t.} \\ \forall \mathbf{v}_1 \in \mathbf{X}_1, \forall q_2 \in M_2, \quad 2\nu(\mathbf{D}(\mathbf{u}_1), \mathbf{D}(\mathbf{v}_1))_{\Omega_1} + (\mathbf{u}_1 \cdot \nabla \mathbf{u}_1, \mathbf{v}_1)_{\Omega_1} - (p_1, \nabla \cdot \mathbf{v}_1)_{\Omega_1} \\ + (\varphi_2 - \frac{1}{2} \mathbf{u}_1 \cdot \mathbf{u}_1, \mathbf{v}_1 \cdot \mathbf{n}_{12})_{\Gamma_{12}} + \frac{1}{G} (\mathbf{u}_1 \cdot \boldsymbol{\tau}_{12}, \mathbf{v}_1 \cdot \boldsymbol{\tau}_{12})_{\Gamma_{12}} - (\mathbf{u}_1 \cdot \mathbf{n}_{12}, q_2)_{\Gamma_{12}} \\ + (\mathbf{K} \nabla \varphi_2, \nabla q_2)_{\Omega_2} = (\mathbf{f}_1, \mathbf{v}_1)_{\Omega_1} + (f_2, q_2)_{\Omega_2} - (\mathbf{K} \nabla p_D, \nabla q_2)_{\Omega_2} + (g_N, q_2)_{\Gamma_{2N}}, \\ \forall q_1 \in M_1, \quad (\nabla \cdot \mathbf{u}_1, q_1)_{\Omega_1} = 0. \end{array} \right.$$

The second variational form (W_B) does not include the inertial forces on the balance of forces on the interface:

$$(W_B) \left\{ \begin{array}{l} \text{Find } \mathbf{u}_1 \in \mathbf{X}_1, p_1 \in M_1, p_2 = \varphi_2 + p_D, \text{ with } \varphi_2 \in M_2, \text{ s.t.} \\ \forall \mathbf{v}_1 \in \mathbf{X}_1, \forall q_2 \in M_2, \quad 2\nu(\mathbf{D}(\mathbf{u}_1), \mathbf{D}(\mathbf{v}_1))_{\Omega_1} + (\mathbf{u}_1 \cdot \nabla \mathbf{u}_1, \mathbf{v}_1)_{\Omega_1} - (p_1, \nabla \cdot \mathbf{v}_1)_{\Omega_1} \\ + \frac{1}{G}(\mathbf{u}_1 \cdot \boldsymbol{\tau}_{12}, \mathbf{v}_1 \cdot \boldsymbol{\tau}_{12})_{\Gamma_{12}} - (\mathbf{u}_1 \cdot \mathbf{n}_{12}, q_2)_{\Gamma_{12}} + (\mathbf{K}\nabla\varphi_2, \nabla q_2)_{\Omega_2} \\ = (\mathbf{f}_1, \mathbf{v}_1)_{\Omega_1} + (f_2, q_2)_{\Omega_2} - (\mathbf{K}\nabla p_D, \nabla q_2)_{\Omega_2} + (g_N, q_2)_{\Gamma_{2N}}, \\ \forall q_1 \in M_1, \quad (\nabla \cdot \mathbf{u}_1, q_1)_{\Omega_1} = 0. \end{array} \right.$$

The problems (W_A) and (W_B) differ only by the term $(\frac{1}{2}\mathbf{u}_1 \cdot \mathbf{u}_1, \mathbf{v}_1 \cdot \mathbf{n}_{12})_{\Gamma_{12}}$ arising from the balance of forces condition. The first step is to show that the variational formulations are equivalent to the model problem.

Lemma 2. *If $(\mathbf{u}_1, p_1, p_2) \in \mathbf{X}_1 \times M_1 \times H^1(\Omega_2)$ satisfies (2.1)-(2.12), then it is also a solution to problem (W_A). If $(\mathbf{u}_1, p_1, p_2) \in \mathbf{X}_1 \times M_1 \times H^1(\Omega_2)$ satisfies (2.1) - (2.11) and (2.13) then it is also a solution to problem (W_B). The converse of both statements is also true.*

Proof. First consider the model problem introduced in Chapter (2) (2.1) - (2.12 and (2.13) with a solution $(\mathbf{u}_1, p_1, p_2) \in \mathbf{X}_1 \times M_1 \times H^1(\Omega_2)$. Multiply (2.1), (2.2) and (2.5) by test functions $\mathbf{v}_1 \in \mathbf{X}_1, q_1 \in M_1$ and $q_2 \in M_2$ respectively and use Green's theorem and boundary conditions:

$$\begin{aligned} & 2\nu(\mathbf{D}(\mathbf{u}_1), \mathbf{D}(\mathbf{v}_1))_{\Omega_1} - (p_1, \nabla \cdot \mathbf{v}_1)_{\Omega_1} + (\mathbf{u}_1 \cdot \nabla \mathbf{u}_1, \mathbf{v}_1)_{\Omega_1} \\ & + ((-2\nu\mathbf{D}(\mathbf{u}_1) + p_1\mathbf{I})\mathbf{n}_{12}, \mathbf{v}_1)_{\Gamma_{12}} = (\mathbf{f}_1, \mathbf{v}_1)_{\Omega_1}, \end{aligned} \quad (3.17)$$

$$(\nabla \cdot \mathbf{u}_1, q_1) = 0, \quad (3.18)$$

$$(\mathbf{K}\nabla p_2, \nabla q_2)_{\Omega_2} + (\mathbf{K}\nabla p_2 \cdot \mathbf{n}_{12}, q_2)_{\Gamma_{12}} = (f_2, q_2)_{\Omega_2} + (g_N, q_2)_{\Gamma_{2N}}. \quad (3.19)$$

Rewriting $\mathbf{v}_1 = (\mathbf{v}_1 \cdot \mathbf{n}_{12})\mathbf{n}_{12} + (\mathbf{v}_1 \cdot \boldsymbol{\tau}_{12})\boldsymbol{\tau}_{12}$, adding (3.17) and (3.19) and using the

interface conditions (2.11)- (2.13), we obtain:

$$\begin{aligned}
& 2\nu(\mathbf{D}(\mathbf{u}_1), \mathbf{D}(\mathbf{v}_1))_{\Omega_1} - (p_1, \nabla \cdot \mathbf{v}_1)_{\Omega_1} + (\mathbf{u}_1 \cdot \nabla \mathbf{u}_1, \mathbf{v}_1)_{\Omega_1} + (\mathbf{K} \nabla p_2, \nabla q_2)_{\Omega_2} \\
& + (p_2 - \frac{1}{2} \mathbf{u}_1 \cdot \mathbf{u}_1, \mathbf{v}_1 \cdot \mathbf{n}_{12})_{\Gamma_{12}} + \frac{1}{G} (\mathbf{u}_1 \cdot \boldsymbol{\tau}_{12}, \mathbf{v}_1 \cdot \boldsymbol{\tau}_{12})_{\Gamma_{12}} - (\mathbf{u}_1 \cdot \mathbf{n}_{12}, q_2)_{\Gamma_{12}} \\
& = (\mathbf{f}_1, \mathbf{v})_{\Omega_1} + (f_2, q_2)_{\Omega_2} + (g_N, q_2)_{\Gamma_{2N}}, \\
& (\nabla \cdot \mathbf{u}_1, q_1)_{\Omega_1} = 0.
\end{aligned}$$

Due to the lift on the nonhomogeneous boundary condition, $\varphi_2 = p_2 - p_D$. The choice of test functions (3.15) means that the trace $p_2 = \varphi_2$ on Γ_{12} . We obtain the resulting equations:

$$\begin{aligned}
& 2\nu(\mathbf{D}(\mathbf{u}_1), \mathbf{D}(\mathbf{v}_1))_{\Omega_1} - (p_1, \nabla \cdot \mathbf{v}_1)_{\Omega_1} + (\mathbf{u}_1 \cdot \nabla \mathbf{u}_1, \mathbf{v}_1)_{\Omega_1} + (\mathbf{K} \nabla \varphi_2, \nabla q_2)_{\Omega_2} \\
& + (\varphi_2 - \frac{1}{2} \mathbf{u}_1 \cdot \mathbf{u}_1, \mathbf{v}_1 \cdot \mathbf{n}_{12})_{\Gamma_{12}} + \frac{1}{G} (\mathbf{u}_1 \cdot \boldsymbol{\tau}_{12}, \mathbf{v}_1 \cdot \boldsymbol{\tau}_{12})_{\Gamma_{12}} - (\mathbf{u}_1 \cdot \mathbf{n}_{12}, q_2)_{\Gamma_{12}} \\
& = (\mathbf{f}_1, \mathbf{v}_1)_{\Omega_1} + (f_2, q_2)_{\Omega_2} + (g_N, q_2)_{\Gamma_{2N}} - (\mathbf{K} \nabla p_D, \nabla q_2)_{\Omega_2}, \\
& (\nabla \cdot \mathbf{u}_1, q_1)_{\Omega_1} = 0,
\end{aligned}$$

which correspond to problem (W_A) . Conversely, assume that (\mathbf{u}_1, p_1, p_2) is a solution to (W_A) . By choosing appropriate test functions, we recover the equations (2.1), (2.2) and (2.5) in a distributional sense. First, take $\mathbf{v}_1 \in \mathcal{D}(\Omega_1)$, $q_1 = q_2 = 0$. This yields:

$$-\nabla \cdot (2\nu \mathbf{D}(\mathbf{u}_1) - p_1 \mathbf{I}) + \mathbf{u}_1 \cdot \nabla \mathbf{u}_1 = \mathbf{f}_1 \quad (3.20)$$

in a distributional sense. Second, take $q_1 \in \mathcal{D}(\Omega_1)$, $\mathbf{v}_1 = \mathbf{0}$, $q_2 = 0$:

$$\nabla \cdot \mathbf{u}_1 = 0. \quad (3.21)$$

Third, take $q_2 \in \mathcal{D}(\Omega_2)$, $\mathbf{v}_1 = \mathbf{0}$, $q_1 = 0$:

$$-\nabla \cdot \mathbf{K} \nabla (\varphi_2 + p_D) = f_2. \quad (3.22)$$

To recover the interface conditions, multiply (3.20), (3.22) by functions $\mathbf{v}_1 \in \mathbf{X}_1$ and $q_2 \in M_2$ respectively, use Green's theorem, add the two equations and compare with

(W_A) :

$$\begin{aligned} & (\varphi_2 - \frac{1}{2}(\mathbf{u}_1 \cdot \mathbf{u}_1), \mathbf{v}_1 \cdot \mathbf{n}_{12})_{\Gamma_{12}} - (\mathbf{u}_1 \cdot \mathbf{n}_{12}, q_2)_{\Gamma_{12}} + \frac{1}{G}(\mathbf{u}_1 \cdot \boldsymbol{\tau}_{12}, \mathbf{v}_1 \cdot \boldsymbol{\tau}_{12})_{\Gamma_{12}} - (g_N, q_2)_{\Gamma_{2N}} \\ & = ((-2\nu\mathbf{D}(\mathbf{u}_1) + p_1\mathbf{I})\mathbf{n}_{12}, \mathbf{v}_1)_{\Gamma_{12}} + (\mathbf{K}\nabla p_2 \cdot \mathbf{n}_{12}, q_2)_{\Gamma_{12}} - (\mathbf{K}\nabla p_2 \cdot \mathbf{n}_2, q_2)_{\Gamma_{2N}}. \end{aligned} \quad (3.23)$$

By choosing $\mathbf{v}_1 = \mathbf{0}$ and either $q_2|_{\Gamma_{12}} = 0$ we obtain

$$(\mathbf{K}\nabla p_2 \cdot \mathbf{n}_2, q_2)_{\Gamma_{2N}} = (g_N, q_2)_{\Gamma_{2N}}$$

the Neumann boundary condition (2.8). If we choose $\mathbf{v}_1 = 0$ and $p_2|_{\Gamma_{12}}$ we have

$$(\mathbf{u}_1 \cdot \mathbf{n}_{12}, q_2)_{\Gamma_{12}} = -(\mathbf{K}\nabla p_2 \cdot \mathbf{n}_{12}, q_2)_{12},$$

the continuity of the normal component on the interface (2.10). Next, by choosing $q_2 = 0$ and $\mathbf{v}_1 = v_1\mathbf{n}_{12}$ where v_1 is a smooth function defined on each curvilinear segment of Γ_{12} and vanishing in a neighborhood of $\partial\Omega_1 \setminus \Gamma_{12}$:

$$((-2\nu\mathbf{D}(\mathbf{u}_1) + p_1\mathbf{I})\mathbf{n}_{12}, \mathbf{v}_1)_{\Gamma_{12}} = (\varphi_2 - \frac{1}{2}(\mathbf{u}_1 \cdot \mathbf{u}_1), \mathbf{v}_1 \cdot \mathbf{n}_{12})_{\Gamma_{12}},$$

the interface condition (2.12) by noting that $p_2 = \varphi_2$ on Γ_{12} due to (3.15). Finally, choosing $q_2 = 0$ and $\mathbf{v}_1 = v_1\boldsymbol{\tau}_{12}$ where v_1 is a smooth function defined on each curvilinear segment of Γ_{12} and vanishing in a neighborhood of $\partial\Omega_1 \setminus \Gamma_{12}$, we recover

$$\frac{1}{G}(\mathbf{u}_1 \cdot \boldsymbol{\tau}_{12}, \mathbf{v}_1 \cdot \boldsymbol{\tau}_{12})_{\Gamma_{12}} = ((-2\nu\mathbf{D}(\mathbf{u}_1))\mathbf{n}_{12}, \mathbf{v}_1 \cdot \boldsymbol{\tau}_{12})_{\Gamma_{12}}$$

the interface condition (2.11). Similarly problem W_B is equivalent to (2.1) - (2.11) and (2.13). \square

The next step is to show the existence of a weak solution to the problems W_A and W_B .

3.3 Existence of a weak solution

In this section we prove existence of weak solutions to problems W_A and W_B . The Navier-Stokes velocity and pressure finite element spaces satisfy a continuous inf-sup condition proved in [24]:

$$\inf_{q_1 \in M_1} \sup_{(v_1, q_2) \in \mathbf{X}_1 \times M_2} \frac{|(\nabla \cdot v_1, q_1)_{\Omega_1}|}{(\|\nabla v_1\|_{L^2(\Omega_1)}^2 + \|\nabla q_2\|_{L^2(\Omega_2)}^2)^{1/2} \|q_1\|_{L^2(\Omega_1)}} \geq \beta > 0. \quad (3.24)$$

The velocity test functions are restricted to the space of weakly divergence free functions:

$$\mathbf{V}_1 = \{v_1 \in \mathbf{X}_1, \quad \nabla \cdot v_1 = 0\}.$$

This space is a well defined closed subspace of \mathbf{X}_1 . The variational formulation for problem W_A becomes:

$$(\tilde{W}_A) \left\{ \begin{array}{l} \text{Find } \mathbf{u}_1 \in \mathbf{V}_1, p_2 = \varphi_2 + p_D, \text{ with } \varphi_2 \in M_2, \text{ s.t.} \\ \forall v_1 \in \mathbf{V}_1, \forall q_2 \in M_2, \quad 2\nu(D(\mathbf{u}_1), D(v_1))_{\Omega_1} + (\mathbf{u}_1 \cdot \nabla \mathbf{u}_1, v_1)_{\Omega_1} \\ + (\varphi_2 - \frac{1}{2} \mathbf{u}_1 \cdot \mathbf{u}_1, v_1 \cdot \mathbf{n}_{12})_{\Gamma_{12}} + \frac{1}{G} (\mathbf{u}_1 \cdot \boldsymbol{\tau}_{12}, v_1 \cdot \boldsymbol{\tau}_{12})_{\Gamma_{12}} - (\mathbf{u}_1 \cdot \mathbf{n}_{12}, q_2)_{\Gamma_{12}} \\ + (K \nabla \varphi_2, \nabla q_2)_{\Omega_2} = (\mathbf{f}_1, v_1)_{\Omega_1} + (f_2, q_2)_{\Omega_2} - (K \nabla p_D, \nabla q_2)_{\Omega_2} + (g_N, q_2)_{\Gamma_{2N}}. \end{array} \right.$$

Similarly for problem W_B the variational form becomes:

$$(\tilde{W}_B) \left\{ \begin{array}{l} \text{Find } \mathbf{u}_1 \in \mathbf{V}_1, p_2 = \varphi_2 + p_D, \text{ with } \varphi_2 \in M_2, \text{ s.t.} \\ \forall v_1 \in \mathbf{V}_1, \forall q_2 \in M_2, \quad 2\nu(D(\mathbf{u}_1), D(v_1))_{\Omega_1} + (\mathbf{u}_1 \cdot \nabla \mathbf{u}_1, v_1)_{\Omega_1} \\ + (\varphi_2, v_1 \cdot \mathbf{n}_{12})_{\Gamma_{12}} + \frac{1}{G} (\mathbf{u}_1 \cdot \boldsymbol{\tau}_{12}, v_1 \cdot \boldsymbol{\tau}_{12})_{\Gamma_{12}} - (\mathbf{u}_1 \cdot \mathbf{n}_{12}, q_2)_{\Gamma_{12}} \\ + (K \nabla \varphi_2, \nabla q_2)_{\Omega_2} = (\mathbf{f}_1, v_1)_{\Omega_1} + (f_2, q_2)_{\Omega_2} - (K \nabla p_D, \nabla q_2)_{\Omega_2} + (g_N, q_2)_{\Gamma_{2N}}. \end{array} \right.$$

Therefore, for $\alpha = A, B$ we now focus on the existence and uniqueness of the solution to (\tilde{W}_α) . The problems (W_α) and (\tilde{W}_α) are equivalent because if (\mathbf{u}_1, p_1, p_2) is a solution to W_α then (\mathbf{u}_1, p_2) is also a solution to \tilde{W}_α . Conversely if (\mathbf{u}_1, p_2) is a solution to (\tilde{W}_α) there exists a unique p_1 such that (\mathbf{u}_1, p_1, p_2) is a solution to W_α , this result follows from the inf-sup condition (3.24). The following corollary of Brouwer's

fixed point theorem will be applied to prove existence of a solution to the problems \tilde{W}_α and \tilde{W}_α .

Lemma 3. *Let H be a finite dimensional Hilbert space with inner-product $(\cdot, \cdot)_H$ and norm $\|\cdot\|_H$. Let \mathcal{F} be a continuous mapping from H into H . Assume there is a constant \mathcal{R} such that*

$$\forall v \in H \text{ with } \|v\|_H = \mathcal{R}, \quad (\mathcal{F}(v), v)_H \geq 0.$$

Then, there exists an element $v_0 \in H$ such that

$$\mathcal{F}(v_0) = 0, \quad \|v_0\|_H \leq \mathcal{R}.$$

Theorem 4. *There exists a solution to problem \tilde{W}_A .*

Proof. We use the Galerkin approach. Since the spaces \mathbf{V}_1 and M_2 are separable, they contain countable dense sets. Let $\{(\mathbf{w}_m, t_m)\}_{m \geq 1}$ be a sequence of smooth functions that form a basis of $Y = \mathbf{V}_1 \times M_2$. Consider the finite dimensional space $Y_m = \text{span}\{(\mathbf{w}_i, t_i) : 1 \leq i \leq m\}$ equipped with the inner-product:

$$((\mathbf{v}, q), (\mathbf{w}, t))_Y = 2\nu(\mathbf{D}(\mathbf{v}), \mathbf{D}(\mathbf{w}))_{\Omega_1} + (\mathbf{K}\nabla q, \nabla t)_{\Omega_2}.$$

We restrict problem (\tilde{W}_A) to Y_m and obtain a finite dimensional problem:

$$(\tilde{W}_{A,m}) \begin{cases} \text{Find } (\mathbf{u}_m, \varphi_m) \in Y_m \text{ s.t.} \\ \forall 1 \leq i \leq m, \quad 2\nu(\mathbf{D}(\mathbf{u}_m), \mathbf{D}(\mathbf{w}_i))_{\Omega_1} + (\mathbf{u}_m \cdot \nabla \mathbf{u}_m, \mathbf{w}_i)_{\Omega_1} \\ + (\varphi_m - \frac{1}{2} \mathbf{u}_m \cdot \mathbf{u}_m, \mathbf{w}_i \cdot \mathbf{n}_{12})_{\Gamma_{12}} + \frac{1}{G} (\mathbf{u}_m \cdot \boldsymbol{\tau}_{12}, \mathbf{w}_i \cdot \boldsymbol{\tau}_{12})_{\Gamma_{12}} - (\mathbf{u}_m \cdot \mathbf{n}_{12}, t_i)_{\Gamma_{12}} \\ + (\mathbf{K}\nabla \varphi_m, \nabla t_i)_{\Omega_2} = (\mathbf{f}_1, \mathbf{w}_i)_{\Omega_1} + (f_2, t_i)_{\Omega_2} - (\mathbf{K}\nabla p_D, \nabla t_i)_{\Omega_2} + (g_N, t_i)_{\Gamma_{2N}}. \end{cases}$$

We then define a continuous mapping $\Psi_{A,m} : Y_m \rightarrow Y_m$:

$$\begin{aligned} (\Psi_{A,m}(\mathbf{v}, q), (\mathbf{w}, t))_Y &= 2\nu(\mathbf{D}(\mathbf{v}), \mathbf{D}(\mathbf{w}))_{\Omega_1} + (\mathbf{v} \cdot \nabla \mathbf{v}, \mathbf{w})_{\Omega_1} + (q - \frac{1}{2}\mathbf{v} \cdot \mathbf{v}, \mathbf{w} \cdot \mathbf{n}_{12})_{\Gamma_{12}} \\ &+ \frac{1}{G}(\mathbf{v} \cdot \boldsymbol{\tau}_{12}, \mathbf{w} \cdot \boldsymbol{\tau}_{12})_{\Gamma_{12}} - (\mathbf{v} \cdot \mathbf{n}_{12}, t)_{\Gamma_{12}} + (\mathbf{K}\nabla q, \nabla t)_{\Omega_2} \\ &- (\mathbf{f}_1, \mathbf{w})_{\Omega_1} - (f_2, t)_{\Omega_2} + (\mathbf{K}\nabla p_D, \nabla t)_{\Omega_2} - (g_N, t)_{\Gamma_{2N}}. \end{aligned}$$

A zero of $\Psi_{A,m}$ is a solution to problem (\tilde{W}_m) . The proof will proceed by applying Lemma (3) to conclude that there is at least one zero of $\Psi_{A,m}$ is a ball of a certain radius centered at the origin.

$$\begin{aligned} (\Psi_{A,m}(\mathbf{v}, q), (\mathbf{v}, q))_Y &= 2\nu(\mathbf{D}(\mathbf{v}), \mathbf{D}(\mathbf{v}))_{\Omega_1} + (\mathbf{v} \cdot \nabla \mathbf{v}, \mathbf{v})_{\Omega_1} + (q - \frac{1}{2}\mathbf{v} \cdot \mathbf{v}, \mathbf{v} \cdot \mathbf{n}_{12})_{\Gamma_{12}} \\ &+ \frac{1}{G}(\mathbf{v} \cdot \boldsymbol{\tau}_{12}, \mathbf{v} \cdot \boldsymbol{\tau}_{12})_{\Gamma_{12}} - (\mathbf{v} \cdot \mathbf{n}_{12}, q)_{\Gamma_{12}} + (\mathbf{K}\nabla q, \nabla q)_{\Omega_2} \\ &- (\mathbf{f}_1, \mathbf{v})_{\Omega_1} - (f_2, q)_{\Omega_2} + (\mathbf{K}\nabla p_D, \nabla q)_{\Omega_2} - (g_N, q)_{\Gamma_{2N}}. \end{aligned}$$

For $\mathbf{v} \in \mathbf{V}_1$, $\nabla \cdot \mathbf{v} = 0$ so:

$$(\mathbf{v} \cdot \nabla \mathbf{v}, \mathbf{v})_{\Omega_1} = -\frac{1}{2}(\nabla \cdot \mathbf{v}, \mathbf{v} \cdot \mathbf{v})_{\Omega_1} + \frac{1}{2}(\mathbf{v} \cdot \mathbf{n}_1, \mathbf{v} \cdot \mathbf{v})_{\partial\Omega_1} = \frac{1}{2}(\mathbf{v} \cdot \mathbf{n}_1, \mathbf{v} \cdot \mathbf{v})_{\partial\Omega_1}. \quad (3.25)$$

Therefore since $\mathbf{v} = 0$ on Γ_1 :

$$(\mathbf{v} \cdot \nabla \mathbf{v}, \mathbf{v})_{\Omega_1} + (q - \frac{1}{2}\mathbf{v} \cdot \mathbf{v}, \mathbf{v} \cdot \mathbf{n}_{12})_{\Gamma_{12}} - (\mathbf{v} \cdot \mathbf{n}_{12}, q)_{\Gamma_{12}} = 0,$$

which results in

$$\begin{aligned} (\Psi_m(\mathbf{v}, q), (\mathbf{v}, q))_Y &= 2\nu\|\mathbf{D}(\mathbf{v})\|_{L^2(\Omega_1)}^2 + \frac{1}{G}\|\mathbf{v} \cdot \boldsymbol{\tau}_{12}\|_{L^2(\Gamma_{12})}^2 + \|\mathbf{K}^{1/2}\nabla q\|_{L^2(\Omega_2)}^2 \\ &- (\mathbf{f}_1, \mathbf{v})_{\Omega_1} - (f_2, q)_{\Omega_2} + (\mathbf{K}\nabla p_D, \nabla q)_{\Omega_2} - (g_N, q)_{\Gamma_{2N}}. \end{aligned} \quad (3.26)$$

We now bound the terms in the second line of (3.26). Using (3.5), (3.8), (3.9) and (3.7), we obtain

$$\begin{aligned} |(\mathbf{f}_1, \mathbf{v})_{\Omega_1}| &\leq \|\mathbf{f}_1\|_{L^2(\Omega_1)}\|\mathbf{v}\|_{L^2(\Omega_1)} \\ &\leq \mathcal{P}_1 C_1 \|\mathbf{D}(\mathbf{v})\|_{L^2(\Omega_1)}\|\mathbf{f}_1\|_{L^2(\Omega_1)} \leq \frac{\nu}{2}\|\mathbf{D}(\mathbf{v})\|_{L^2(\Omega_1)}^2 + \frac{\mathcal{P}_1^2 C_1^2}{2\nu}\|\mathbf{f}_1\|_{L^2(\Omega_1)}^2. \end{aligned}$$

Similarly, using (3.5), (3.11), (3.13) and (3.7), we have

$$(f_2, q)_{\Omega_2} \leq \frac{1}{4} \|\mathbf{K}^{1/2} \nabla q\|_{L^2(\Omega_2)}^2 + \frac{1}{\lambda_{\min}} \mathcal{P}_2^2 \|f_2\|_{L^2(\Omega_2)}^2.$$

Using the bounds (3.16), (3.5) and (3.13), we have

$$(\mathbf{K} \nabla p_D, \nabla q)_{\Omega_2} \leq \frac{1}{4} \|\mathbf{K}^{1/2} \nabla q\|_{L^2(\Omega_2)}^2 + C_0^2 \lambda_{\max} \|g_D\|_{H^{1/2}(\Gamma_{2D})}^2.$$

Finally, using (3.5), (3.12), (3.13) and (3.7), we obtain

$$(g_N, q)_{\Gamma_{2N}} \leq \frac{1}{4} \|\mathbf{K}^{1/2} \nabla q\|_{L^2(\Omega_2)}^2 + \frac{C_3^2}{\lambda_{\min}} \|g_N\|_{L^2(\Gamma_{2N})}^2.$$

Therefore

$$\begin{aligned} (\Psi_{A,m}(\mathbf{v}, q), (\mathbf{v}, q))_Y &\geq \frac{1}{4} \left(2\nu \|\mathbf{D}(\mathbf{v})\|_{L^2(\Omega_1)}^2 + \|\mathbf{K}^{1/2} \nabla q\|_{L^2(\Omega_2)}^2 \right) \\ &\quad - \left(\frac{\mathcal{P}_1^2 C_1^2}{2\nu} \|\mathbf{f}_1\|_{L^2(\Omega_1)}^2 + \frac{\mathcal{P}_2^2}{\lambda_{\min}} \|f_2\|_{L^2(\Omega_2)}^2 + C_0^2 \lambda_{\max} \|g_D\|_{H^{1/2}(\Gamma_{2D})}^2 + \frac{C_3^2}{\lambda_{\min}} \|g_N\|_{L^2(\Gamma_{2N})}^2 \right), \end{aligned}$$

so $(\Psi_m(\mathbf{v}, q), (\mathbf{v}, q))_Y \geq 0$ provided $\|(\mathbf{v}, q)\|_Y = ((\mathbf{v}, q), (\mathbf{v}, q))_Y^{1/2} = \mathcal{R}_0$ with

$$\mathcal{R}_0 = 2 \left(\frac{\mathcal{P}_1^2 C_1^2}{2\nu} \|\mathbf{f}_1\|_{L^2(\Omega_1)}^2 + \frac{\mathcal{P}_2^2}{\lambda_{\min}} \|f_2\|_{L^2(\Omega_2)}^2 + C_0^2 \lambda_{\max} \|g_D\|_{H^{1/2}(\Gamma_{2D})}^2 + \frac{C_3^2}{\lambda_{\min}} \|g_N\|_{L^2(\Gamma_{2N})}^2 \right)^{1/2}. \quad (3.27)$$

Therefore, for any m , there is a solution $(\mathbf{u}_m, \varphi_m)$ of problem $(\tilde{W}_{A,m})$ satisfying:

$$\|(\mathbf{u}_m, \varphi_m)\|_Y \leq \mathcal{R}_0.$$

We have thus constructed a bounded sequence in the Hilbert space $\mathbf{V}_1 \times M_2$. Therefore, there exists a subsequence, still denoted by $\{(\mathbf{u}_m, \varphi_m)\}_m$, that converges weakly to an element $(\mathbf{u}_1, \varphi_2) \in \mathbf{V}_1 \times M_2$. Using a standard argument and Sobolev imbeddings, we can pass to the limit in the equation of problem $(\tilde{W}_{A,m})$ as m tends to infinity. Denoting $p_2 = \varphi_2 + p_D$, we then obtain that (\mathbf{u}_1, p_2) is a solution to problem $(\tilde{W}_{A,m})$. Using the same argument as above, we can show that any solution $(\mathbf{u}_1, \varphi_2)$ to problem (\tilde{W}_A) is bounded:

$$2\nu \|\mathbf{D}(\mathbf{u})\|_{L^2(\Omega_1)}^2 + \|\mathbf{K}^{1/2} \nabla \varphi_2\|_{L^2(\Omega_2)}^2 \leq \mathcal{R}_0^2. \quad (3.28)$$

This yields the bound:

$$2\nu\|\mathbf{D}(\mathbf{u})\|_{L^2(\Omega_1)}^2 + \|\mathbf{K}^{1/2}\nabla p\|_{L^2(\Omega_2)}^2 \leq \mathcal{R}_1^2, \quad (3.29)$$

where

$$\mathcal{R}_1^2 = \mathcal{R}_0^2 + 2\|\mathbf{K}^{1/2}\nabla p_D\|_{L^2(\Omega_2)}^2. \quad (3.30)$$

□

The next theorem proves the existence of a solution to \tilde{W}_B under the assumption of a small data condition.

Theorem 5. *Let \mathcal{R}_0 be defined by (3.27). Assume that*

$$\mathcal{R}_0 < \frac{2\nu^3}{C_1^6 \mathcal{P}_4^4}.$$

Then, there exists a solution to problem \tilde{W}_B satisfying (3.28).

Proof. The problem \tilde{W}_B is restricted to Y_m defined in the proof of Theorem (4) to obtain a finite dimensional problem:

$$(\tilde{W}_{B,m}) \left\{ \begin{array}{l} \text{Find } (\mathbf{u}_m, \varphi_m) \in Y_m \text{ s.t.} \\ \forall 1 \leq i \leq m, \quad 2\nu(\mathbf{D}(\mathbf{u}_m), \mathbf{D}(\mathbf{w}_i))_{\Omega_1} + (\mathbf{u}_m \cdot \nabla \mathbf{u}_m, \mathbf{w}_i)_{\Omega_1} \\ + (\varphi_m, \mathbf{w}_i \cdot \mathbf{n}_{12})_{\Gamma_{12}} + \frac{1}{G}(\mathbf{u}_m \cdot \boldsymbol{\tau}_{12}, \mathbf{w}_i \cdot \boldsymbol{\tau}_{12})_{\Gamma_{12}} - (\mathbf{u}_m \cdot \mathbf{n}_{12}, t_i)_{\Gamma_{12}} \\ + (\mathbf{K}\nabla\varphi_m, \nabla t_i)_{\Omega_2} = (\mathbf{f}_1, \mathbf{w}_i)_{\Omega_1} + (f_2, t_i)_{\Omega_2} - (\mathbf{K}\nabla p_D, \nabla t_i)_{\Omega_2} + (g_N, t_i)_{\Gamma_{2N}}. \end{array} \right.$$

As in the proof of Theorem (4) the finite dimensional problem yields a continuous mapping $\Psi_{B,m} : Y_m \rightarrow Y_m$:

$$\begin{aligned} (\Psi_{B,m}(v, q), (\mathbf{w}, t))_Y &= 2\nu(\mathbf{D}(v), \mathbf{D}(\mathbf{w}))_{\Omega_1} + (v \cdot \nabla v, \mathbf{w})_{\Omega_1} + (q, \mathbf{w} \cdot \mathbf{n}_{12})_{\Gamma_{12}} \\ &+ \frac{1}{G}(v \cdot \boldsymbol{\tau}_{12}, \mathbf{w} \cdot \boldsymbol{\tau}_{12})_{\Gamma_{12}} - (v \cdot \mathbf{n}_{12}, t)_{\Gamma_{12}} + (\mathbf{K}\nabla q, \nabla t)_{\Omega_2} - (\mathbf{f}_1, \mathbf{w})_{\Omega_1} \\ &- (f_2, t)_{\Omega_2} + (\mathbf{K}\nabla p_D, \nabla t)_{\Omega_2} - (g_N, t)_{\Gamma_{2N}}. \end{aligned}$$

First we bound the term $(\mathbf{v} \cdot \nabla \mathbf{v}, \mathbf{v})_{\Omega_1}$:

$$\begin{aligned} (\mathbf{v} \cdot \nabla \mathbf{v}, \mathbf{v})_{\Omega_1} &\leq \|\mathbf{v}\|_{L^4(\Omega_1)}^2 \|\nabla \mathbf{v}\|_{L^2(\Omega_1)} \\ &\leq C_1^3 \mathcal{P}_4^2 \|\mathbf{D}(\mathbf{v})\|_{L^2(\Omega_1)}^3 \end{aligned}$$

Bounding the rest of the terms in $(\Psi_{B,m}(\mathbf{v}, q), (\mathbf{w}, t))_Y$ as in Theorem (4) we note that

$$(\Psi_{B,m}(\mathbf{v}, q), (\mathbf{w}, t))_Y \geq \frac{1}{4} (\|\mathbf{v}, q\|_Y^2 - \mathcal{R}_0^2)$$

provided:

$$2\nu \|\mathbf{D}(\mathbf{v})\|_{L^2(\Omega_1)}^2 \leq \frac{2\nu^3}{C_1^6 \mathcal{P}_4^4}.$$

Therefore, if the condition

$$\mathcal{R}_0^2 < \frac{2\nu^3}{C_1^6 \mathcal{P}_4^4}, \quad (3.31)$$

holds there is a ball of radius \mathcal{R}_0 on which $(\Psi_{B,m}(\mathbf{v}, q), (\mathbf{w}, t))_Y \geq 0$. Thus we obtain a solution $(\mathbf{u}_m, \varphi_m)$ of the problem $(W_{B,m})$ that lies inside a ball of radius \mathcal{R}_0 , we obtain a solution to the problem (W_B) by passing to the limit. This solution also satisfies (3.28). \square

Having shown existence of weak solutions for problems W_A and W_B , the next step is to prove uniqueness of the solutions.

3.4 Uniqueness of weak solution

Theorem 6. *Assuming that the data satisfies:*

$$\begin{aligned} \frac{16\nu^3}{C_1^6 (\mathcal{P}_4^2 + \frac{3}{2} C_4^2 C_2)^2} &> \frac{2\mathcal{P}_1^2 C_1^2}{\nu} \|\mathbf{f}_1\|_{L^2(\Omega_1)}^2 + \frac{4\mathcal{P}_2^2}{\lambda_{\min}} \|f_2\|_{L^2(\Omega_2)}^2 \\ &+ 4C_0^2 \lambda_{\max} \|g_D\|_{H^{1/2}(\Gamma_{2D})}^2 + \frac{4C_3^2}{\lambda_{\min}} \|g_N\|_{L^2(\Gamma_{2N})}^2. \end{aligned}$$

Then problem (\tilde{W}_A) has a unique weak solution.

Proof. Assume that (\mathbf{u}_1^1, p_2^1) and (\mathbf{u}_1^2, p_2^2) are two solutions of problem (\tilde{W}_A) . Their difference, say (\mathbf{w}_1, z_2) , belongs to the space $\mathbf{V}_1 \times M_2$ and satisfies:

$$\begin{aligned} \forall (\mathbf{v}_1, q_2) \in \mathbf{V}_1 \times M_2, \quad & 2\nu(\mathbf{D}(\mathbf{w}_1), \mathbf{D}(\mathbf{v}_1))_{\Omega_1} + (\mathbf{K}\nabla z_2, \nabla q_2)_{\Omega_2} + (\mathbf{w}_1 \cdot \nabla \mathbf{u}_1^1, \mathbf{v}_1)_{\Omega_1} \\ & + (\mathbf{u}_1^2 \cdot \nabla \mathbf{w}_1, \mathbf{v}_1)_{\Omega_1} + \frac{1}{G}(\mathbf{w}_1 \cdot \boldsymbol{\tau}_{12}, \mathbf{v}_1 \cdot \boldsymbol{\tau}_{12})_{\Gamma_{12}} + (z_2 - \frac{1}{2}(\mathbf{w}_1 \cdot \mathbf{u}_1^1), \mathbf{v}_1 \cdot \mathbf{n}_{12})_{\Gamma_{12}} \\ & - (\mathbf{w}_1 \cdot \mathbf{n}_{12}, q_2)_{\Gamma_{12}} - \frac{1}{2}(\mathbf{u}_1^2 \cdot \mathbf{w}_1, \mathbf{v}_1 \cdot \mathbf{n}_{12})_{\Gamma_{12}} = 0. \end{aligned}$$

By choosing $(\mathbf{v}_1, q_2) = (\mathbf{w}_1, z_2) \in \mathbf{V}_1 \times M_2$ and applying Green's formula and the boundary condition on the functions of \mathbf{X}_1 , this equation becomes

$$\begin{aligned} 2\nu\|\mathbf{D}(\mathbf{w}_1)\|_{L^2(\Omega_1)}^2 + \|\mathbf{K}^{1/2}\nabla z_2\|_{L^2(\Omega_2)}^2 + \frac{1}{G}\|\mathbf{w}_1 \cdot \boldsymbol{\tau}_{12}\|_{L^2(\Gamma_{12})}^2 + (\mathbf{w}_1 \cdot \nabla \mathbf{u}_1^1, \mathbf{w}_1)_{\Omega_1} \\ + \frac{1}{2}\left((\mathbf{w}_1 \cdot \mathbf{w}_1, \mathbf{u}_1^2 \cdot \mathbf{n}_{12})_{\Gamma_{12}} - (\mathbf{w}_1 \cdot (\mathbf{u}_1^1 + \mathbf{u}_1^2), \mathbf{w}_1 \cdot \mathbf{n}_{12})_{\Gamma_{12}}\right) = 0. \end{aligned} \quad (3.32)$$

Applying (3.8) and (3.9), the first non-linear term in the second line of (3.32) is bounded above by

$$\|\mathbf{w}_1\|_{L^4(\Omega_1)}^2 \|\nabla \mathbf{u}_1^1\|_{L^2(\Omega_1)} \leq C_1^3 \mathcal{P}_4^2 \frac{1}{\sqrt{\nu}} \|\mathbf{D}(\mathbf{w}_1)\|_{L^2(\Omega_1)}^2 (\sqrt{\nu} \|\mathbf{D}(\mathbf{u}_1^1)\|_{L^2(\Omega_1)}).$$

Similarly, applying formulas (3.8)–(3.10), the second term in the second line of (3.32) is bounded above by

$$\begin{aligned} \frac{1}{2}\|\mathbf{w}_1\|_{L^4(\Gamma_{12})}^2 (\|\mathbf{u}_1^1\|_{L^2(\Gamma_{12})} + 2\|\mathbf{u}_1^2\|_{L^2(\Gamma_{12})}) \\ \leq \frac{1}{2}C_4^2 C_2 C_1^3 \frac{1}{\sqrt{\nu}} \|\mathbf{D}(\mathbf{w}_1)\|_{L^2(\Omega_1)}^2 (\sqrt{\nu} \|\mathbf{D}(\mathbf{u}_1^1)\|_{L^2(\Omega_1)} + 2\sqrt{\nu} \|\mathbf{D}(\mathbf{u}_1^2)\|_{L^2(\Omega_1)}). \end{aligned}$$

Hence, using the a priori estimate (3.29), the second line in (3.32) is bounded above by

$$\frac{C_1^3}{\sqrt{2\nu}} \left(\mathcal{P}_4^2 + \frac{3}{2}C_4^2 C_2 \right) \mathcal{R}_1 \|\mathbf{D}(\mathbf{w}_1)\|_{L^2(\Omega_1)}^2.$$

Thus if

$$(2\nu)^{3/2} > C_1^3 \left(\mathcal{P}_4^2 + \frac{3}{2}C_4^2 C_2 \right) \mathcal{R}_1,$$

then $(\mathbf{w}_1, z_2) = (\mathbf{0}, 0)$, which proves the uniqueness of the solution. \square

Theorem 7. *The solution to problem (W_B) cannot be shown to be bounded, therefore we can only prove uniqueness of the solution inside a certain ball. Assuming that the data satisfies the condition:*

$$\frac{2\nu^3}{C_1^6 \mathcal{P}_4^4} > \frac{2\mathcal{P}_1^2 C_1^2}{\nu} \|\mathbf{f}_1\|_{L^2(\Omega_1)}^2 + \frac{4\mathcal{P}_2^2}{\lambda_{min}} \|f_2\|_{L^2(\Omega_2)}^2 + 4C_0^2 \lambda_{max} \|g_D\|_{H^{1/2}(\Gamma_{2D})}^2 + \frac{4C_3^2}{\lambda_{min}} \|g_N\|_{L^2(\Gamma_{2N})}^2 \quad (3.33)$$

then the problem \tilde{W}_B has at most one weak solution satisfying:

$$\|\mathbf{D}(\mathbf{u})\|_{L^2(\Omega_1)} \leq \frac{\mathcal{R}_0}{\sqrt{2\nu}}$$

Proof. The proof of uniqueness of a solution for W_B is similar to Theorem (6).

□

Conclusion

The weak formulations for the coupled Navier-Stokes/Darcy models with or without inertial forces have been presented. We have also shown existence and uniqueness results for the weak solution for the coupled problem when the balance of forces is written with or without the inertial forces. The next step is to show existence and uniqueness of a numerical solution to the model.

Chapter 4

Numerical Analysis

Introduction

This chapter introduces the discrete spaces that will be used to approximate the Navier-Stokes velocity and pressure and the Darcy pressure. Existence and Uniqueness proofs for the numerical schemes for the problems W_A and W_B as well as a priori error estimates will be presented. Let \mathcal{E}_1^h be a conforming triangulation of the free flow domain Ω_1 and let \mathcal{E}_2^h be a general subdivision of the porous medium domain Ω_2 . The parameter h denotes the maximum diameter of the elements. In the case when the discontinuous Galerkin method is used to approximate the solution in the porous medium, \mathcal{E}_2^h may contain some hanging nodes. The mesh $\mathcal{E}^h = \mathcal{E}_1^h \cup \mathcal{E}_2^h$ is assumed to be regular [11]. The free fluid and porous medium domains are separated by an interface Γ_{12} a polygonal line with nodes in the mesh \mathcal{E}^h .

4.1 Discrete Spaces for Navier-Stokes Equations

The Navier-Stokes velocity and pressure is approximated by conforming finite element spaces $\mathbf{X}_1^h \subset \mathbf{X}_1$ and $M_1^h \subset M_1$ respectively that satisfy the discrete inf-sup condition with condition β_* independent of h :

$$\inf_{q \in M_1^h} \sup_{\mathbf{v}_1 \in \mathbf{X}_1^h} \frac{|(\nabla \cdot \mathbf{v}_1, q_1)_{\Omega_1}|}{\|\nabla \mathbf{v}_1\|_{L^2(\Omega_1)} \|q_1\|_{L^2(\Omega_1)}} \geq \beta_* > 0 \quad (4.1)$$

Examples of spaces include the Taylor-Hood element of order 2 in which the velocity is approximated by continuous piecewise quadratics and the pressure by continuous

piecewise linears [12]. In this work the MINI finite element space [2] of order $k = 1$ element space has been implemented to approximate the Navier-Stokes velocity and pressure. The Navier-Stokes velocity is approximated by piecewise linear elements enhanced by bubble functions and the pressure is approximated by piecewise linear functions [2]. More examples of finite element spaces for the Navier-Stokes equations can be found in [32, 41].

4.2 Discrete Space for Darcy Problem

The solution for the Darcy problem is obtained by approximating p_2 , the Darcy pressure and numerically differentiating the result to obtain the Darcy velocity. The discontinuous Galerkin method is used to approximate the Darcy pressure. Recall the broken Sobolev space for any real number s :

$$H^s(\mathcal{E}_2^h) = \{p_2 \in L^2(\Omega) : \forall E \in \mathcal{E}_2^h, p_2|_E \in H^s(E)\}$$

endowed with broken Sobolev norm:

$$\|p_2\|_{H^s(\mathcal{E}_2^h)} = \left(\sum_{E \in \mathcal{E}_2^h} \|p_2\|_{H^s(E)}^2 \right)^{1/2}.$$

The function space $\mathbb{P}_{k_2}(E)$ is the space of polynomials of degree less than or equal to k_2 which can be discontinuous across the edges of the mesh. For the discontinuous Galerkin method, the interior edges of \mathcal{E}_2^h are denoted by Γ_2^h . Each edge is associated with a unit normal vector \mathbf{n}_e . If the function $q_2 \in H^1(\mathcal{E}_2^h)$, the trace on each element is well defined. In the case of interior edges with neighbors E_1^e and E_2^e , there are two traces of q_2 along e . For a given \mathbf{n}_e pointing from E_1^e to E_2^e the average and jump for p_2 :

$$\{q_2\} = \frac{1}{2}(q_2|_{E_1^e}) + \frac{1}{2}(q_2|_{E_2^e}), \quad [q_2] = (q_2|_{E_1^e}) - (q_2|_{E_2^e}) \quad \forall e = \partial E_1^e \cap \partial E_2^e.$$

For an integer $k_2 \geq 1$, the finite element space for the Darcy pressure is

$$M_2^h = \{q_2 \in L^2(\Omega_2); q_2|_{\Gamma_{2D}} = 0 \quad \text{and} \quad \forall E \in \mathcal{E}_2^h, \quad q_2|_E \in \mathbb{P}_{k_2}(E)\},$$

equipped with the usual DG norm:

$$\forall q_2 \in M_2^h, \quad |||q_2||| = \left(\sum_{E \in \mathcal{E}_2^h} \|\mathbf{K}^{1/2} \nabla q_2\|_{L^2(E)}^2 + \sum_{e \in \Gamma_h^2} \frac{1}{|e|} \|[q_2]\|_{L^2(e)}^2 \right)^{1/2}. \quad (4.2)$$

The following Lemma is necessary to handle the non-homogeneous Dirichlet boundary conditions on the porous medium domain.

Lemma 8. *Assume that $p_D \in H^{k_2+1}(\Omega_2)$ is the lift defined in (3.14)-(3.16). Then, there exists $P_D \in M_2^h$ and a constant C independent of h satisfying:*

$$P_D = 0, \quad \text{on} \quad \Gamma_{12}, \quad (4.3)$$

$$|||p_D - P_D||| \leq Ch^{k_2} \|p_D\|_{H^{k_2+1}(\Omega_2)}. \quad (4.4)$$

4.3 Numerical Scheme

In the rest of the chapter, C a generic constant independent of h and ν , that takes different values at different places. Discretizations of the viscous term, pressure term and nonlinear term in the Navier-Stokes equations will be denoted by: $a_{\text{NS}}, b_{\text{NS}}, c_{\text{NS}}$ respectively; a_D is the discretization of the diffusion term in the Darcy equations; and

γ_α , $\alpha = A, B$ is the form containing terms related to the interface Γ_{12} .

$$\begin{aligned}
& \forall \mathbf{v}_1, \mathbf{w}_1 \in \mathbf{X}_1^h, \quad a_{\text{NS}}(\mathbf{v}_1, \mathbf{w}_1) = 2\nu(\mathbf{D}(\mathbf{v}_1), \mathbf{D}(\mathbf{w}_1))_{\Omega_1}, \\
& \forall \mathbf{v}_1 \in \mathbf{X}_1^h, \forall q_1 \in M_1^h, \quad b_{\text{NS}}(\mathbf{v}_1, q_1) = -(q_1, \nabla \cdot \mathbf{v}_1)_{\Omega_1}, \\
& \forall \mathbf{z}_1, \mathbf{v}_1, \mathbf{w}_1 \in \mathbf{X}_1^h, \quad c_{\text{NS}}(\mathbf{z}_1, \mathbf{v}_1, \mathbf{w}_1) = \frac{1}{2}(\mathbf{z}_1 \cdot \nabla \mathbf{v}_1, \mathbf{w}_1)_{\Omega_1} - \frac{1}{2}(\mathbf{z}_1 \cdot \nabla \mathbf{w}_1, \mathbf{v}_1)_{\Omega_1} \\
& \quad \quad \quad + \frac{1}{2}(\mathbf{z}_1 \cdot \mathbf{n}_{12}, \mathbf{v}_1 \cdot \mathbf{w}_1)_{\Gamma_{12}}, \\
& \forall q_2, t_2 \in M_2^h, \quad a_{\text{D}}(q_2, t_2) = \sum_{E \in \mathcal{E}_2^h} (\mathbf{K} \nabla q_2, \nabla t_2)_E - \sum_{e \in \Gamma_2^h} (\{\mathbf{K} \nabla q_2 \cdot \mathbf{n}_e\} [t_2])_e \\
& \quad \quad \quad + \epsilon \sum_{e \in \Gamma_h^2} (\{\mathbf{K} \nabla t_2 \cdot \mathbf{n}_e\}, [q_2])_e + \sum_{e \in \Gamma_h^2} \frac{\sigma_e}{|e|} ([q_2], [t_2])_e, \\
& \forall \mathbf{v}_1, \mathbf{w}_1 \in \mathbf{X}_1^h, \quad \forall q_2, t_2 \in M_2^h, \quad \gamma_B(\mathbf{v}_1, q_2; \mathbf{w}_1, t_2) = (q_2, \mathbf{w}_1 \cdot \mathbf{n}_{12})_{\Gamma_{12}} + \frac{1}{G} (\mathbf{v}_1 \cdot \boldsymbol{\tau}_{12}, \mathbf{w}_1 \cdot \boldsymbol{\tau}_{12})_{\Gamma_{12}} \\
& \quad \quad \quad - (\mathbf{v}_1 \cdot \mathbf{n}_{12}, t_2)_{\Gamma_{12}}, \\
& \forall \mathbf{v}_1, \mathbf{w}_1 \in \mathbf{X}_1^h, \quad \forall q_2, t_2 \in M_2^h, \quad \gamma_A(\mathbf{v}_1, q_2; \mathbf{w}_1, t_2) = \gamma_B(\mathbf{v}_1, q_2; \mathbf{w}_1, t_2) - \frac{1}{2} (\mathbf{v}_1 \cdot \mathbf{v}_1, \mathbf{w}_1 \cdot \mathbf{n}_{12})_{\Gamma_{12}}.
\end{aligned}$$

In the definition of a_{D} the parameter ϵ yields a symmetric bilinear form if $\epsilon = -1$ and a non-symmetric bilinear form if $\epsilon = 0$ or $\epsilon = 1$. The parameter σ_e is a penalty parameter that varies with respect to the edge in \mathcal{E}_2^h . The bilinear form a_{D} is coercive and corresponds to the Nonsymmetric interior penalty Galerkin method (NIPG) ($\epsilon = 1$), symmetric interior penalty Galerkin method (SIPG) ($\epsilon = -1$) or the incomplete interior penalty Galerkin method (IIPG) ($\epsilon = 0$) methods [52, 25, 13]. There exists a constant $\kappa > 0$ independent of h such that:

$$\forall q_2 \in M_2^h, \quad \kappa \| \|q_2\| \|^2 \leq a_{\text{D}}(q_2, q_2). \quad (4.5)$$

It has been shown that if $\epsilon \in \{-1, 0\}$, property (4.5) is valid if the penalty parameter is large enough [46]. From [16], the lower bound for the penalty parameter is:

$$\forall e = \partial E_e^1 \cap \partial E_e^2, \quad \sigma_e \geq \frac{3\lambda_{\max}^2}{2\lambda_{\min}} k_2 (k_2 + 1) (\cot \theta_{E_e^1} + \cot \theta_{E_e^2}),$$

where $\theta_{E_e^i}$ denotes the smallest angle in the triangle E_e^i . We also define the form L :

$$\begin{aligned} \forall \mathbf{v}_1 \in \mathbf{X}_1^h, \quad \forall q_2 \in M_2^h, \quad L(\mathbf{v}_1, q_2) = & (\mathbf{f}_1, \mathbf{v}_1)_{\Omega_1} + (f_2, q_2)_{\Omega_2} + (g_N, q_2)_{\Gamma_{2N}} \\ & - \sum_{E \in \mathcal{E}_2^h} (\mathbf{K} \nabla p_D, \nabla q_2)_E + \sum_{e \in \Gamma_2^h} (\{\mathbf{K} \nabla p_D \cdot \mathbf{n}_e\}, [q_2])_e. \end{aligned}$$

Having defined the bilinear forms the numerical schemes to problem (W_A) and problem (W_B) are:

$$(W_A^h) \left\{ \begin{array}{l} \text{Find } \mathbf{U}_1 \in \mathbf{X}_1^h, P_1 \in M_1^h, P_2 = \Phi_2 + P_D \text{ with } \Phi_2 \in M_2^h, \text{ s.t} \\ \forall \mathbf{v}_1 \in \mathbf{X}_1^h, q_2 \in M_2^h : a_{\text{NS}}(\mathbf{U}_1, \mathbf{v}_1) + b_{\text{NS}}(\mathbf{v}_1, P_1) + c_{\text{NS}}(\mathbf{U}_1; \mathbf{U}_1, \mathbf{v}_1) \\ + a_D(\Phi_2, q_2) + \gamma_A(\mathbf{U}_1, \Phi_2; \mathbf{v}_1, q_2) = L(\mathbf{v}_1, q_2), \\ \forall q_1 \in M_1^h, b_{\text{NS}}(\mathbf{U}_1, q_1) = 0. \end{array} \right.$$

$$(W_B^h) \left\{ \begin{array}{l} \text{Find } \mathbf{U}_1 \in \mathbf{X}_1^h, P_1 \in M_1^h, P_2 = \Phi_2 + P_D \text{ with } \Phi_2 \in M_2^h, \text{ s.t} \\ \forall \mathbf{v}_1 \in \mathbf{X}_1^h, q_2 \in M_2^h, q_1 \in M_1^h : a_{\text{NS}}(\mathbf{U}_1, \mathbf{v}_1) + b_{\text{NS}}(\mathbf{v}_1, P_1) + c_{\text{NS}}(\mathbf{U}_1; \mathbf{U}_1, \mathbf{v}_1) \\ + a_D(\Phi_2, q_2) + \gamma_B(\mathbf{U}_1, \Phi_2; \mathbf{v}_1, q_2) = L(\mathbf{v}_1, q_2), \\ \forall q_1 \in M_1^h, b_{\text{NS}}(\mathbf{U}_1, q_1) = 0. \end{array} \right.$$

The following are some important properties of the discrete spaces and the continuity property of the bilinear form c_{NS} .

Approximation properties. Assume that $(\mathbf{v}_1, p_1, p_2) \in \mathbf{X}_1 \times M_1 \times M_2$ is smooth enough, i.e. $\mathbf{v}_1 \in H^{k_1+1}(\Omega_1)$, $p_1 \in H^{k_1}(\Omega_1)$ and $p_2 \in H^{k_2+1}(\Omega_2)$ for integers k_1, k_2 . Then, there exists an approximation $(\tilde{\mathbf{v}}_1, \tilde{p}_1, \tilde{p}_2) \in \mathbf{X}_1^h \times M_1^h \times M_2^h$ such that

$$\|\nabla(\mathbf{v}_1 - \tilde{\mathbf{v}}_1)\|_{L^2(\Omega_1)} \leq Ch^{k_1} \|\mathbf{v}_1\|_{H^{k_1+1}(\Omega_1)}, \quad (4.6)$$

$$\forall q_1 \in M_1^h, \quad (\nabla \cdot (\mathbf{v}_1 - \tilde{\mathbf{v}}_1), q_1)_{\Omega_1} = 0, \quad (4.7)$$

$$\|p_1 - \tilde{p}_1\|_{L^2(\Omega_1)} \leq Ch^{k_1} \|p_1\|_{H^{k_1}(\Omega_1)}, \quad (4.8)$$

$$i = 0, 1, \quad \sum_{E \in \Omega_2} \|\nabla^i(p_2 - \tilde{p}_2)\|_{L^2(E)} \leq Ch^{k_2+1-i} \|p_2\|_{H^{k_2+1}(\Omega_2)}. \quad (4.9)$$

Approximation (4.9) implies

$$\|p_2 - \tilde{p}_2\| \leq Ch^{k_2} \|p_2\|_{H^{k_2+1}(\Omega_2)}. \quad (4.10)$$

L^2 bound. There exists a constant $C_5 > 0$ independent of h such that

$$\forall q_2 \in M_2^h, \quad \|q_2\|_{L^2(\Omega_2)} \leq C_5 \|q_2\|. \quad (4.11)$$

Trace theorem. There exists a constant $C_6 > 0$ independent of h such that

$$\forall q_2 \in M_2^h, \quad \|q_2\|_{L^2(\Gamma_{12})} \leq C_6 \|q_2\|. \quad (4.12)$$

The proof of (4.11) is given in Lemma 6.2 of [25] and the proof of (4.12) is given in Theorem 4.4 of [24]. We next show that the form c_{NS} is continuous.

Lemma 9. *The bilinear form c_{NS} is continuous. There exists a constant C_7 such that*

$$\forall \mathbf{z}_1, \mathbf{v}_1, \mathbf{w}_1 \in \mathbf{X}_1, \quad c_{NS}(\mathbf{z}_1; \mathbf{v}_1, \mathbf{w}_1) \leq C_7 \|\mathbf{D}(\mathbf{z}_1)\|_{L^2(\Omega_1)} \|\mathbf{D}(\mathbf{v}_1)\|_{L^2(\Omega_1)} \|\mathbf{D}(\mathbf{w}_1)\|_{L^2(\Omega_1)}. \quad (4.13)$$

An expression for the constant C_7 is

$$C_7 = C_1^3 (\mathcal{P}_4^2 + \frac{1}{2} C_2 C_4^2).$$

Proof. Using (3.5), we have

$$\begin{aligned} c_{NS}(\mathbf{z}_1; \mathbf{v}_1, \mathbf{w}_1) &= \frac{1}{2} (\mathbf{z}_1 \cdot \nabla \mathbf{v}_1, \mathbf{w}_1)_{\Omega_1} - \frac{1}{2} (\mathbf{z}_1 \cdot \nabla \mathbf{w}_1, \mathbf{v}_1)_{\Omega_1} + \frac{1}{2} (\mathbf{z}_1 \cdot \mathbf{n}_{12}, \mathbf{v}_1 \cdot \mathbf{w}_1)_{\Gamma_{12}} \\ &\leq \frac{1}{2} \|\mathbf{z}_1\|_{L^4(\Omega_1)} (\|\nabla \mathbf{v}_1\|_{L^2(\Omega_1)} \|\mathbf{w}_1\|_{L^4(\Omega_1)} + \|\nabla \mathbf{w}_1\|_{L^2(\Omega_1)} \|\mathbf{v}_1\|_{L^4(\Omega_1)}) \\ &\quad + \frac{1}{2} \|\mathbf{z}_1\|_{L^2(\Gamma_{12})} \|\mathbf{v}_1\|_{L^4(\Gamma_{12})} \|\mathbf{w}_1\|_{L^4(\Gamma_{12})}. \end{aligned}$$

Using (3.8), (3.10) and (3.9) we have

$$\begin{aligned} c_{NS}(\mathbf{z}_1; \mathbf{v}_1, \mathbf{w}_1) &\leq (\mathcal{P}_4^2 + \frac{1}{2} C_2 C_4^2) \|\nabla \mathbf{z}_1\|_{L^2(\Omega_1)} \|\nabla \mathbf{v}_1\|_{L^2(\Omega_1)} \|\nabla \mathbf{w}_1\|_{L^2(\Omega_1)} \\ &\leq C_1^3 (\mathcal{P}_4^2 + \frac{1}{2} C_2 C_4^2) \|\mathbf{D}(\mathbf{z}_1)\|_{L^2(\Omega_1)} \|\mathbf{D}(\mathbf{v}_1)\|_{L^2(\Omega_1)} \|\mathbf{D}(\mathbf{w}_1)\|_{L^2(\Omega_1)}. \end{aligned}$$

□

The next task is to show the equivalence between the weak problem and the equations of the coupled Navier-Stokes and Darcy problem.

4.4 Consistency

Lemma 10. *Let (\mathbf{u}_1, p_1, p_2) be the solution to the coupled Navier-Stokes and Darcy equations without inertial forces on the balance of forces on the interface (2.1)-(2.11) that is smooth enough. Define $\varphi_2 = p_2 - p_D$ where p_D satisfied (8). Then, we have for all $v_1 \in \mathbf{X}_1^h, q_2 \in \mathbf{M}_2^h, q_1 \in \mathbf{M}_1^h$:*

$$a_{\text{NS}}(\mathbf{u}_1, \mathbf{v}_1) + b_{\text{NS}}(\mathbf{v}_1, p_1) + c_{\text{NS}}(\mathbf{u}_1; \mathbf{u}_1, \mathbf{v}_1) + a_{\text{D}}(\varphi_2, q_2) \quad (4.14)$$

$$+\gamma_A(\mathbf{u}_1, \varphi_2; \mathbf{v}_1, q_2) = L(\mathbf{v}_1, q_2), \quad (4.15)$$

$$b_{\text{NS}}(\mathbf{u}_1, q_1) = 0. \quad (4.16)$$

Proof. Equation (4.16) is obtained by multiplying (2.2) by $q_1 \in M_1^h$ and integrating over Ω_1 . Next, we multiply (2.1) by a test function $\mathbf{v}_1 \in \mathbf{X}_1^h$, integrate over Ω_1 and use Green's theorem. The resulting equation is:

$$\begin{aligned} & 2\nu(\mathbf{D}(\mathbf{u}_1), \mathbf{D}(\mathbf{v}_1))_{\Omega_1} - (p_1, \nabla \cdot \mathbf{v}_1)_{\Omega_1} + (\mathbf{u}_1 \cdot \nabla \mathbf{u}_1, \mathbf{v}_1)_{\Omega_1} \\ & + ((-2\nu \mathbf{D}(\mathbf{u}_1) + p_1 \mathbf{I}) \mathbf{n}_{12}, \mathbf{v}_1)_{\Gamma_{12}} = (\mathbf{f}_1, \mathbf{v}_1)_{\Omega_1}, \end{aligned} \quad (4.17)$$

Finally, we multiply (2.5) by a test function $q_2 \in M_2^h$, integrate over one element E , apply Green's theorem and sum over all elements in \mathcal{E}_2^h .

$$\begin{aligned} & \sum_{E \in \mathcal{E}_2^h} (\mathbf{K} \nabla p_2, \nabla q_2)_E - \sum_{e \in \Gamma_2^h} (\{\mathbf{K} \nabla p_2 \cdot \mathbf{n}_e\}, [q_2])_e + \sum_{e \in \Gamma_{12}} (\mathbf{K} \nabla p_2 \cdot \mathbf{n}_{12}, q_2)_{\Gamma_{12}} \\ & = (f_2, q_2)_{\Omega_2} + (g_N, q_2)_{\Gamma_{12}}. \end{aligned}$$

Using the splitting $p_2 = \varphi_2 + p_D$, we obtain:

$$\begin{aligned} & \sum_{E \in \mathcal{E}_2^h} (\mathbf{K} \nabla \varphi_2, \nabla q_2)_E - \sum_{e \in \Gamma_2^h} (\{\mathbf{K} \nabla \varphi_2 \cdot \mathbf{n}_e\}, [q_2])_e + \sum_{e \in \Gamma_{12}} (\mathbf{K} \nabla p_2 \cdot \mathbf{n}_{12}, q_2)_{\Gamma_{12}} \\ & = (f_2, q_2)_{\Omega_2} + (g_N, q_2)_{\Gamma_{12}} - \sum_{E \in \mathcal{E}_2^h} (\mathbf{K} \nabla p_D, \nabla q_2)_E + \sum_{e \in \Gamma_2^h} (\{\mathbf{K} \nabla p_D \cdot \mathbf{n}_e\}, [q_2])_e. \end{aligned} \quad (4.18)$$

We then add (4.17) and (4.18), and use the fact that $[\varphi_2]|_e = 0$ in $L^2(e)$ for all $e \in \Gamma_2^h$.

$$\begin{aligned}
& 2\nu(\mathbf{D}(\mathbf{u}_1), \mathbf{D}(\mathbf{v}_1))_{\Omega_1} - (p_1, \nabla \cdot \mathbf{v}_1)_{\Omega_1} + (\mathbf{u}_1 \cdot \nabla \mathbf{u}_1, \mathbf{v}_1)_{\Omega_1} \\
& + \sum_{E \in \mathcal{E}_2^h} (\mathbf{K} \nabla \varphi_2, \nabla q_2)_E - \sum_{e \in \Gamma_2^h} (\{\mathbf{K} \nabla \varphi_2 \cdot \mathbf{n}_e\}, [q_2])_e + \epsilon \sum_{e \in \Gamma_2^h} (\{\mathbf{K} \nabla q_2 \cdot \mathbf{n}_e\}, [\varphi_2])_e \\
& + \sum_{e \in \Gamma_{12}} (\mathbf{K} \nabla p_2 \cdot \mathbf{n}_{12}, q_2)_{\Gamma_{12}} + ((-2\nu \mathbf{D}(\mathbf{u}_1) + p_1 \mathbf{I}) \mathbf{n}_{12}, \mathbf{v}_1)_{\Gamma_{12}} \\
& = (\mathbf{f}_1, \mathbf{v}_1)_{\Omega_1} + (f_2, q_2)_{\Omega_2} + (g_N, q_2)_{\Gamma_{12}} - \sum_{E \in \mathcal{E}_2^h} (\mathbf{K} \nabla p_D, \nabla q_2)_E + \sum_{e \in \Gamma_2^h} (\{\mathbf{K} \nabla p_D \cdot \mathbf{n}_e\}, [q_2])_e.
\end{aligned} \tag{4.19}$$

In (4.19), the terms $\sum_{e \in \Gamma_{12}} (\mathbf{K} \nabla p_2 \cdot \mathbf{n}_{12}, q_2)_{\Gamma_{12}} + ((-2\nu \mathbf{D}(\mathbf{u}_1) + p_1 \mathbf{I}) \mathbf{n}_{12}, \mathbf{v}_1)_{\Gamma_{12}}$ are handled by choosing test functions $\mathbf{v}_1|_{\Gamma_{12}} = 0$ and $q_2|_{\Gamma_{12}} = 0$. The solution $\mathbf{u}_1 \in \mathbf{V}_1$, thus we have

$$(\mathbf{u}_1 \cdot \nabla \mathbf{u}_1, \mathbf{v}_1)_{\Omega_1} = -(\mathbf{u}_1 \cdot \nabla \mathbf{v}_1, \mathbf{u}_1)_{\Omega_1} + (\mathbf{u}_1 \cdot \mathbf{n}_{12}, \mathbf{v}_1 \cdot \mathbf{u}_1)_{\Gamma_{12}},$$

which yields easily:

$$(\mathbf{u}_1 \cdot \nabla \mathbf{u}_1, \mathbf{v}_1)_{\Omega_1} = c_{\text{NS}}(\mathbf{u}_1, \mathbf{u}_1, \mathbf{v}_1).$$

Combining this result with (4.19), we obtain equation (4.15). \square

Lemma (11) is proved in the same way as the only difference is the term γ_B which has less terms and they have been handled in the proof of (10).

Lemma 11. *Let (\mathbf{u}_1, p_1, p_2) be the solution to (2.1)-(2.11) that is smooth enough. Define $\varphi_2 = p_2 - p_D$. Then, we have for all $\mathbf{v}_1 \in \mathbf{X}_1^h, q_2 \in \mathbf{M}_2^h, q_1 \in \mathbf{M}_1^h$:*

$$a_{\text{NS}}(\mathbf{u}_1, \mathbf{v}_1) + b_{\text{NS}}(\mathbf{v}_1, p_1) + c_{\text{NS}}(\mathbf{u}_1; \mathbf{u}_1, \mathbf{v}_1) + a_D(\varphi_2, q_2) + \gamma_B(\mathbf{u}_1, \varphi_2; \mathbf{v}_1, q_2) = L(\mathbf{v}_1, q_2), \tag{4.20}$$

$$b_{\text{NS}}(\mathbf{u}_1, q_1) = 0. \tag{4.21}$$

The next step is to prove existence of a numerical solution for problems (W_A^h) and (W_B^h) .

4.5 Existence of Numerical Solution

Theorem 12. *Let \mathcal{R}_2 be defined by*

$$\begin{aligned} \mathcal{R}_2 = & (\max(\frac{3}{4}, \frac{\kappa}{2}))^{1/2} \left(\frac{\mathcal{P}_1^2 C_1^2}{2\nu} \|\mathbf{f}_1\|_{L^2(\Omega_1)}^2 + \frac{2C_5^2}{\kappa} \|f_2\|_{L^2(\Omega_2)}^2 + \frac{2C_6^2}{\kappa} \|g_N\|_{L^2(\Gamma_{2N})}^2 \right. \\ & \left. + \frac{2\lambda_{\max}}{\kappa} \|p_D\|_{H^1(\Omega_1)}^2 + \frac{2C_t^2}{\kappa} \sum_{E \in \mathcal{E}_2^h} \|p_D\|_{H^2(E)}^2 \right)^{1/2}. \end{aligned} \quad (4.22)$$

There exists an unique solution (\mathbf{U}_1, P_1, P_2) of (W_A^h) satisfying

$$2\nu \|\mathbf{D}(\mathbf{U}_1)\|_{L^2(\Omega_1)}^2 + \|P_2\|^2 \leq \mathcal{R}_2^2. \quad (4.23)$$

If the data satisfies

$$\mathcal{R}_2^2 < \frac{32\nu^3}{C_1^6 C_2^2 C_4^4},$$

then there exists a solution (\mathbf{U}_1, P_1, P_2) of (W_B^h) satisfying (7.19).

Proof. To prove existence of a unique solution to problem (W_A^h) , first the velocity test functions are restricted to the space of weakly divergence-free functions:

$$\mathbf{V}_1^h = \{\mathbf{v}_1 \in \mathbf{X}_1^h : \forall q_1 \in M_1^h, \quad b_{NS}(\mathbf{v}_1, q_1) = 0\}.$$

The solution $\mathbf{U}_1 \in \mathbf{V}_1^h$ so that the scheme reduces to:

$$\begin{aligned} \forall \mathbf{v}_1 \in \mathbf{X}_1^h, \forall q_2 \in M_2^h, \quad a_{NS}(\mathbf{U}_1, \mathbf{v}_1) + b_{NS}(\mathbf{v}_1, P_1) + c_{NS}(\mathbf{U}_1; \mathbf{U}_1, \mathbf{v}_1) \\ + a_D(P_2, q_2) + \gamma_A(\mathbf{U}_1, P_2; \mathbf{v}_1, q_2) = L(\mathbf{v}_1, q_2). \end{aligned} \quad (4.24)$$

If (\mathbf{U}_1, P_1, P_2) is a solution to (5.1)-(5.2), then (\mathbf{U}_1, P_2) is a solution to (4.24). Conversely, assume that (\mathbf{U}_1, P_2) is a solution to (4.24). Then, the discrete inf-sup (4.1) implies that there exists a unique $P_1 \in M_1^h$ such that (\mathbf{U}_1, P_1, P_2) is a solution to (5.1)-(5.2). Based on this equivalence between the two problems, it suffices to show that there exists a solution $(\mathbf{U}_1, P_2) \in \mathbf{V}_1^h \times M_2^h$ of (4.24). As in the proof of the

existence of a weak solution an inner product is defined on $Y^h = \mathbf{V}_1^h \times M_2^h$:

$$((\mathbf{v}_1, q_2), (\mathbf{w}_1, t_2))_{Y^h} = 2\nu(\mathbf{D}(\mathbf{v}_1), \mathbf{D}(\mathbf{w}_1))_{\Omega_1} + \sum_{E \in \mathcal{E}_h^2} (\mathbf{K} \nabla q_2, \nabla t_2)_E + \sum_{e \in \Gamma_h^2} \frac{1}{|e|} ([q_2], [t_2])_e. \quad (4.25)$$

Next define $\Psi_A^h : Y^h \rightarrow Y^h$ such that:

$$\begin{aligned} (\Psi^h(\mathbf{v}_1, q_2), (\mathbf{w}_1, t_2))_{Y^h} &= a_{\text{NS}}(\mathbf{v}_1, \mathbf{w}_1) + c_{\text{NS}}(\mathbf{v}_1; \mathbf{v}_1, \mathbf{w}_1) + a_{\text{D}}(q_2, t_2) \\ &\quad + \gamma_A(\mathbf{v}_1, q_2; \mathbf{w}_1, t_2) - L(\mathbf{w}_1, t_2). \end{aligned}$$

Using coercivity of the bilinear form a_{D} and the definitions of the bilinear forms, a lower bound of $(\Psi_A^h(\mathbf{v}_1, q_2), (\mathbf{v}_1, q_2))_{Y^h}$ is:

$$(\Psi_A^h(\mathbf{v}_1, q_2), (\mathbf{v}_1, q_2))_{Y^h} \geq 2\nu \|\mathbf{D}(\mathbf{v}_1)\|_{L^2(\Omega_1)}^2 + \kappa \|q_2\|^2 + \frac{1}{G} \|\mathbf{v}_1 \cdot \boldsymbol{\tau}_{12}\|_{L^2(\Gamma_{12})}^2 - L(\mathbf{v}_1, q_2).$$

From (3.5), (3.7) and (4.11), we have for any $\delta > 0$:

$$(f_2, q_2)_{\Omega_2} \leq \frac{\delta}{2} \|q_2\|^2 + \frac{C_5^2}{2\delta} \|f_2\|_{L^2(\Omega_2)}^2. \quad (4.26)$$

Similarly, from (3.5), (3.7) and (4.12), we have for any $\delta > 0$:

$$(g_{\text{N}}, q_2)_{\Gamma_{12}} \leq \frac{\delta}{2} \|q_2\|^2 + \frac{C_6^2}{2\delta} \|g_{\text{N}}\|_{L^2(\Gamma_{12})}^2. \quad (4.27)$$

Using a trace theorem [48], (3.5), (3.7) and (3.13), we have for any $\delta > 0$:

$$\begin{aligned} \left| - \sum_{E \in \mathcal{E}_2^h} (\mathbf{K} \nabla p_{\text{D}}, \nabla q_2)_E + \sum_{e \in \Gamma_2^h} (\{\mathbf{K} \nabla p_{\text{D}} \cdot \mathbf{n}_e\}, [q_2])_e \right| &\leq \delta \|q_2\|^2 + \frac{\lambda_{\max}}{2\delta} \|p_{\text{D}}\|_{H^1(\Omega_2)}^2 \\ &\quad + \frac{C_t^2}{2\delta} \sum_{E \in \mathcal{E}_2^h} \|p_{\text{D}}\|_{H^2(E)}^2. \end{aligned} \quad (4.28)$$

Combining the bounds (4.26), (4.27), (4.28) and (3.27), we obtain:

$$\begin{aligned} (\Psi_A^h(\mathbf{v}_1, q_2), (\mathbf{v}_1, q_2))_{Y^h} &\geq \frac{3\nu}{2} \|\mathbf{D}(\mathbf{v}_1)\|_{L^2(\Omega_1)}^2 + \frac{\kappa}{2} \|q_2\|^2 + \frac{1}{G} \|\mathbf{v}_1 \cdot \boldsymbol{\tau}_{12}\|_{L^2(\Gamma_{12})}^2 \\ &\quad - \left(\frac{P_1^2 C_1^2}{2\nu} \|\mathbf{f}_1\|_{L^2(\Omega_1)}^2 + \frac{2C_5^2}{\kappa} \|f_2\|_{L^2(\Omega_2)}^2 + \frac{2C_6^2}{\kappa} \|g_{\text{N}}\|_{L^2(\Gamma_{2\text{N}})}^2 + \frac{2\lambda_{\max}}{\kappa} \|p_{\text{D}}\|_{H^1(\Omega_1)}^2 \right. \\ &\quad \left. + \frac{2C_t^2}{\kappa} \sum_{E \in \mathcal{E}_2^h} \|p_{\text{D}}\|_{H^2(E)}^2 \right). \end{aligned}$$

Therefore, $(\Psi_A^h(\mathbf{v}_1, q_2), (\mathbf{v}_1, q_2))_{Y^h} \geq 0$ provided that $\|(\mathbf{v}_1, q_2)\|_{Y^h} = \mathcal{R}_2$ with

$$\begin{aligned} \mathcal{R}_2 = & (\max(\frac{3}{4}, \frac{\kappa}{2}))^{1/2} \left(\frac{\mathcal{P}_1^2 C_1^2}{2\nu} \|\mathbf{f}_1\|_{L^2(\Omega_1)}^2 + \frac{2C_5^2}{\kappa} \|f_2\|_{L^2(\Omega_2)}^2 + \frac{2C_6^2}{\kappa} \|g_N\|_{L^2(\Gamma_{2N})}^2 \right. \\ & \left. + \frac{2\lambda_{\max}}{\kappa} \|p_D\|_{H^1(\Omega_1)}^2 + \frac{2C_t^2}{\kappa} \sum_{E \in \mathcal{E}_2^h} \|p_D\|_{H^2(E)}^2 \right)^{1/2}. \end{aligned} \quad (4.29)$$

This concludes the proof of existence of a solution (\mathbf{U}_1, P_2) of (4.24). The solution (\mathbf{U}_1, P_2) of (4.24) is bounded as follows:

$$2\nu \|\mathbf{D}(\mathbf{U}_1)\|_{L^2(\Omega_1)}^2 + \|P_2\|^2 \leq \mathcal{R}_2^2. \quad (4.30)$$

To prove existence of a solution to (W_B^h) , the difficulty arises due to the nonlinear term $\frac{1}{2}(\mathbf{z}_1 \cdot \mathbf{n}_{12}, \mathbf{v}_1 \cdot \mathbf{w}_1)_{\Gamma_{12}}$ that remains from the c_{NS} form. As above, define $\Psi_B^h : Y^h \rightarrow Y^h$ such that:

$$\begin{aligned} (\psi_B^h(\mathbf{v}_1, q_2), (\mathbf{w}_1, t_2))_{Y^h} = & a_{NS}(\mathbf{v}_1, \mathbf{w}_1) + c_{NS}(\mathbf{v}_1; \mathbf{v}_1, \mathbf{w}_1) + a_D(q_2, t_2) \\ & + \gamma_B(\mathbf{v}_1, q_2; \mathbf{w}_1, t_2) - L(\mathbf{w}_1, t_2) \end{aligned}$$

Using the bound

$$\frac{1}{2}(\mathbf{v}_1 \cdot \mathbf{n}_{12}, \mathbf{v}_1 \cdot \mathbf{v}_1)_{\Gamma_{12}} \leq \frac{C_1^3 C_2 C_4^2}{2} \|\mathbf{D}(\mathbf{v}_1)\|_{L^2(\Omega_1)}^3$$

and 4.26, (4.27), (4.28) and (3.27), $(\psi_B^h(\mathbf{v}_1, q_2), (\mathbf{v}_1, q_2)) \geq 0$ provided that $\|(\mathbf{v}_1, q_2)\|_{Y^h} = \mathcal{R}_2$ and that

$$2\nu \|\mathbf{D}(\mathbf{v}_1)\|_{L^2(\Omega_1)}^2 \leq \frac{32\nu^3}{C_1^6 C_2^2 C_4^4}.$$

These conditions are compatible if

$$\mathcal{R}_2^2 < \frac{32\nu^3}{C_1^6 C_2^2 C_4^4}.$$

The existence of a solution follows from the corollary of Brouwer's fixed point theorem.

□

4.6 Uniqueness of Numerical Solution

Theorem 13. *Let \mathcal{R}_2 be defined by (4.29). Under the condition*

$$\nu^{3/2} > \frac{C_1^3}{\sqrt{2}}(\mathcal{P}_4^2 + C_2 C_4^2) \mathcal{R}_2 \quad (4.31)$$

problem (W_A^h) admits a unique solution.

Proof. To prove uniqueness, we assume that (U_1^1, P_2^1) and (U_1^2, P_2^2) are two solutions of problem (4.24), and let $\mathbf{W}_1 = U_1^1 - U_1^2$ and $\chi_2 = P_2^1 - P_2^2$.

$$\begin{aligned} & a_{NS}(\mathbf{W}_1, \mathbf{v}_1) + c_{NS}(U_1^1, U_1^1, \mathbf{v}_1) - c_{NS}(U_1^2, U_1^2, \mathbf{v}_1) + a_D(\chi_2, q_2) + (\chi_2, \mathbf{v}_1 \cdot \mathbf{n}_{12})_{\Gamma_{12}} \\ & - \frac{1}{2}(U_1^1 \cdot U_1^1, \mathbf{v}_1 \cdot \mathbf{n}_{12})_{\Gamma_{12}} + \frac{1}{2}(U_1^2 \cdot U_1^2, \mathbf{v}_1 \cdot \mathbf{n}_{12})_{\Gamma_{12}} + \frac{1}{G}(\mathbf{W}_1 \cdot \tau_{12}, \mathbf{v}_1 \cdot \tau_{12})_{\Gamma_{12}} \\ & - (\mathbf{W}_1 \cdot \mathbf{n}_{12}, q_2)_{\Gamma_{12}} = 0. \end{aligned}$$

In particular, we choose $\mathbf{v}_1 = \mathbf{W}_1$ and $q_2 = \chi_2$.

$$\begin{aligned} & a_{NS}(\mathbf{W}_1, \mathbf{W}_1) + a_D(\chi_2, \chi_2) + \frac{1}{G} \|\mathbf{W}_1 \cdot \tau_{12}\|_{L^2(\Gamma_{12})}^2 + c_{NS}(U_1^1, U_1^1, \mathbf{W}_1) - c_{NS}(U_1^2, U_1^2, \mathbf{W}_1) \\ & + (\chi_2, \mathbf{W}_1 \cdot \mathbf{n}_{12})_{\Gamma_{12}} - \frac{1}{2}(U_1^1 \cdot U_1^1, \mathbf{W}_1 \cdot \mathbf{n}_{12})_{\Gamma_{12}} \\ & + \frac{1}{2}(U_1^2 \cdot U_1^2, \mathbf{W}_1 \cdot \mathbf{n}_{12})_{\Gamma_{12}} - (\mathbf{W}_1 \cdot \mathbf{n}_{12}, \chi_2)_{\Gamma_{12}} = 0. \end{aligned}$$

Using continuity of the form c_{NS} and rewriting the nonlinear terms as

$$\begin{aligned} & c_{NS}(U_1^1, U_1^1, \mathbf{W}_1) - c_{NS}(U_1^2, U_1^2, \mathbf{W}_1) = c_{NS}(\mathbf{W}_1, U_1^1, \mathbf{W}_1) + c_{NS}(U_1^2, \mathbf{W}_1, \mathbf{W}_1), \\ & - \frac{1}{2}(U_1^1 \cdot U_1^1, \mathbf{W}_1 \cdot \mathbf{n}_{12})_{\Gamma_{12}} + \frac{1}{2}(U_1^2 \cdot U_1^2, \mathbf{W}_1 \cdot \mathbf{n}_{12})_{\Gamma_{12}} \\ & = -\frac{1}{2}(\mathbf{W}_1 \cdot U_1^1, \mathbf{W}_1 \cdot \mathbf{n}_{12})_{\Gamma_{12}} - \frac{1}{2}(\mathbf{W}_1 \cdot U_1^2, \mathbf{W}_1 \cdot \mathbf{n}_{12})_{\Gamma_{12}}, \end{aligned}$$

we obtain

$$\begin{aligned} & 2\nu \|\mathbf{D}(\mathbf{W}_1)\|_{L^2(\Omega_1)}^2 + \kappa \|\chi_2\|^2 + \frac{1}{G} \|\mathbf{W}_1 \cdot \tau_{12}\|_{L^2(\Gamma_{12})}^2 \\ & + c_{NS}(\mathbf{W}_1, U_1^1, \mathbf{W}_1) + c_{NS}(U_1^2, \mathbf{W}_1, \mathbf{W}_1) - \frac{1}{2}(\mathbf{W}_1 \cdot U_1^1, \mathbf{W}_1 \cdot \mathbf{n}_{12})_{\Gamma_{12}} \\ & - \frac{1}{2}(\mathbf{W}_1 \cdot U_1^2, \mathbf{W}_1 \cdot \mathbf{n}_{12})_{\Gamma_{12}} \leq 0. \end{aligned}$$

From Lemma (9), we have

$$\begin{aligned} & c_{\text{NS}}(\mathbf{W}_1; \mathbf{U}_1^1, \mathbf{W}_1) + c_{\text{NS}}(\mathbf{U}_1^2; \mathbf{W}_1, \mathbf{W}_1) \\ & \leq C_7 \|\mathbf{D}(\mathbf{W}_1)\|_{L^2(\Omega_1)} (\|\mathbf{D}(\mathbf{U}_1^1)\|_{L^2(\Omega_1)} + \|\mathbf{D}(\mathbf{U}_1^2)\|_{L^2(\Omega_1)}). \end{aligned}$$

Similarly, using (3.10) and (3.9), we have

$$\begin{aligned} & \frac{1}{2}(\mathbf{W}_1 \cdot \mathbf{U}_1^1, \mathbf{W}_1 \cdot \mathbf{n}_{12})_{\Gamma_{12}} + \frac{1}{2}(\mathbf{W}_1 \cdot \mathbf{U}_1^2, \mathbf{W}_1 \cdot \mathbf{n}_{12})_{\Gamma_{12}} \\ & \leq \frac{1}{2} C_4^2 C_2 C_1^3 \|\mathbf{D}(\mathbf{W}_1)\|_{L^2(\Omega_1)}^2 (\|\mathbf{D}(\mathbf{U}_1^1)\|_{L^2(\Omega_1)} + \|\mathbf{D}(\mathbf{U}_1^2)\|_{L^2(\Omega_1)}). \end{aligned}$$

Combining the two bounds above with (7.19), we obtain:

$$(2\nu - \frac{\mathcal{R}_2}{\sqrt{\nu}}(\sqrt{2}C_7 + \frac{1}{\sqrt{2}}C_1^3 C_2 C_4^2)) \|\mathbf{D}(\mathbf{W}_1)\|_{L^2(\Omega_1)}^2 + \kappa \|\chi_2\|^2 + \frac{1}{G} \|\mathbf{W}_1 \cdot \tau_{12}\|_{L^2(\Gamma_{12})}^2 \leq 0.$$

This clearly implies that $\mathbf{W}_1 = \mathbf{0}$ and $\chi_2 = 0$ if the condition

$$2\nu > \frac{\mathcal{R}_2}{\sqrt{\nu}}(\sqrt{2}C_7 + \frac{1}{\sqrt{2}}C_1^3 C_2 C_4^2)$$

is satisfied. This condition is equivalent to (4.31). \square

The proof of uniqueness for the solution W_B^h involves less terms but is only valid in a ball of fixed radius. The result is summarized in the following theorem.

Theorem 14. *Let \mathcal{R}_2 be defined by 4.29. Under the condition*

$$\nu^{3/2} > \frac{C_1^3}{\sqrt{2}}(\mathcal{P}_4^2 + C_2 C_4^2) \mathcal{R}_2 \tag{4.32}$$

and

$$\mathcal{R}_2^2 < \frac{32\nu^3}{C_1^6 C_2^2 C_4^4},$$

problem (W_B^h) admits at most one solution satisfying

$$2\nu \|\mathbf{D}(\mathbf{U}_1)\|_{L^2(\Omega_1)}^2 + \|\mathbf{P}_2\|^2 \leq \mathcal{R}_2^2. \tag{4.33}$$

4.7 A Priori Error Estimates

Theorem 15. *Assume that the solution to problem (W_A) is smooth enough, i.e. $\mathbf{u}_1 \in (H^{k_1+1}(\Omega_1))^2$, $p_1 \in H^{k_1}(\Omega_1)$ and $p_2 = \varphi_2 + p_D$ with $\varphi_2 \in H^{k_2+1}(\Omega_2)$. Let \mathcal{R}_1 be defined by (3.30) and let \mathcal{R}_2 be defined by (4.29). Assume that the data satisfies:*

$$\nu^{3/2} > \frac{C_1^3}{\sqrt{2}}(\mathcal{P}_4^2 + C_2 C_4^2)(\mathcal{R}_1 + \mathcal{R}_2).$$

Then, there exists a constant C independent of h and ν such that

$$\begin{aligned} & \nu \|\mathbf{D}(\mathbf{u}_1 - \mathbf{U}_1)\|_{L^2(\Omega_1)}^2 + \|\varphi_2 - \Phi_2\|^2 + \|(\mathbf{u}_1 - \mathbf{U}_1) \cdot \boldsymbol{\tau}_{12}\|_{L^2(\Gamma_{12})}^2 \leq \\ & C \left(1 + \frac{(\mathcal{R}_1 + \mathcal{R}_2)^2}{\nu^2}\right) h^{2k_1} \|\mathbf{u}_1\|_{H^{k_1+1}(\Omega_1)}^2 + C \left(1 + \frac{1}{\nu}\right) h^{2k_2} \|\varphi_2\|_{H^{k_2+1}(\Omega_2)}^2 + C \frac{1}{\nu} h^{2k_1} \|p_1\|_{H^{k_1}(\Omega_1)}^2. \end{aligned}$$

Proof. Let $\tilde{\mathbf{u}}_1, \tilde{p}_1, \tilde{\varphi}_2$ be approximations to $\mathbf{u}_1, p_1, \varphi_2$ in the spaces \mathbf{X}_1^h, M_1^h and M_2^h respectively. Assume that the error bounds (4.6), (4.8) and (4.9) hold. Let

$$\begin{aligned} \boldsymbol{\chi}_1 &= \mathbf{U}_1 - \tilde{\mathbf{u}}_1, & \xi_1 &= P_1 - \tilde{p}_1, & \xi_2 &= \Phi_2 - \tilde{\varphi}_2, \\ \boldsymbol{\zeta}_1 &= \mathbf{u}_1 - \tilde{\mathbf{u}}_1, & \eta_1 &= p_1 - \tilde{p}_1, & \eta_2 &= \varphi_2 - \tilde{\varphi}_2. \end{aligned}$$

Subtracting (4.15)-(4.16) from (5.1)-(5.2), we obtain the error equations:

$$\begin{aligned} & \forall \mathbf{v}_1 \in \mathbf{X}_1^h, \forall q_2 \in M_2^h, \quad a_{\text{NS}}(\boldsymbol{\chi}_1, \mathbf{v}_1) + a_{\text{D}}(\xi_2, q_2) + b_{\text{NS}}(\mathbf{v}_1, \xi_1) + c_{\text{NS}}(\mathbf{U}_1; \mathbf{U}_1, \mathbf{v}_1) \\ & - c_{\text{NS}}(\mathbf{u}_1; \mathbf{u}_1, \mathbf{v}_1) + \gamma_A(\mathbf{U}_1, \Phi_2; \mathbf{v}_1, q_2) - \gamma_A(\mathbf{u}_1, \varphi_2; \mathbf{v}_1, q_2) = a_{\text{NS}}(\boldsymbol{\zeta}_1, \mathbf{v}_1) + a_{\text{D}}(\eta_2, q_2) \\ & \quad + b_{\text{NS}}(\mathbf{v}_1, \eta_1), \\ & \forall q_1 \in M_1^h, \quad b_{\text{NS}}(\boldsymbol{\chi}_1, q_1) = b_{\text{NS}}(\boldsymbol{\zeta}_1, q_1). \end{aligned}$$

Let $\mathbf{v}_1 = \boldsymbol{\chi}_1, q_1 = \xi_1, q_2 = \xi_2$, then from (4.5), we have

$$\begin{aligned} & 2\nu \|\mathbf{D}(\boldsymbol{\chi}_1)\|_{L^2(\Omega_1)}^2 + \kappa \|\xi_2\|^2 + c_{\text{NS}}(\mathbf{U}_1; \mathbf{U}_1, \boldsymbol{\chi}_1) - c_{\text{NS}}(\mathbf{u}_1; \mathbf{u}_1, \boldsymbol{\chi}_1) \\ & + \gamma_A(\mathbf{U}_1, \Phi_2; \boldsymbol{\chi}_1, \xi_2) - \gamma_A(\mathbf{u}_1, \varphi_2; \boldsymbol{\chi}_1, \xi_2) \leq a_{\text{NS}}(\boldsymbol{\zeta}_1, \boldsymbol{\chi}_1) + a_{\text{D}}(\eta_2, \xi_2) \end{aligned} \quad (4.34)$$

$$+ b_{\text{NS}}(\boldsymbol{\chi}_1, \eta_1) - b_{\text{NS}}(\boldsymbol{\zeta}_1, \xi_1). \quad (4.35)$$

First expand the terms involving the linear form γ_A :

$$\begin{aligned} \gamma_A(\mathbf{U}_1, \Phi_2; \chi_1, \xi_2) - \gamma_A(\mathbf{u}_1, \varphi_2; \chi_1, \xi_2) &= -\frac{1}{2}(\mathbf{U}_1 \cdot \mathbf{U}_1, \chi_1 \cdot \mathbf{n}_{12})_{\Gamma_{12}} \\ &+ \frac{1}{2}(\mathbf{u}_1 \cdot \mathbf{u}_1, \chi_1 \cdot \mathbf{n}_{12})_{\Gamma_{12}} + \frac{1}{G} \|\chi_1 \cdot \boldsymbol{\tau}_{12}\|_{L^2(\Gamma_{12})}^2 - \frac{1}{G} (\zeta_1 \cdot \boldsymbol{\tau}_{12}, \chi_1 \cdot \boldsymbol{\tau}_{12})_{\Gamma_{12}} \end{aligned} \quad (4.36)$$

$$-(\eta_2, \chi_1 \cdot \mathbf{n}_{12})_{\Gamma_{12}} + (\xi_2, \zeta_1 \cdot \mathbf{n}_{12})_{\Gamma_{12}}. \quad (4.37)$$

The nonlinear terms are rewritten as

$$\begin{aligned} A_1 &= -\frac{1}{2}(\mathbf{U}_1 \cdot \mathbf{U}_1, \chi_1 \cdot \mathbf{n}_{12})_{\Gamma_{12}} + \frac{1}{2}(\mathbf{u}_1 \cdot \mathbf{u}_1, \chi_1 \cdot \mathbf{n}_{12})_{\Gamma_{12}} = \frac{1}{2}(\mathbf{U}_1 \cdot \chi_1, \chi_1 \cdot \mathbf{n}_{12})_{\Gamma_{12}} \\ &+ \frac{1}{2}(\chi_1 \cdot \mathbf{u}_1, \chi_1 \cdot \mathbf{n}_{12})_{\Gamma_{12}} - \frac{1}{2}(\mathbf{U}_1 \cdot \zeta_1, \chi_1 \cdot \mathbf{n}_{12})_{\Gamma_{12}} - \frac{1}{2}(\zeta_1 \cdot \mathbf{u}_1, \chi_1 \cdot \mathbf{n}_{12})_{\Gamma_{12}}, \end{aligned} \quad (4.38)$$

and bounded by using (3.5), (3.7), (3.10), (3.9), (3.29) and (7.19)

$$\begin{aligned} A_1 &\leq \frac{1}{2} C_1^3 C_2 C_4^2 \|\mathbf{D}(\chi_1)\|_{L^2(\Omega_1)}^2 (\|\mathbf{D}(\mathbf{U}_1)\|_{L^2(\Omega_1)} + \|\mathbf{D}(\mathbf{u}_1)\|_{L^2(\Omega_1)}) \\ &+ C \|\mathbf{D}(\chi_1)\|_{L^2(\Omega_1)} \|\nabla \zeta_1\|_{L^2(\Omega_1)} (\|\mathbf{D}(\mathbf{U}_1)\|_{L^2(\Omega_1)} + \|\mathbf{D}(\mathbf{u}_1)\|_{L^2(\Omega_1)}) \\ &\leq \frac{\nu}{5} \|\mathbf{D}(\chi_1)\|_{L^2(\Omega_1)}^2 + \frac{1}{2} C_1^3 C_2 C_4^2 \frac{\mathcal{R}_1 + \mathcal{R}_2}{\sqrt{2\nu}} \|\mathbf{D}(\chi_1)\|_{L^2(\Omega_1)}^2 \\ &+ \frac{C(\mathcal{R}_1 + \mathcal{R}_2)^2}{\nu^2} \|\nabla \zeta_1\|_{L^2(\Omega_1)}^2. \end{aligned}$$

The linear terms in (4.37) are bounded by (3.5), (3.7), (3.10), (3.9) and (4.12)

$$\begin{aligned} \frac{1}{G} (\zeta_1 \cdot \boldsymbol{\tau}_{12}, \chi_1 \cdot \boldsymbol{\tau}_{12})_{\Gamma_{12}} &\leq \frac{1}{2G} \|\chi_1 \cdot \boldsymbol{\tau}_{12}\|_{L^2(\Gamma_{12})}^2 + C \|\nabla \zeta_1\|_{L^2(\Omega_1)}^2 \\ (\eta_2, \chi_1 \cdot \mathbf{n}_{12})_{\Gamma_{12}} &\leq \frac{\nu}{5} \|\mathbf{D}(\chi_1)\|_{L^2(\Omega_1)}^2 + \frac{C}{\nu} \|\eta_2\|^2, \\ (\xi_2, \zeta_1 \cdot \mathbf{n}_{12})_{\Gamma_{12}} &\leq \frac{\kappa}{5} \|\xi_2\|^2 + C \|\nabla \zeta_1\|_{L^2(\Omega_1)}^2. \end{aligned}$$

Rewriting the nonlinear terms involving c_{NS} in (4.35) in a similar way as with the term A_1 defined in (4.7). We obtain a bound by using the continuity of the bilinear

from c_{NS} .

$$\begin{aligned}
c_{NS}(\mathbf{U}_1; \mathbf{U}_1, \boldsymbol{\chi}_1) - c_{NS}(\mathbf{u}_1; \mathbf{u}_1, \boldsymbol{\chi}_1) &= c_{NS}(\mathbf{U}_1; \boldsymbol{\chi}_1, \boldsymbol{\chi}_1) + c_{NS}(\boldsymbol{\chi}_1; \mathbf{u}_1, \boldsymbol{\chi}_1) \\
&\quad - c_{NS}(\mathbf{U}_1; \boldsymbol{\zeta}_1, \boldsymbol{\chi}_1) - c_{NS}(\boldsymbol{\zeta}_1; \mathbf{u}, \boldsymbol{\chi}_1) \\
&\leq \frac{\nu}{5} \|\mathbf{D}(\boldsymbol{\chi}_1)\|_{L^2(\Omega_1)}^2 + C_7 \frac{\mathcal{R}_1 + \mathcal{R}_2}{\sqrt{2\nu}} \|\mathbf{D}(\boldsymbol{\chi}_1)\|_{L^2(\Omega_1)}^2 \\
&\quad + C \frac{(\mathcal{R}_1 + \mathcal{R}_2)^2}{\nu^2} \|\nabla \boldsymbol{\zeta}_1\|_{L^2(\Omega_1)}^2.
\end{aligned}$$

The term $a_{NS}(\boldsymbol{\zeta}_1, \boldsymbol{\chi}_1)$ is bounded using Cauchy-Schwarz and Young's inequalities.

$$a_{NS}(\boldsymbol{\zeta}_1, \boldsymbol{\chi}_1) \leq \frac{\nu}{5} \|\mathbf{D}(\boldsymbol{\chi}_1)\|_{L^2(\Omega_1)}^2 + C\nu \|\mathbf{D}(\boldsymbol{\zeta}_1)\|_{L^2(\Omega_1)}^2.$$

The term $b_{NS}(\boldsymbol{\zeta}_1, \boldsymbol{\xi}_1)$ vanishes because of property (4.7). The term $a_D(\boldsymbol{\eta}_2, \boldsymbol{\xi}_2)$ is bounded using standard DG techniques and the approximation property (4.9):

$$a_D(\boldsymbol{\eta}_2, \boldsymbol{\xi}_2) \leq \frac{\kappa}{4} \|\boldsymbol{\xi}_2\|^2 + Ch^{2k_2} \|\varphi_2\|_{H^{k_2+1}(\Omega_2)}^2.$$

Finally, the term $b_{NS}(\boldsymbol{\chi}_1, \boldsymbol{\eta}_1)$ is bounded as:

$$b_{NS}(\boldsymbol{\chi}_1, \boldsymbol{\eta}_1) \leq \frac{\nu}{5} \|\mathbf{D}(\boldsymbol{\chi}_1)\|_{L^2(\Omega_1)}^2 + \frac{C}{\nu} \|\boldsymbol{\eta}_1\|_{L^2(\Omega_1)}^2.$$

Combining the results above, the error equation (4.35) becomes:

$$\begin{aligned}
&\left(\nu - \left(\frac{1}{2} C_1^3 C_2 C_4^2 + C_7 \right) \frac{\mathcal{R}_1 + \mathcal{R}_2}{\sqrt{2\nu}} \right) \|\mathbf{D}(\boldsymbol{\chi}_1)\|_{L^2(\Omega_1)}^2 + \frac{\kappa}{2} \|\boldsymbol{\xi}_2\|^2 + \frac{1}{2G} \|\boldsymbol{\chi}_1 \cdot \boldsymbol{\tau}_{12}\|_{L^2(\Gamma_{12})}^2 \\
&\leq C \left(1 + \frac{(\mathcal{R}_1 + \mathcal{R}_2)^2}{\nu^2} \right) \|\nabla \boldsymbol{\zeta}_1\|_{L^2(\Omega_1)}^2 + C \frac{1}{\nu} \|\boldsymbol{\eta}_2\|^2 + Ch^{2k_2} \|\varphi_2\|_{H^{k_2+1}(\Omega_2)}^2 + C \frac{1}{\nu} \|\boldsymbol{\eta}_1\|_{L^2(\Omega_1)}^2.
\end{aligned}$$

The final result is obtained by using the approximation properties (4.6), (4.8), (4.10), a trace theorem and the inequalities:

$$\begin{aligned}
\|\mathbf{D}(\mathbf{u}_1 - \mathbf{U}_1)\|_{L^2(\Omega_1)}^2 &\leq C \|\mathbf{D}(\boldsymbol{\chi}_1)\|_{L^2(\Omega_1)}^2 + C \|\mathbf{D}(\boldsymbol{\zeta}_1)\|_{L^2(\Omega_1)}^2, \\
\|(\mathbf{u}_1 - \mathbf{U}_1) \cdot \boldsymbol{\tau}_{12}\|_{L^2(\Gamma_{12})}^2 &\leq C \|(\boldsymbol{\chi}_1) \cdot \boldsymbol{\tau}_{12}\|_{L^2(\Gamma_{12})}^2 + C \|(\boldsymbol{\zeta}_1) \cdot \boldsymbol{\tau}_{12}\|_{L^2(\Gamma_{12})}^2, \\
\|p_2 - P_2\|^2 &\leq C \|\boldsymbol{\xi}_2\|^2 + C \|\boldsymbol{\eta}_2\|^2.
\end{aligned}$$

□

A straight consequence of Lemma (8) and Theorem (15) is a bound on the pressure error.

Corollary 16. *Under the assumptions of Theorem (15) and if the function p_D belongs to $H^{k_2+1}(\Omega_2)$, there exists a constant C independent of h and ν such that*

$$\begin{aligned} \| \|p_2 - P_2\| \|^2 &\leq C \left(1 + \frac{(\mathcal{R}_1 + \mathcal{R}_2)^2}{\nu^2}\right) h^{2k_1} \| \mathbf{u}_1 \|_{H^{k_1+1}(\Omega_1)}^2 + C \left(1 + \frac{1}{\nu}\right) h^{2k_2} \| \varphi_2 \|_{H^{k_2+1}(\Omega_2)}^2 \\ &\quad + Ch^{2k_2} \| p_D \|_{H^{k_2+1}(\Omega_2)}^2 + C \frac{1}{\nu} h^{2k_1} \| p_1 \|_{H^{k_1}(\Omega_1)}^2. \end{aligned}$$

Theorem 17. *Under the assumptions of Theorem (15) and Corollary (16), there exists a constant C independent of h such that*

$$\| p_1 - P_1 \|_{L^2(\Omega_1)} \leq Ch^{k_1} \| p_1 \|_{H^{k_1}(\Omega_1)} + Ch^{k_1} \| \mathbf{u}_1 \|_{H^{k_1+1}(\Omega_1)} + Ch^{k_2} (\| \varphi_2 \|_{H^{k_2+1}(\Omega_2)} + \| p_D \|_{H^{k_2+1}(\Omega_2)}).$$

Proof. Using the same notation as in the proof of Theorem (15), we can rewrite the error equation by taking $q_2 = 0$:

$$\begin{aligned} b_{\text{NS}}(\mathbf{v}_1, \xi_1) &= b_{\text{NS}}(\mathbf{v}_1, \eta_1) + a_{\text{NS}}(\mathbf{u}_1 - \mathbf{U}_1, \mathbf{v}_1) - \frac{1}{2}(\mathbf{u}_1 \cdot \mathbf{u}_1 - \mathbf{U}_1 \cdot \mathbf{U}_1, \mathbf{v}_1 \cdot \mathbf{n}_{12})_{\Gamma_{12}} \\ &\quad + c_{\text{NS}}(\mathbf{u}_1; \mathbf{u}_1, \mathbf{v}_1) - c_{\text{NS}}(\mathbf{U}_1; \mathbf{U}_1, \mathbf{v}_1) + (\varphi_2 - \Phi_2, \mathbf{v}_1 \cdot \mathbf{n}_{12})_{\Gamma_{12}} \\ &\quad + \frac{1}{G}((\mathbf{u}_1 - \mathbf{U}_1) \cdot \boldsymbol{\tau}_{12}, \mathbf{v}_1 \cdot \boldsymbol{\tau}_{12})_{\Gamma_{12}}. \end{aligned}$$

We now bound all terms in the right-hand side. Cauchy-Schwarz's inequality yields

$$\begin{aligned} b_{\text{NS}}(\mathbf{v}_1, \eta_1) &\leq C \| \nabla \mathbf{v}_1 \|_{L^2(\Omega_1)} \| \eta_1 \|_{L^2(\Omega_1)}, \\ a_{\text{NS}}(\mathbf{u}_1 - \mathbf{U}_1, \mathbf{v}_1) &\leq C \nu \| \nabla \mathbf{v}_1 \|_{L^2(\Omega_1)} \| \mathbf{D}(\mathbf{u}_1 - \mathbf{U}_1) \|_{L^2(\Omega_1)}. \end{aligned}$$

The nonlinear terms are handled like the term A_1 in (4.7).

$$\begin{aligned}
\frac{1}{2}(\mathbf{u}_1 \cdot \mathbf{u}_1 - \mathbf{U}_1 \cdot \mathbf{U}_1, \mathbf{v}_1 \cdot \mathbf{n}_{12})_{\Gamma_{12}} &= \frac{1}{2}(\mathbf{U}_1 \cdot \boldsymbol{\chi}_1, \mathbf{v}_1 \cdot \mathbf{n}_{12})_{\Gamma_{12}} + \frac{1}{2}(\boldsymbol{\chi}_1 \cdot \mathbf{u}_1, \mathbf{v}_1 \cdot \mathbf{n}_{12})_{\Gamma_{12}} \\
&\quad - \frac{1}{2}(\mathbf{U}_1 \cdot \boldsymbol{\zeta}_1, \mathbf{v}_1 \cdot \mathbf{n}_{12})_{\Gamma_{12}} - \frac{1}{2}(\boldsymbol{\zeta}_1 \cdot \mathbf{u}_1, \mathbf{v}_1 \cdot \mathbf{n}_{12})_{\Gamma_{12}} \\
&\leq \frac{C(\mathcal{R}_1 + \mathcal{R}_2)}{\sqrt{\nu}} \|\nabla \mathbf{v}_1\|_{L^2(\Omega_1)} (\|\mathbf{D}(\boldsymbol{\chi}_1)\|_{L^2(\Omega_1)} + \|\nabla \boldsymbol{\zeta}_1\|_{L^2(\Omega_1)}), \\
c_{\text{NS}}(\mathbf{u}_1; \mathbf{u}_1, \mathbf{v}_1) - c_{\text{NS}}(\mathbf{U}_1; \mathbf{U}_1, \mathbf{v}_1) &= c_{\text{NS}}(\mathbf{U}_1; \boldsymbol{\chi}_1, \mathbf{v}_1) + c_{\text{NS}}(\boldsymbol{\chi}_1; \mathbf{u}_1, \mathbf{v}_1) \\
&\quad - c_{\text{NS}}(\mathbf{U}_1; \boldsymbol{\zeta}_1, \mathbf{v}_1) - c_{\text{NS}}(\boldsymbol{\zeta}_1; \mathbf{u}_1, \mathbf{v}_1) \\
&\leq \frac{C(\mathcal{R}_1 + \mathcal{R}_2)}{\sqrt{\nu}} \|\nabla \mathbf{v}_1\|_{L^2(\Omega_1)} (\|\mathbf{D}(\boldsymbol{\chi}_1)\|_{L^2(\Omega_1)} + \|\nabla \boldsymbol{\zeta}_1\|_{L^2(\Omega_1)}).
\end{aligned}$$

Finally, the last two terms are bounded as:

$$\begin{aligned}
(\varphi_2 - \Phi_2, \mathbf{v}_1 \cdot \mathbf{n}_{12})_{\Gamma_{12}} &\leq C(\|\xi_2\| + \|\eta_2\|_{L^2(\Gamma_{12})}) \|\nabla \mathbf{v}_1\|_{L^2(\Omega_1)}, \\
\frac{1}{G}((\mathbf{u}_1 - \mathbf{U}_1) \cdot \boldsymbol{\tau}_{12}, \mathbf{v}_1 \cdot \boldsymbol{\tau}_{12})_{\Gamma_{12}} &\leq C\|(\mathbf{u}_1 - \mathbf{U}_1) \cdot \boldsymbol{\tau}_{12}\|_{L^2(\Omega_1)} \|\nabla \mathbf{v}_1\|_{L^2(\Omega_1)}.
\end{aligned}$$

Therefore, we obtain:

$$b_{\text{NS}}(\mathbf{v}_1, \xi_1) \leq C\Theta \|\nabla \mathbf{v}_1\|_{L^2(\Omega_1)},$$

with

$$\begin{aligned}
\Theta &= \|\eta_1\|_{L^2(\Omega_1)} + \nu \|\mathbf{D}(\mathbf{u}_1 - \mathbf{U}_1)\|_{L^2(\Omega_1)} + \frac{\mathcal{R}_1 + \mathcal{R}_2}{\sqrt{\nu}} (\|\mathbf{D}(\boldsymbol{\chi}_1)\|_{L^2(\Omega_1)} + \|\nabla \boldsymbol{\zeta}_1\|_{L^2(\Omega_1)}) \\
&\quad + \|\xi_2\| + \|\eta_2\|_{L^2(\Gamma_{12})} + \|(\mathbf{u}_1 - \mathbf{U}_1) \cdot \boldsymbol{\tau}_{12}\|_{L^2(\Omega_1)}.
\end{aligned}$$

The inf-sup condition (4.1) then yields

$$\|\xi_1\|_{L^2(\Omega_1)} \leq \frac{C}{\beta_*} \Theta.$$

Using the approximation results (4.6), (4.8), (4.9) and Theorem (15) yields the result. \square

The bounds for W_B^h are obtained in the same way, the result is stated below.

Theorem 18. *Assume that the solution to problem (W_B^h) is smooth enough, i.e $\mathbf{u}_1 \in (H^{k_1+1}(\Omega_1))^2$, $p_1 \in H^{k_1}(\Omega_1)$ and $p_2 = \phi_2 + p_D$ with $\phi_2 \in H^{k_2+1}(\Omega_2)$ and p_D belongs to $H^{k_2+1}(\Omega_2)$. Let \mathcal{R}_1 be defined by (3.30) and let \mathcal{R}_2 be defined by (4.29). Assume that the data satisfies:*

$$\nu^{3/2} > \frac{C_1^3}{\sqrt{2}}(\mathcal{P}_4^2 + \frac{1}{2}C_2C_4^2)(\mathcal{R}_1 + \mathcal{R}_2).$$

Let (\mathbf{U}_1, P_1, P_2) be a solution to problem (W_B^h) . Then, there exists a constant C independent of h and ν such that

$$\begin{aligned} & \nu \|\mathbf{D}(\mathbf{u}_1 - \mathbf{U}_1)\|_{L^2(\Omega_1)}^2 + \|p_2 - P_2\|^2 + \|(\mathbf{u}_1 - \mathbf{U}_1) \cdot \boldsymbol{\tau}_{12}\|_{L^2(\Gamma_{12})}^2 \\ & \leq C(1 + \frac{(\mathcal{R}_1 + \mathcal{R}_2)^2}{\nu^2})h^{2k_1}\|\mathbf{u}_1\|_{H^{k_1+1}(\Omega_1)}^2 + C(1 + \frac{1}{\nu})h^{2k_2}\|\varphi_2\|_{H^{k_2+1}(\Omega_2)}^2 \\ & \quad + C\frac{1}{\nu}h^{2k_1}\|p_1\|_{H^{k_1}(\Omega_1)}^2 + Ch^{2k_2}\|p_D\|_{H^{k_2+1}(\Omega_2)}. \end{aligned}$$

In addition, there exists a constant C independent of h such that

$$\begin{aligned} \|p_1 - P_1\|_{L^2(\Omega_1)} & \leq Ch^{k_1}\|p_1\|_{H^{k_1}(\Omega_1)} + Ch^{k_1}\|\mathbf{u}_1\|_{H^{k_1+1}(\Omega_1)} \\ & \quad + Ch^{k_2}(\|\varphi_2\|_{H^{k_2+1}(\Omega_2)} + \|p_D\|_{H^{k_2+1}(\Omega_2)}) \end{aligned}$$

Conclusion

This chapter deals with the existence and uniqueness of a numerical solution to the problem coupled problems W_A^h and W_B^h . If the inertial forces are included in the balance of forces across the interface, existence of the numerical solutions is obtained unconditionally. A small data condition is needed if one does not include inertial forces. In addition convergence of the discrete solution has been proved with respect to the mesh size. The next step is to verify these results with numerical experiments in the following chapter.

Chapter 5

Numerical Results

Introduction

This chapter introduces the numerical discretization of the coupled Navier-Stokes and Darcy problem. Grid tests are used to check theoretical convergence rates with respect grid parameter h . The motivation behind this model is to understand the coupling of free flow with flow in porous medial. With this application in mind the coupled problem is solved under various conditions that test the robustness of the model with respect to the viscosity ν and hydraulic conductivity \mathbf{K} . This chapter also investigates the effect of the balance of forces on the interface.

5.1 Software

I have written software in C using the Petsc Libraries for the numerical results presented in this and subsequent chapters.

5.2 Numerical Schemes

The numerical scheme presented in this thesis couples the continuous finite element method in the free flow region with the discontinuous Galerkin method in the porous media region. To show the effectiveness of this choice, results from an implementation with the CG method and DG method in both domains will also be presented for comparison. The triangulation \mathcal{E}^h (h is the maximum diameter of of a mesh element) of

the computational domain $\Omega = \Omega_1 \cup \Omega_2$ is assumed to be regular. The aim is to find an approximation U_1^h of the Navier-Stokes velocity, P_1^h of the Navier-Stokes pressure and P_h^2 of the Darcy pressure in the finite dimensional spaces $\mathbf{X}_1^h, M_1^h, M_2^h$ respectively. Because the discretization of the different operators will depend on the choice of the finite element method, the following is a list of bilinear forms corresponding to various discretizations:

- Assume that the operator $-2\nu\nabla \cdot D(\mathbf{u})$ has been discretized by a bilinear form $a_{\text{NS}} : \mathbf{X}_1^h \times \mathbf{X}_1^h \rightarrow \mathbb{R}$.
- Assume that the operator ∇p has been discretized by a bilinear form $b_{\text{NS}} : \mathbf{X}_1^h \times M_1^h \rightarrow \mathbb{R}$.
- Assume that the operator $\mathbf{u} \cdot \nabla \mathbf{u}$ has been discretized by a trilinear form $c_{\text{NS}} : \mathbf{X}_1^h \times \mathbf{X}_1^h \times \mathbf{X}_1^h \rightarrow \mathbb{R}$.
- Assume that the operator $-\nabla \cdot \mathbf{K} \nabla p$ has been discretized by a bilinear form $a_{\text{D}} : M_2^h \times M_2^h \rightarrow \mathbb{R}$.
- Assume that the input data (body forces \mathbf{f}_1 and f_2 and boundary conditions) are incorporated into a bilinear form $L : \mathbf{X}_1^h \times M_2^h \rightarrow \mathbb{R}$.

The interface conditions are taken into account by a form γ_A in the case when inertial forces are included in the balance of forces on the interface (see (2.12) and xrefeq:ch1:forces2). We recall the bilinear forms for the interface:

$$\begin{aligned} \forall \mathbf{v}, \mathbf{w} \in \mathbf{X}_1^h, \quad \forall q_2, t_2 \in M_2^h, \quad \gamma_A(\mathbf{v}, q_2; \mathbf{w}, t_2) &= (q_2 - \frac{1}{2} \mathbf{v}_1 \cdot \mathbf{v}_1, \mathbf{w} \cdot \mathbf{n}_{12})_{\Gamma_{12}} \\ &+ \frac{1}{G} (\mathbf{v} \cdot \boldsymbol{\tau}_{12}, \mathbf{w} \cdot \boldsymbol{\tau}_{12})_{\Gamma_{12}} - (\mathbf{v} \cdot \mathbf{n}_{12}, t_2)_{\Gamma_{12}}. \end{aligned}$$

In the case where the inertial forces are included, the interface bilinear form becomes

$$\begin{aligned} \forall \mathbf{v}, \mathbf{w} \in \mathbf{X}_1^h, \quad \forall q_2, t_2 \in M_2^h, \quad \gamma_B(\mathbf{v}, q_2; \mathbf{w}, t_2) &= (q_2, \mathbf{w} \cdot \mathbf{n}_{12})_{\Gamma_{12}} \\ &+ \frac{1}{G} (\mathbf{v} \cdot \boldsymbol{\tau}_{12}, \mathbf{w} \cdot \boldsymbol{\tau}_{12})_{\Gamma_{12}} - (\mathbf{v} \cdot \mathbf{n}_{12}, t_2)_{\Gamma_{12}}. \end{aligned}$$

The interface term is independent of the discretization that is used.

Using the operator discretizations as “black boxes”, the coupled Navier-Stokes and Darcy problem is solved by the general scheme: find $\mathbf{U}^h \in \mathbf{X}_1^h, P_1^h \in M_1^h, P_2^h \in M_2^h$ such that

$$\begin{aligned} \forall \mathbf{v} \in \mathbf{X}_1^h, \forall q_2 \in M_2^h, \quad a_{\text{NS}}(\mathbf{U}^h, \mathbf{v}) + b_{\text{NS}}(\mathbf{v}, P_1^h) + c_{\text{NS}}(\mathbf{U}^h; \mathbf{U}^h, \mathbf{v}) + a_{\text{D}}(P_2^h, q_2) \\ + \gamma_{\alpha}(\mathbf{U}^h, P_2^h; \mathbf{v}, q_2) = L(\mathbf{v}_1, q_2), \quad \alpha = A, B \end{aligned} \quad (5.1)$$

$$\forall q_1 \in M_1^h, \quad b_{\text{NS}}(\mathbf{U}^h, q_1) = 0. \quad (5.2)$$

Three algorithms based on the classical continuous finite element method and the primal discontinuous Galerkin method will be presented. In each scheme the solution for the approximation to the Navier-Stokes velocity is obtained from a Picard iteration starting with an initial guess $\mathbf{U}_0 = \mathbf{0}$: find $\mathbf{U}_{n+1}^h \in \mathbf{X}_1^h, P_1^h \in M_1^h, P_2^h \in M^h$ such that

$$\begin{aligned} \forall \mathbf{v} \in \mathbf{X}_1^h, \forall q_2 \in M_2^h, \quad a_{\text{NS}}(\mathbf{U}_{n+1}^h, \mathbf{v}) + b_{\text{NS}}(\mathbf{v}, P_1^h) + c_{\text{NS}}(\mathbf{U}_n^h; \mathbf{U}_{n+1}^h, \mathbf{v}) + a_{\text{D}}(P_2^h, q_2) \\ + \gamma_{\alpha}(\mathbf{U}^h, P_2^h; \mathbf{v}, q_2) = L(\mathbf{v}_1, q_2), \quad \alpha = A, B \end{aligned} \quad (5.3)$$

$$\forall q_1 \in M_1^h, \quad b_{\text{NS}}(\mathbf{U}_{n+1}^h, q_1) = 0. \quad (5.4)$$

5.2.1 Continuous finite element scheme (CG-CG)

In the CG-CG scheme the continuous finite element method is used in both flow domains. The mesh is assumed to be conforming. Let $\mathbf{X}_1^h \subset \{\mathbf{v} \in H^1(\Omega_1)^2 : \mathbf{v} =$

0 on Γ_1 } and let $M_1^h \subset L^2(\Omega)$ be finite-dimensional subspaces that contain continuous piecewise polynomials of a certain degree. The pair (\mathbf{X}_1^h, M_1^h) satisfies an inf-sup condition and the order of approximation is one: for a given positive integer k :

$$\inf_{\mathbf{w}_h \in \mathbf{X}_1^h} \|\mathbf{u} - \mathbf{w}_h\|_{H^1(\Omega_1)} + \inf_{q_h \in M_1^h} \|p_1 - q_h\|_{L^2(\Omega_1)} = \mathcal{O}(h)$$

In this thesis, the MINI finite element space [2] (with order $k = 1$), in which the Navier-Stokes velocity is approximated by continuous piecewise linears enriched with bubbles and the Navier-Stokes pressure by continuous piecewise linear functions has been implemented. Another example is the Taylor-Hood elements (with order $k = 2$) in which the velocity is approximated by continuous piecewise quadratics and the pressure by continuous piecewise linear functions [12]. The discrete space for the Darcy pressure is

$$M_2^h \subset \{q_2 \in H^1(\Omega_2) : q_2 = 0 \text{ on } \Gamma_2\},$$

that contains continuous piecewise polynomials of degree one. We define the following bilinear forms:

$$\begin{aligned} \forall \mathbf{v}, \mathbf{w} \in \mathbf{X}^h, \quad a_{\text{NS}}(\mathbf{v}, \mathbf{w}) &= 2\nu(\mathbf{D}(\mathbf{v}), \mathbf{D}(\mathbf{w}))_{\Omega_1}, \\ \forall \mathbf{v} \in \mathbf{X}^h, \forall q_1 \in M_1^h, \quad b_{\text{NS}}(\mathbf{v}, q_1) &= -(q_1, \nabla \cdot \mathbf{v})_{\Omega_1}, \\ \forall \mathbf{z}, \mathbf{v}, \mathbf{w} \in \mathbf{X}^h, \quad c_{\text{NS}}(\mathbf{z}, \mathbf{v}, \mathbf{w}) &= \frac{1}{2}(\mathbf{z} \cdot \nabla \mathbf{v}, \mathbf{w})_{\Omega_1} - \frac{1}{2}(\mathbf{z} \cdot \nabla \mathbf{w}, \mathbf{v})_{\Omega_1} + \frac{1}{2}(\mathbf{z} \cdot \mathbf{n}_{12}, \mathbf{v} \cdot \mathbf{w})_{\Gamma_{12}}, \\ \forall q_2, t_2 \in M^h, \quad a_{\text{D}}(q_2, t_2) &= (\mathbf{K} \nabla q_2, \nabla t_2)_{\Omega_2} \\ \forall \mathbf{v} \in \mathbf{X}_1^h, \forall q_2 \in M^h, \quad L(\mathbf{v}, q_2) &= (\mathbf{f}_1, \mathbf{v})_{\Omega_1} + (\mathbf{f}_2, q_2)_{\Omega_2} + (g_N, q_2)_{\Gamma_{2N}} \\ &\quad - (\mathbf{K} \nabla g_D, \nabla t_2)_{\Omega_2}. \end{aligned}$$

5.2.2 Discontinuous Galerkin finite element scheme (DG-DG)

The mesh \mathcal{E}^h is allowed to be non-conforming in the interior of each free flow region or each porous medium. The mesh $\mathcal{E}^h = \mathcal{E}_1^h \cup \mathcal{E}_2^h$ where \mathcal{E}_i^h is the mesh restricted to Ω_i . The unknowns are approximated by discontinuous piecewise polynomials. The finite-dimensional spaces are defined for any positive integers k_1 and k_2 :

$$\mathbf{X}_1^h = \{\mathbf{v} \in (L^2(\Omega_1))^2 : \mathbf{v}|_E \in \mathbb{P}_{k_1}(E)\},$$

$$M_1^h = \{q_1 \in L^2(\Omega_1) : q_1|_E \in \mathbb{P}_{k_1-1}(E)\},$$

$$M_2^h = \{q_2 \in L^2(\Omega_2) : q_2|_E \in \mathbb{P}_{k_2}(E)\}.$$

Before defining the bilinear forms, we recall some notation that is standard to the DG method. Let Γ_1^h (resp. Γ_2^h) denote the set of interior edges to Ω_1 (resp. Ω_2) and boundary edges that belong to Γ_1 (resp. Γ_{2D}). For each edge e in $\Gamma_1^h \cup \Gamma_2^h$ we fix a unit normal vector denoted \mathbf{n}_e . If the edge e is a boundary edge, the vector \mathbf{n}_e coincides with the unit normal vector exterior to Ω . For any two triangles E_i and E_j (with $i < j$) that share a common edge e , the jump function $[v]$ and average function $\{v\}$ of a discontinuous piecewise polynomial v is given by:

$$\{v\} = \frac{1}{2}(v|_{E_i}) + \frac{1}{2}(v|_{E_j}), \quad [v] = (v|_{E_i}) - (v|_{E_j}).$$

The trace of v on a boundary edge is denoted by $v = [v] = \{v\}$. The bilinear forms are defined as follows:

$$\begin{aligned}
\forall \mathbf{v}, \mathbf{w} \in \mathbf{X}^h, \quad a_{\text{NS}}(\mathbf{v}, \mathbf{w}) &= 2\nu \sum_{E \in \mathcal{E}_1^h} (\mathbf{D}(\mathbf{v}), \mathbf{D}(\mathbf{w}))_E + \sum_{e \in \Gamma_1^h} \frac{\sigma_e}{|e|} ([v], [w])_e \\
&\quad - 2\nu \sum_{e \in \Gamma_1^h} (\{D(\mathbf{v})\mathbf{n}_e\}, [w])_e + 2\nu\epsilon_1 \sum_{e \in \Gamma_1^h} (\{D(\mathbf{w})\mathbf{n}_e\}, [v])_e, \\
\forall \mathbf{v} \in \mathbf{X}^h, \forall q_1 \in M_1^h, \quad b_{\text{NS}}(\mathbf{v}, q_1) &= - \sum_{E \in \mathcal{E}_1^h} (q_1, \nabla \cdot \mathbf{v})_E + \sum_{e \in \Gamma_1^h} (\{q_1\}, [v] \cdot \mathbf{n}_e)_e, \\
\forall q_2, t_2 \in M^h, \quad a_{\text{D}}(q_2, t_2) &= \sum_{E \in \mathcal{E}_2^h} (\mathbf{K}\nabla q_2, \nabla t_2)_E + \sum_{e \in \Gamma_2^h} \frac{\sigma_e}{|e|} ([q_2], [t_2])_e \\
&\quad - \sum_{e \in \Gamma_2^h} (\{\mathbf{K}\nabla q_2 \cdot \mathbf{n}_e\}, [t_2])_e + \epsilon_2 \sum_{e \in \Gamma_2^h} (\{\mathbf{K}\nabla t_2 \cdot \mathbf{n}_e\}, [q_2])_e, \\
\forall \mathbf{v} \in \mathbf{X}_1^h, \forall q_2 \in M_2^h, \quad \forall t_2 \in M_2^h, \forall \mathbf{v} \in \mathbf{X}_1^h, \quad L(\mathbf{v}, t_2) &= (\mathbf{f}_1, \mathbf{v})_{\Omega_1} + (f_2, t_2)_{\Omega_2} \\
&\quad + \epsilon \sum_{e \in \Gamma_{2D}} (\mathbf{K}\nabla t_2 \cdot \mathbf{n}_e, g_D)_e + \sum_{e \in \Gamma_{2D}} \frac{\sigma_e}{|e|} (g_D, t_2)_e + \sum_{e \in \Gamma_{2N}} (g_N, t_2)_e
\end{aligned}$$

The length of one edge e is denoted by $|e|$. The parameter $\sigma_e \geq 0$ is the penalty parameter. The coefficients $\epsilon_1, \epsilon_2 \in \{-1, +1\}$ are the symmetrization parameters. The DG discretization of the nonlinear operator $\mathbf{u} \cdot \nabla \mathbf{u}$ is based on an upwinding technique [26] and its definition requires additional notation.

For an element $E \in \mathcal{E}_1^h$, \mathbf{n}_E the outward normal to E , and we denote by \mathbf{v}^{int} (resp. \mathbf{v}^{ext}) the trace of the function \mathbf{v} on a side of E coming from the interior of E (resp. the exterior of E). When the side of E belongs to Γ_1 , then by convention we set $\mathbf{v}^{\text{int}} = \mathbf{v}$ and $\mathbf{v}^{\text{ext}} = \mathbf{0}$. Then we define:

$$\begin{aligned}
\forall \mathbf{z}, \mathbf{v}, \mathbf{w} \in \mathbf{X}_1^h, \quad c_{\text{NS}}(\mathbf{z}; \mathbf{v}, \mathbf{w}) &= \sum_{E \in \mathcal{E}_1^h} (\mathbf{z} \cdot \nabla \mathbf{v}, \mathbf{w})_E + \frac{1}{2} \sum_{E \in \mathcal{E}_1^h} (\nabla \cdot \mathbf{z}, \mathbf{v} \cdot \mathbf{w})_E \\
&\quad - \frac{1}{2} \sum_{e \in \Gamma_1^h} ([z] \cdot \mathbf{n}_e, \{\mathbf{v} \cdot \mathbf{w}\})_e + \sum_{E \in \mathcal{E}_1^h} (|\{z\} \cdot \mathbf{n}_E| (\mathbf{v}^{\text{int}} - \mathbf{v}^{\text{ext}}), \mathbf{w}^{\text{int}})_{\partial E_-(z) \setminus \Gamma_{12}},
\end{aligned}$$

where

$$\partial E_-(z) = \{x \in \partial E; \{z(x)\} \cdot \mathbf{n}_E < 0\}.$$

5.2.3 Coupled continuous finite element with discontinuous Galerkin method scheme (CG-DG)

The continuous finite element method in Ω_1 is coupled with the discontinuous Galerkin method in Ω_2 for several reasons. First, the coupled problem has two domains with very different kinds of flow, and the continuous finite element method has proven to be effective in solving the free flow problem. On the other hand, it was shown that continuous finite element method can produce non-physical flow in a fractured porous medium [30]. As DG methods are locally mass conservative, they are appropriate for flow and transport problems in heterogeneous porous media [46]. The discontinuous Galerkin method is thus well suited for solving the part of the coupled problem in the porous medium region. Second, there exist legacy codes for solving the Navier-Stokes equation with the classical finite element method whereas DG software for these problems is not readily available.

In this multinumerics scheme, the forms a_{NS}, b_{NS}, c_{NS} defined in Section (5.2.1). Recall that the spaces $\mathbf{X}_1^h \subset \{\mathbf{v} \in H^1(\Omega_1)^2 : \mathbf{v} = 0 \text{ on } \Gamma_1\}$ and $M_1^h \subset L^2(\Omega)$ satisfy an inf-sup condition and of order k_1 . The space M_2^h consists of discontinuous piecewise polynomials of degree k_2 . In this multi-numerics scheme, Navier-Stokes flow is approximated by the MINI finite element, whereas Darcy flow is approximated by discontinuous piecewise polynomials. The bilinear forms have been defined in Sections (5.2.1) and (5.2.2).

5.3 Numerical Convergence

In this section the CG-CG and CG-DG schemes are tested with respect to the grid parameter h . The computational domain $\Omega \subset \mathbb{R}^2$ is divided into $\Omega_1 = (0, 1) \times (1, 2)$

and $\Omega_2 = (0, 1) \times (0, 1)$ with interface $\Gamma_{12} = (0, 1) \times \{1\}$. For each example, numerical errors and convergence rates are tabulated and discussed for both the CG-CG scheme and the CG-DG scheme. The L^2 errors for velocity and pressure in both regions, as well as the H^1 error for the Navier-Stokes velocity are computed at for each mesh. The coarse mesh consists of 8 triangles with a mesh size $h = 1/4$ and the finest mesh contains 4096 triangles with a mesh size $h = 1/32$. In the first example numerical convergence rates are presented for each scheme for both the cases with and without the inertial forces on the balance of forces on the interface.

Example 19. *The boundary conditions are chosen in such a way that the exact solution to the coupled Navier-Stokes and Darcy problem is*

$$\begin{aligned} \mathbf{u}_1 &= (y^2 - 2y + 2x, x^2 - x + 2y), \quad p_1 = -x^2y + xy + y^2 - 4.0, \\ p_2 &= x^2y + xy + y^2, \end{aligned}$$

in the case when inertial forces are not included on the interface. The boundary conditions are then modified to include inertial forces, and the exact solution becomes

$$\begin{aligned} \mathbf{u}_1 &= (y^2 - 2y + 2x, x^2 - x + 2y), \quad p_1 = -x^2y + xy + y^2, \\ p_2 &= 4.0 - x^2y + xy + y^2 + 0.5((2x - 1)^2 + (x^2 - x - 2)^2). \end{aligned}$$

Numerical errors for the CG-CG and CG-DG schemes are presented for both choices of boundary conditions. Table (5.1) shows optimal convergence rates for the Navier-Stokes velocity, Darcy pressure and velocity. For the Navier-Stokes pressure we observe a higher than optimal rate of convergence of 1.65.

Tables (5.1)-(5.4) show optimal convergence rates for all the variables in the model. For this particular problem and other problems tested in this chapter, it is clear that the solution obtained from including the inertial forces on the interface is comparable

$1/h$	$\ U_1 - u_1\ _{L^2(\Omega_1)}$	$\ P_1 - p_1\ _{L^2(\Omega_1)}$	$\ D(U_1 - u_1)\ _{L^2(\Omega_1)}$	$\ P_2 - p_2\ _{L^2(\Omega_2)}$	$\ U_2 - u_2\ _{L^2(\Omega_2)}$
2	6.906×10^{-2}	3.308×10^{-1}	2.820×10^{-1}	4.179×10^{-2}	3.763×10^{-1}
4	1.719×10^{-2}	6.645×10^{-2}	1.391×10^{-1}	1.106×10^{-2}	1.885×10^{-1}
8	4.300×10^{-3}	1.975×10^{-2}	6.935×10^{-2}	2.985×10^{-3}	9.357×10^{-2}
16	1.074×10^{-3}	6.254×10^{-3}	3.463×10^{-2}	8.081×10^{-4}	4.664×10^{-2}
32	2.683×10^{-4}	2.013×10^{-3}	1.615×10^{-4}	1.614×10^{-4}	2.330×10^{-2}
rate	2.00	1.65	1.00	1.9	1.00

Table 5.1 : Errors and convergence rates: CG-CG scheme without inertial forces ($k_1 = 1, k_2 = 1$)

$1/h$	$\ U_1 - u_1\ _{L^2(\Omega_1)}$	$\ P_1 - p_1\ _{L^2(\Omega_1)}$	$\ D(U_1 - u_1)\ _{L^2(\Omega_1)}$	$\ P_2 - p_2\ _{L^2(\Omega_2)}$	$\ U_2 - u_2\ _{L^2(\Omega_2)}$
2	6.906×10^{-2}	3.320×10^{-1}	2.820×10^{-1}	4.182×10^{-2}	3.719×10^{-1}
4	1.720×10^{-2}	6.446×10^{-2}	1.391×10^{-2}	1.136×10^{-2}	1.947×10^{-1}
8	4.300×10^{-3}	1.900×10^{-2}	6.936×10^{-2}	2.990×10^{-3}	1.140×10^{-1}
16	1.07×10^{-3}	6.05×10^{-3}	3.464×10^{-2}	7.939×10^{-4}	8.258×10^{-2}
32	2.681×10^{-4}	1.995×10^{-3}	1.731×10^{-2}	1.706×10^{-4}	7.259×10^{-2}
rate	2.00	1.65	1.00	1.91	1.00

Table 5.2 : Errors and convergence rates: CG-CG scheme with inertial forces ($k_1 = 1, k_2 = 1$)

$1/h$	$\ U_1 - u_1\ _{L^2(\Omega_1)}$	$\ P_1 - p_1\ _{L^2(\Omega_1)}$	$\ D(U_1 - u_1)\ _{L^2(\Omega_1)}$	$\ P_2 - p_2\ _{L^2(\Omega_2)}$	$\ U_2 - u_2\ _{L^2(\Omega_2)}$
2	6.426×10^{-2}	3.345×10^{-1}	2.793×10^{-1}	1.052×10^{-1}	3.507×10^{-1}
4	1.598×10^{-2}	6.889×10^{-2}	1.366×10^{-1}	2.598×10^{-2}	1.625×10^{-1}
8	3.998×10^{-3}	2.909×10^{-2}	6.794×10^{-2}	6.418×10^{-3}	7.811×10^{-2}
16	9.989×10^{-4}	6.754×10^{-3}	3.390×10^{-2}	1.592×10^{-3}	3.841×10^{-2}
32	2.495×10^{-4}	2.248×10^{-3}	1.694×10^{-2}	3.963×10^{-4}	1.907×10^{-2}
rate	2.00	2.00	1.00	2.00	1.00

Table 5.3 : Errors and convergence rates: CG-DG scheme without inertial forces ($k_1 = 1, k_2 = 1$)

$1/h$	$\ U_1 - u_1\ _{L^2(\Omega_1)}$	$\ P_1 - p_1\ _{L^2(\Omega_1)}$	$\ D(U_1 - u_1)\ _{L^2(\Omega_1)}$	$\ P_2 - p_2\ _{L^2(\Omega_2)}$	$\ U_2 - u_2\ _{L^2(\Omega_2)}$
2	6.426×10^{-2}	3.271×10^{-1}	2.793×10^{-1}	1.054×10^{-1}	3.547×10^{-1}
4	1.598×10^{-2}	6.640×10^{-2}	1.367×10^{-1}	2.592×10^{-2}	1.643×10^{-1}
8	4.001×10^{-3}	2.047×10^{-2}	6.794×10^{-2}	6.417×10^{-3}	7.911×10^{-2}
16	1.000×10^{-3}	6.658×10^{-3}	3.390×10^{-2}	1.594×10^{-3}	3.896×10^{-2}
32	2.499×10^{-4}	2.304×10^{-3}	1.594×10^{-2}	3.970×10^{-4}	1.961×10^{-2}
rate	2.00	1.53	1.00	2.00	1.00

Table 5.4 : Errors and convergence rates: CG-DG scheme with inertial forces ($k_1 = 1, k_2 = 2$)

to the one without. However, as it has been shown in Chapter 3, the problem without the inertial forces requires an additional small data condition to prove existence and uniqueness of the weak solution. As mentioned earlier, there is no scientific consensus on the proper interface conditions. Physical experiments might be able to provide better insight as to which condition is better.

Example 20. *The boundary conditions are chosen so that the exact solution to the coupled Navier-Stokes/Darcy problem is:*

$$\begin{aligned} \mathbf{u}_1(x, y) &= \left(-\cos\left(\frac{\pi}{2}y\right) \sin\left(\frac{\pi}{2}x\right) + 1.0, \sin\left(\frac{\pi}{2}y\right) \cos\left(\frac{\pi}{2}x\right) - 1.0 + x \right), \quad \text{in } \Omega_1, \\ p_1(x, y) &= 1 - x, \quad \text{in } \Omega_1 \\ p_2(x, y) &= \frac{2}{\pi} \cos\left(\frac{\pi}{2}x\right) \cos\left(\frac{\pi}{2}y\right) - y(x - 1), \quad \text{in } \Omega_2 \end{aligned}$$

From Table (5.5) optimal convergence rates have been obtained for the Navier-Stokes velocity, pressure and Darcy pressure. The Darcy velocity is obtained through numerical differentiation of the pressure variable in the Darcy region. The only drawback for the continuous finite element method is that higher order approximations in the Darcy region can be obtained only after significant changes to the code. This,

$1/h$	$\ U_1 - u_1\ _{L^2(\Omega_1)}$	$\ P_1 - p_1\ _{L^2(\Omega_1)}$	$\ D(U_1 - u_1)\ _{L^2(\Omega_1)}$	$\ P_2 - p_2\ _{L^2(\Omega_2)}$	$\ U_2 - u_2\ _{L^2(\Omega_2)}$
2	7.173×10^{-2}	4.143×10^0	7.351×10^{-1}	4.080×10^{-2}	2.330×10^{-1}
4	1.812×10^{-2}	5.429×10^{-1}	2.433×10^{-1}	1.270×10^{-2}	1.405×10^{-1}
8	4.445×10^{-3}	1.598×10^{-1}	1.135×10^{-1}	3.417×10^{-3}	7.286×10^{-2}
16	1.097×10^{-3}	5.320×10^{-2}	5.540×10^{-2}	8.959×10^{-4}	3.670×10^{-2}
32	2.730×10^{-4}	1.885×10^{-2}	2.735×10^{-2}	1.962×10^{-4}	1.838×10^{-2}
rate	2.00	1.58	1.00	2.00	1.00

Table 5.5 : Errors and convergence rates: CG-CG scheme ($k_1 = 1, k_2 = 1$)

however, is not the case for the discontinuous Galerkin method.

$1/h$	$\ U_1 - u_1\ _{L^2(\Omega_1)}$	$\ P_1 - p_1\ _{L^2(\Omega_1)}$	$\ D(U_1 - u_1)\ _{L^2(\Omega_1)}$	$P_2 - p_2$	$\ U_2 - u_2\ _{L^2(\Omega_2)}$
2	6.058×10^{-2}	2.809×10^0	6.566×10^{-1}	3.479×10^{-2}	2.025×10^{-1}
4	1.615×10^{-2}	3.999×10^{-1}	2.337×10^{-1}	9.361×10^{-3}	1.026×10^{-2}
8	3.769×10^{-3}	1.201×10^{-1}	1.128×10^{-1}	2.326×10^{-3}	4.948×10^{-2}
16	9.350×10^{-4}	4.188×10^{-2}	5.557×10^{-2}	5.719×10^{-4}	2.427×10^{-2}
32	2.335×10^{-4}	1.482×10^{-2}	2.751×10^{-2}	1.412×10^{-4}	1.201×10^{-2}
rate	2.00	1.50	1.00	2.00	1.00

Table 5.6 : Errors and convergence rates: CG-DG ($k_1 = 1, k_2 = 1$)

Table (5.6) shows the numerical errors and convergence rates if the DG method of order one is used for the Darcy region. The resulting rate is of order one as predicted by the theory. Next the order of approximation in the Darcy region is increased to two for the same problem. The results are presented in Table (5.7). It is clear that the order two approximation achieves higher accuracy on coarser meshes compared to the order one approximation. A higher convergence rate of two for the Darcy pressure in Ω_2 . However, since Ω_1 has a lower order approximation there is no improvement in the quality of the solution in Ω_1 . The implementation of the discontinuous Galerkin method for this thesis has been done using monomial basis functions. Due to this

fact, the code is very flexible, making it is easy to change the order of approximation to an arbitrary degree n to approximate the pressure at any subset of the porous medium.

$1/h$	$\ \mathbf{U}_1 - \mathbf{u}_1\ _{L^2(\Omega_1)}$	$\ P_1 - p_1\ _{L^2(\Omega_1)}$	$\ \mathbf{D}(\mathbf{U}_1 - \mathbf{u}_1)\ _{L^2(\Omega_1)}$	$\ P_2 - p_2\ _{L^2(\Omega_2)}$	$\ \mathbf{U}_2 - \mathbf{u}_2\ _{L^2(\Omega_2)}$
2	6.058×10^{-2}	2.817×10^0	6.566×10^{-1}	4.841×10^{-3}	4.254×10^{-2}
4	1.615×10^{-2}	4.015×10^{-1}	2.337×10^{-1}	1.106×10^{-3}	1.154×10^{-2}
8	3.770×10^{-3}	1.203×10^{-1}	1.129×10^{-1}	3.041×10^{-4}	2.875×10^{-3}
16	9.352×10^{-4}	4.189×10^{-2}	5.557×10^{-2}	7.613×10^{-5}	7.155×10^{-4}
32	2.334×10^{-4}	1.482×10^{-2}	2.751×10^{-2}	1.915×10^{-5}	1.789×10^{-4}
rate	2.00	1.50	1.00	2.00	2.00

Table 5.7 : Numerical errors and convergence rates: CG-DG ($k_1 = 1, k_2 = 2$)

The optimal convergence rates proved in Chapter 4 have been numerically verified for the CG-CG and CG-DG schemes. It is also important to test the numerical solution for different ranges of the physical parameters of the model.

5.4 Effect of Physical Parameters

5.4.1 Permeability

The permeability in the porous medium is important in determining the flow characteristics of ground-water. Some difficulties in modeling porous media flow arise due to cracks, pinches or faults that occur in the domain. These physical features give rise to highly discontinuous permeability fields. First we investigate the effectiveness of each numerical scheme on problems with heterogeneous permeability in the porous medium. The kinematic viscosity ν for all cases is 1.0.

1. *Rock in porous medium*

The free flow domain $\Omega_1 = (0, 1) \times (1, 2)$ and the porous medium $\Omega_2 = (0, 1) \times (0, 1)$. The porous medium has a circular region with permeability $1 \times 10^{-11} \mathbf{I}$ surrounded by a medium with permeability \mathbf{I} . A Dirichlet boundary condition $\mathbf{u}_1 = (0, -1)$ is imposed on $\Gamma_1 = \partial\Omega_1 \setminus \Gamma_{12}$ and zero Dirichlet and Neumann conditions are imposed on the bottom and lateral boundaries of the domain Ω_2 respectively. Figure (5.1)(a) is a plot of the computational domain. Figures (5.1)(b),(c) and (d) are plots of the norm velocity obtained from each scheme from a mesh with 826 triangular elements in the porous medium and 206 elements in the free flow region. The CG-CG and CG-DG schemes are of order one. The DG-DG scheme is of order two. The CG-CG solution is obtained from a system with only 1143 degrees of freedom whereas the CG-DG requires 3199 degrees of freedom. It is clear that we observe the expected flow pattern in both schemes and that the CG-CG scheme is the least expensive method for this problem.

2. *Two intersecting fracture zones*

We test the model on a porous medium $\Omega_2 = (0, 1.6) \times (0, 1.5)$, with permeability of $10^{-8} \mathbf{I}$ with 2 intersecting faults with a permeability of $10^{-5} \mathbf{I}$. The free flow domain $\Omega_1 = (0, 1.6) \times (1.5, 2)$. A Dirichlet boundary condition $\mathbf{u}_1 = (0, -1)$ is imposed on the Navier-Stokes boundary and zero Neumann and Dirichlet boundary conditions are imposed on the porous medial flow boundary.

Figure (5.2) is a plot of the computational domain adapted from work by Kasschieter [30]. Kasschieter has compared the effectiveness of the mixed finite element to the classical finite element on particle tracking problems in saturated groundwater flow and concluded that the finite element method gives

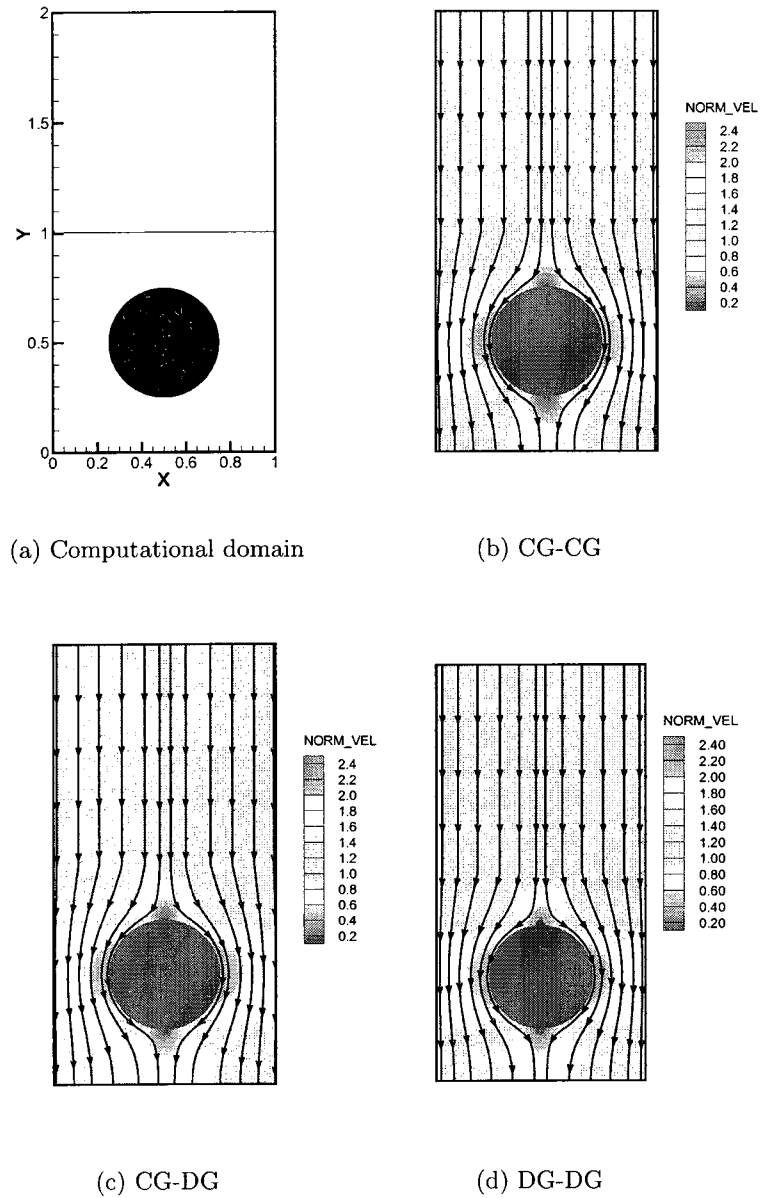


Figure 5.1 : Computational domain and numerical results

unphysical flow in fractured porous media.

Figure (5.3) is a plot of the streamlines and pressure contours of the solution

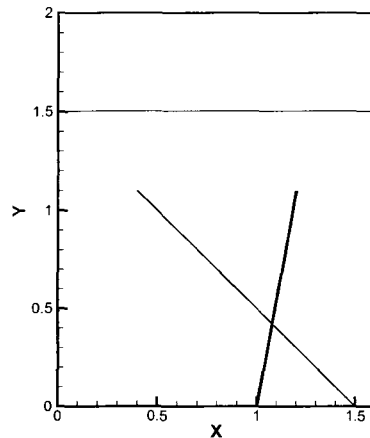


Figure 5.2 : Computational domain adapted from [30]

obtained from the CG-CG scheme from a mesh consisting of 170 elements in the free flow region and 541 elements in the porous medium. It is evident that none of the streamlines that approach the fault make it through the fault line. The flow pattern exhibited by this solution is unphysical as the fault fracture is an area of high permeability compared to the rock surrounding it. This unphysical flow generated by the continuous finite element method for this problem has also been reported in [30]. Figure (5.4) is a plot of the streamlines and pressure contours of the solution obtained from the CG-DG scheme on the same mesh used to produce the CG-CG solution in Figure (5.3). It is clear that the CG-DG solution shows the expected flow because the majority of streamlines entering the relatively high permeable faults exit the fault.

Upon further refinement, the CG-CG scheme produces the expected flow pattern in Figure ((5.5)) on an adaptively refined mesh with 8146 elements. This solution is obtained from a system with 4583 degrees of freedom, while the CG-

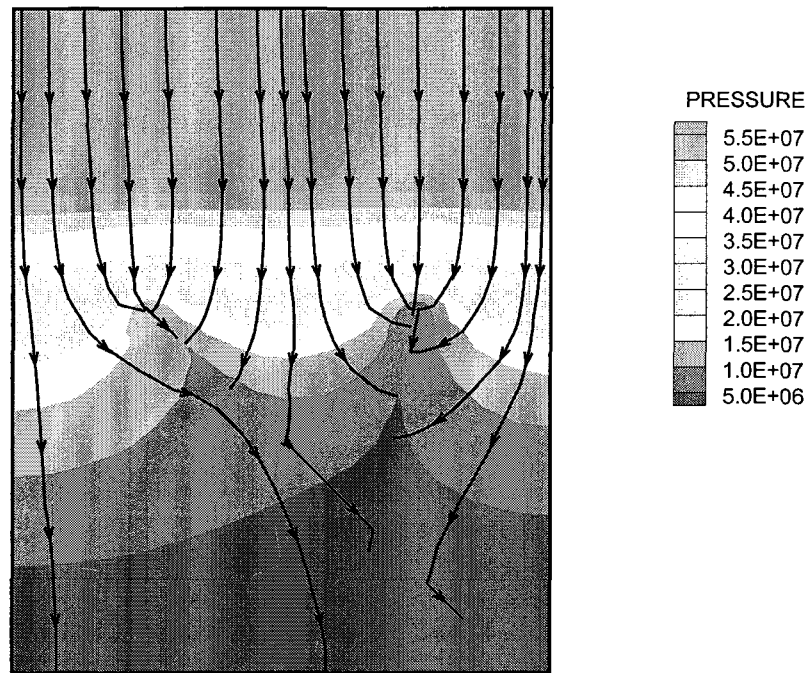


Figure 5.3 : CG-CG: velocity and pressure

DG solution in Figure (5.4) solves the problem with 2229 degrees of freedom. For this example the CG-DG solution is obtained from a smaller linear system therefore the scheme is more efficient.

Figure (5.6) is the solution obtained from the DG-DG scheme of order 2. It is clear from these examples that the CG-DG and DG-DG solutions are able to capture the underlying permeability well. However the DG-DG scheme in both domains is more computationally expensive hence the proposed coupling of the CG-DG scheme in this thesis.

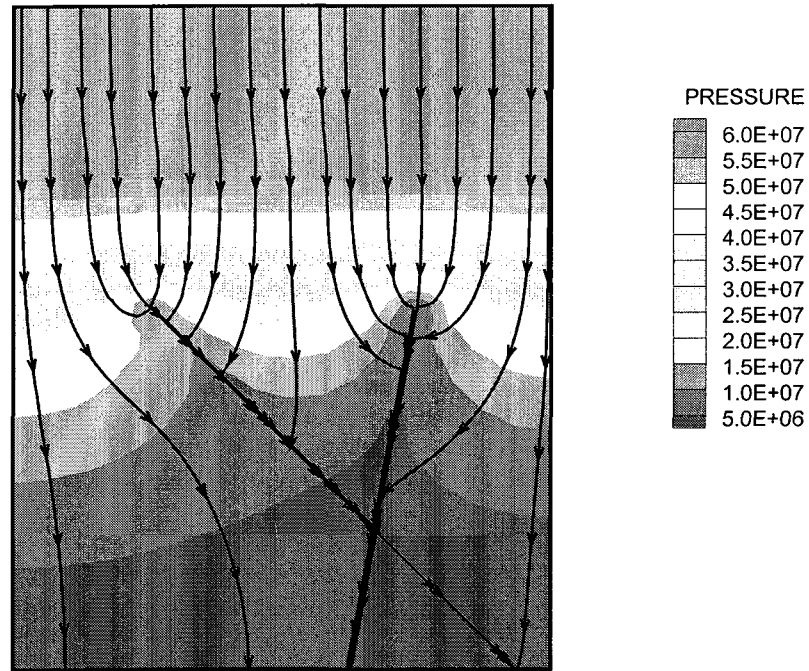


Figure 5.4 : CG-DG: velocity and pressure

Figure (5.7) is a plot of the velocity streamlines and the norm of the velocity at the intersection of the faults. The larger fault on the right has larger volume and therefore it forces the flow moving initially from left to right to move to the left. The above experiment shows that the CG-DG scheme is more robust under highly discontinuous permeability. The CG-CG solution is unphysical on a coarse mesh. The expected flow patterns were observed for the CG-CG scheme only after refining the mesh around the region with the fault. From this example it is clear that using the CG-DG scheme for problems with a high level

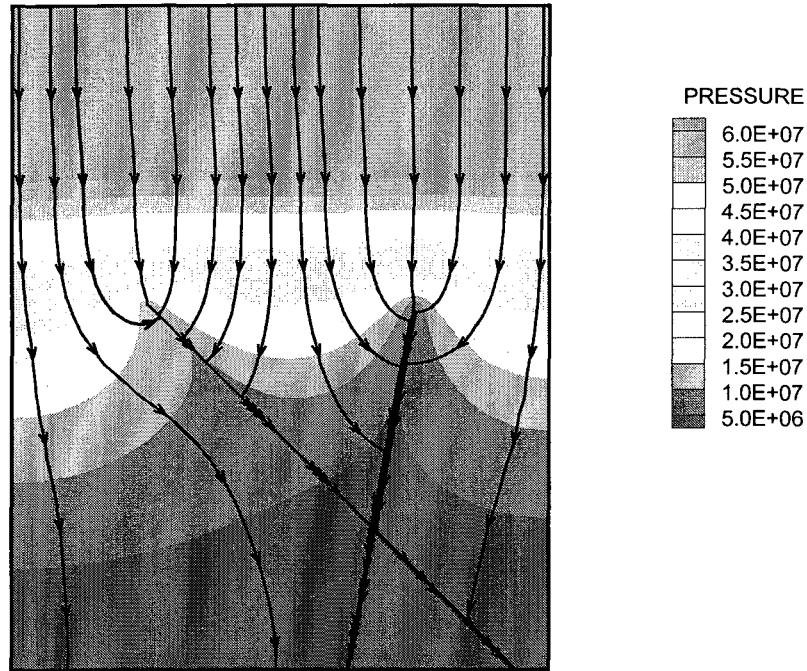


Figure 5.5 : CG-CG on refined mesh: velocity and pressure

of heterogeneity is more efficient than using a CG-CG scheme.

3. *Random Permeability*

In this example, the permeability in the porous medium assumes random values on each element between 0.001 and 1.0. The kinematic viscosity in the free fluid region ν is equal to 1.0. The exact solution of the problem is unknown, however we expect the model to show flow favoring areas of low permeability as it moves down in the porous medium. Figure (5.8) is a plot of the computational

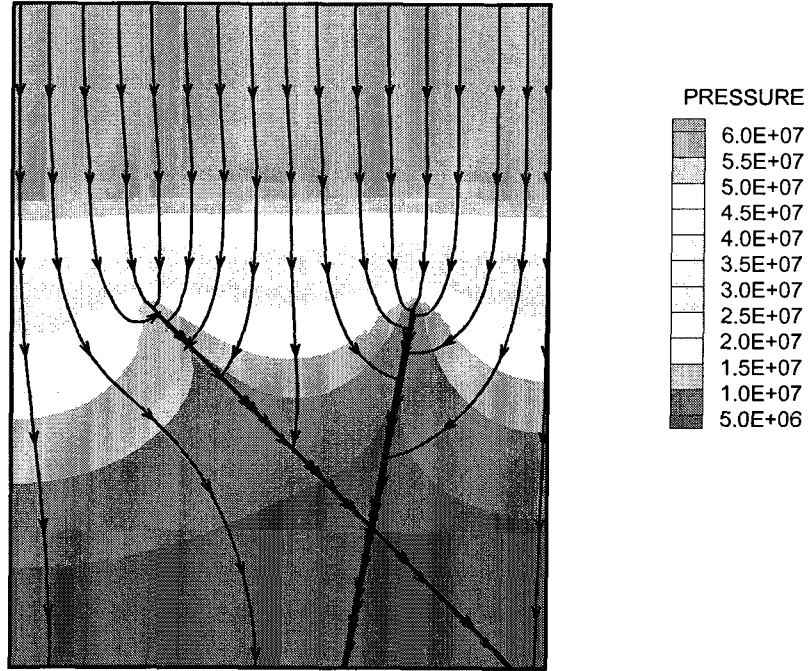


Figure 5.6 : DG-DG scheme of order two: velocity and pressure

domain consisting of 128 elements in the Navier-Stokes and Darcy domains. The underlying values of permeability on each element are also shown. The following boundary conditions are imposed:

$$\mathbf{u}_1 = (\pi - 2 \sin(\pi y), -\pi y) \text{ on } \Gamma_1$$

$$p_2 = \pi x y \text{ in } \Omega_1$$

$$g_D = \pi y^2 \text{ on } \Gamma_{2D}, \quad g_N = 0 \text{ on } \Gamma_{2N}$$

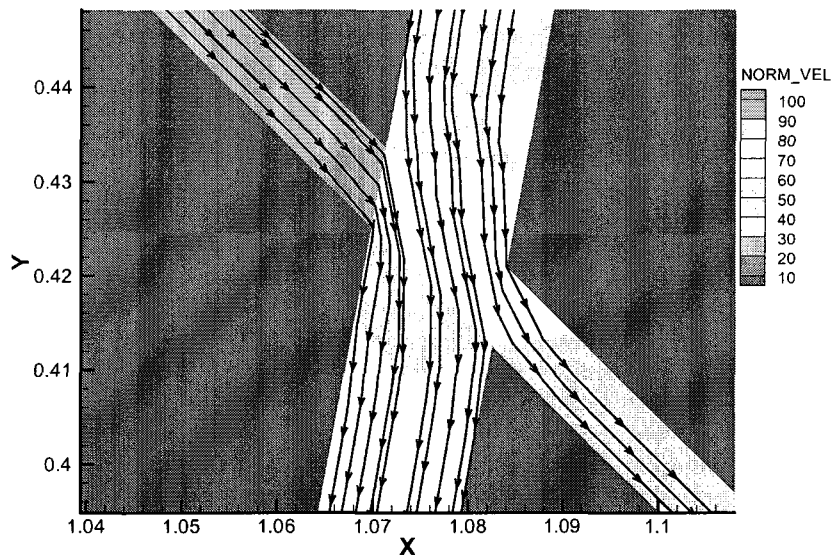


Figure 5.7 : CG-CG: streamlines and norm of velocity at fracture intersection

Figure (5.9) shows the norm of the velocity and the pressure of the solution obtained from the CG-DG scheme using the NIPG method with piecewise quadratic functions approximation the Darcy pressure. The CG-CG and DG-DG schemes give comparable results. The scheme converges in 8 Picard iterations with a set tolerance of 10^{-10} . The observed streamlines in Figure (5.9) (a) are as expected because the fluid particles are seen to avoid regions of the porous medium with low permeability. The pressure is lower in the porous medium because of the relatively low volume of fluid that makes its way across the interface.

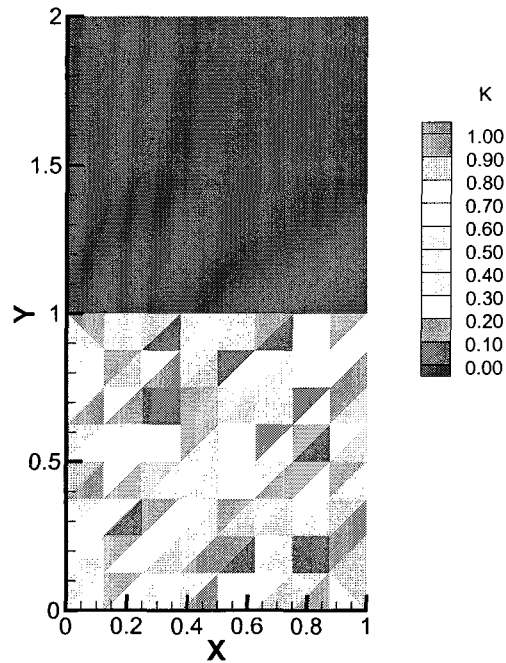


Figure 5.8 : CG-DG: Computational domain on random permeability field

5.4.2 Kinematic Fluid Viscosity

We consider the effect of the kinematic fluid viscosity ν on the CG-DG coupling of the Navier-Stokes Darcy coupling. One of the conditions needed for the proofs of existence of a solution for the coupled model was that the kinematic viscosity ν has to be large enough for a given set of data values. In this section we check optimal convergence rates and errors for decreasing value of ν to test the limits of the model.

Example 21. *The boundary conditions are chosen in such a way that the exact*

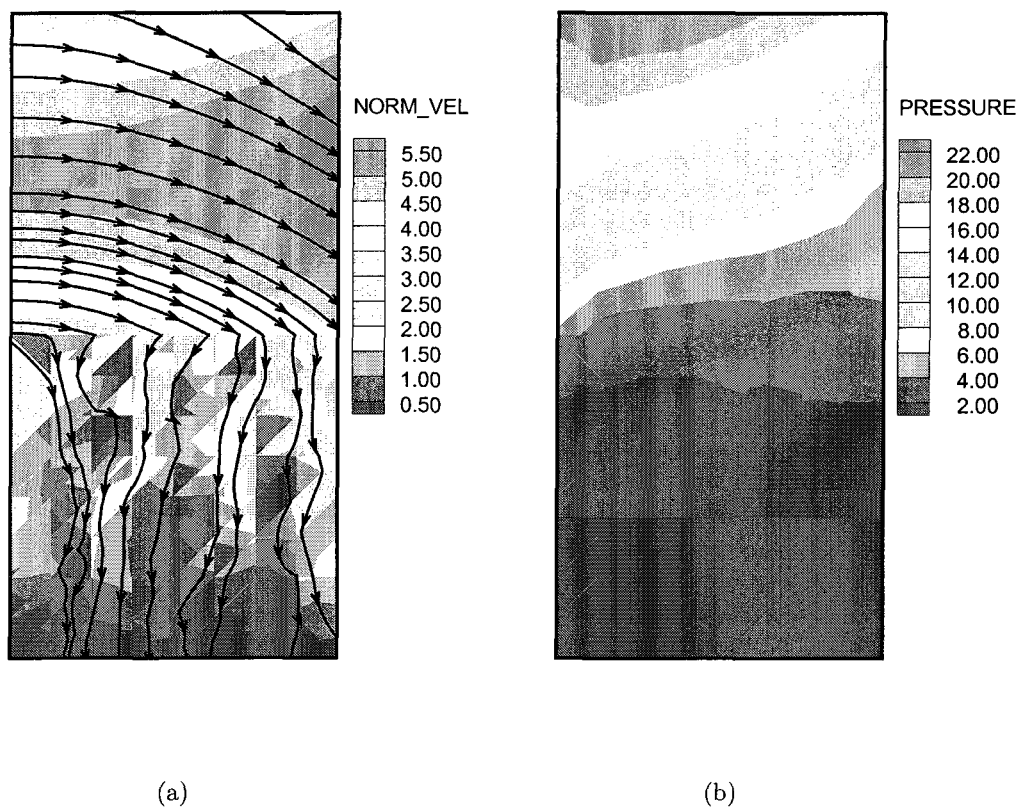


Figure 5.9 : CG-DG: Random permeability (a) Norm velocity and (b) Pressure

solution is:

$$\begin{aligned} \mathbf{u}_1(x, y) &= (y^2 - 2y + 1 + \nu(2x - 1), x^2 - x - (y - 1)2\nu), \\ p_1(x, y) &= 2\nu(x + y - 1.0) + \frac{1}{3k} - 4\nu^2, \\ p_2(x, y) &= \frac{1}{k}(x(1 - x)(y - 1) + \frac{y^3}{3} - y^2 + y) + 2\nu x. \end{aligned}$$

For each value of ν , numerical errors are computed on successive refinements on a coarse mesh with $h = 1/4$.

ν	N	$\ U_1 - u_1\ _{L^2(\Omega_1)}$	$\ P_1 - p_1\ _{L^2(\Omega_1)}$	$\ D(U_1 - u_1)\ _{L^2(\Omega_1)}$	$\ P_2 - p_2\ _{L^2(\Omega_1)}$	$\ U_2 - u_2\ _{L^2(\Omega_1)}$
1	8	6.183×10^{-5} (2.00)	7.208×10^{-4} (1.54)	8.485×10^{-3} (1.00)	6.616×10^{-5} (2.00)	7.100×10^{-3} (1.00)
0.1	10	6.201×10^{-5} (2.00)	8.358×10^{-5} (1.68)	8.485×10^{-3} (1.00)	6.615×10^{-5} (2.00)	7.100×10^{-3} (1.00)
0.01	18	6.329×10^{-5} (2.00)	4.089×10^{-5} (1.97)	8.489×10^{-3} (1.00)	6.612×10^{-5} (2.00)	7.100×10^{-3} (1.00)
0.001	23	6.462×10^{-5} (2.00)	4.074×10^{-5} (1.98)	8.897×10^{-3} (1.00)	6.611×10^{-5} (2.00)	7.101×10^{-3} (1.00)

Table 5.8 : Numerical errors and convergence rates for varying ν : CG-CG

Table (5.8) shows the convergence rates for each variable for different values of ν and error on a fine mesh consisting of 8192 elements using order 1 polynomials in the porous medium. The variable N is the number of Picard iterations required for convergence with a tolerance set at 1×10^{-10} . The hydraulic conductivity \mathbf{K} is the identity matrix. We observe optimal convergence rates for Reynolds number up to 1000 and an increase in the number of Picard iterations required to achieve convergence under the set tolerance.

5.5 Local Mass Conservation: An Application to Filtration Systems

The coupling of viscous flow and porous media flow that has been presented in this thesis can also be found in industrial filtration systems. In [17], a coupled Stokes/Darcy model is proposed for industrial filtration systems and solved using a mixed finite element formulation. Filtration systems play an important role in chemical industries in solid-liquid or solid-gas separations. The CG-CG and DG-DG schemes are applied to the filtration problem posed in [17].

The computational domain is a concentric quarter circular divided into the porous and free flow media domains as shown in Figure (5.5). The thickness of the free fluid

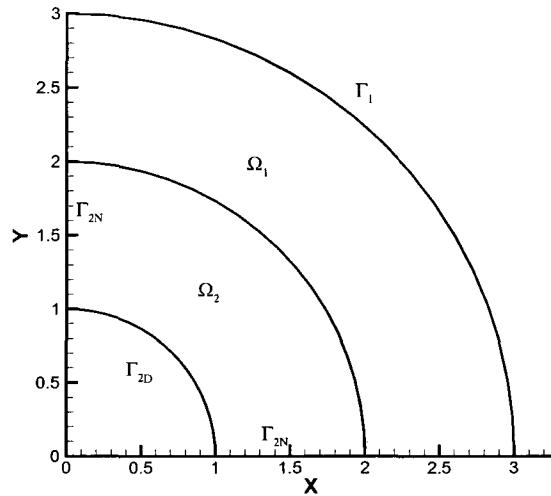


Figure 5.10 : Filter: Computational domain

and porous media domain is 0.02. The Navier-Stokes and Darcy domains consists of 3068 and 1847 triangular elements respectively. We impose $\mathbf{u}_1 = \left(-\frac{x}{30}, -\frac{y}{30}\right)$ on the circular part of circular part of Γ_1 and $\mathbf{u}_1 = (0, -1.0)$, $\mathbf{u}_1 = (-1.0, 0)$ on the lateral and horizontal segments of Γ_1 respectively. We impose zero Dirichlet and Neumann boundary conditions for the Darcy pressure on Γ_{2D} and Γ_{2N} respectively.

The low permeability in the porous medium causes a pressure build up during the filtration process. The life span of filtration equipment is heavily dependent on the hydrostatic pressure gradient that develops across the porous medium during filtration [17], as a result it is important to develop efficient models to determine the pressure gradient before any experiments are done. Mass conservation is an important component of any numerical model that effectively simulates the filtration process. We seek to test mass conservation for the CG-DG and DG-DG schemes. For each

numerical scheme we compute the ratio of mass lost between the inflow and outflow fluxes:

$$\frac{\sum_{e \in \Gamma_1} \int_e \mathbf{u}_1 \cdot \mathbf{n}_e - \sum_{e \in \Gamma_{2D}} \int_e \mathbf{u}_2 \cdot \mathbf{n}_e}{\sum_{e \in \Gamma_1} \int_e \mathbf{u}_1 \cdot \mathbf{n}_e}$$

The flow characteristics in Figure (5.11) are the same as observed in work by Hanspal

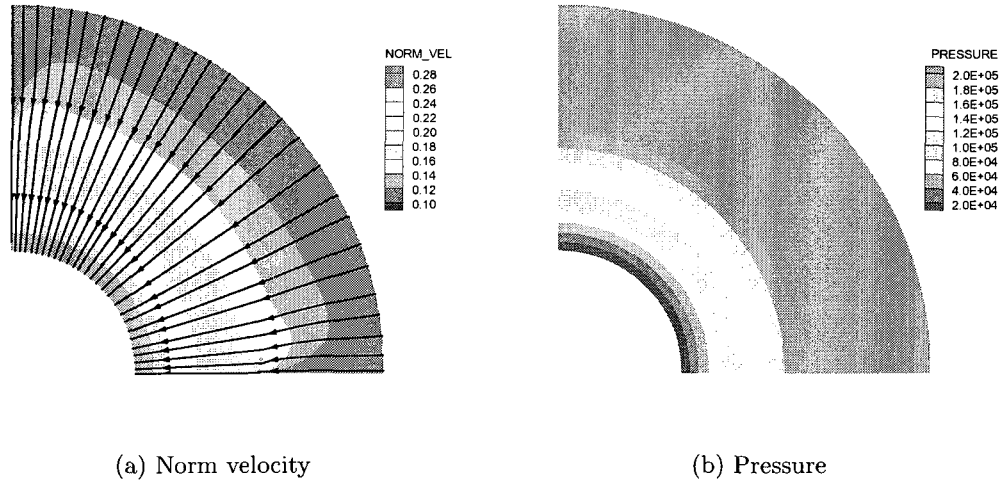


Figure 5.11 : Dead-end filter: CG-DG norm velocity and pressure

et al [17]. There is a 90% drop in the pressure from the interface to the Dirichlet boundary condition of the porous media flow region. This allows the filtration process to occur efficiently. The observed mass loss for the CG-CG scheme is 1.8%, 2.57% for the CG-CG scheme and 0.02% for the DG-DG scheme. The local mass conservation property of the DG method pays off. The DG-DG scheme outperforms the CG-CG and CG-DG schemes. From this it is clear that when local mass conservation is of great importance we have to pay the computational cost of the DG-DG. All

the schemes have a mass loss less than 5% which is very good for most practical applications.

5.6 Comparison of Interface conditions

In this section we perform a numerical study on the effect of the choice of including the inertial forces on the interface. In Chapter (2) we introduced an interface condition that relates the balance of forces in two forms, one including inertial forces and another without. The interface conditions are recalled below:

1. including inertial forces

$$((-2\nu\mathbf{D}(\mathbf{u}_1) + p_1\mathbf{I})\mathbf{n}_{12}) \cdot \mathbf{n}_{12} + \frac{1}{2}(\mathbf{u}_1 \cdot \mathbf{u}_1) = p_2, \quad (5.5)$$

2. without inertial forces

$$((-2\nu\mathbf{D}(\mathbf{u}_1) + p_1\mathbf{I})\mathbf{n}_{12}) \cdot \mathbf{n}_{12} = p_2, \quad (5.6)$$

In consultation with Dr. Matteo Pasquali, the condition with inertial forces can also be written in the following manner:

$$((-2\nu\mathbf{D}(\mathbf{u}_1) + p_1\mathbf{I})\mathbf{n}_{12}) \cdot \mathbf{n}_{12} + \frac{1}{2}\rho(\mathbf{u}_1 \cdot \mathbf{n}_{12})^2 = p_2, \quad (5.7)$$

with ρ the fluid velocity. The techniques that have been used in this work to prove existence and uniqueness do not work with this interface condition. This section provides numerical test cases to try to understand the impact of this condition of the coupling. The purpose of this study is to compare the numerical solutions obtained from the schemes W_A^h and W_B^h resulting from using conditions (5.5) and (5.6) respectively and the scheme denoted by W_C^h using condition (5.7)

First we compare the schemes W_A^h and W_B^h . Next, we compare these two schemes to W_C^h . It is not clear which condition is the most physical. In my view laboratory experiments might shed more light into which is the most suitable condition. These experiments are beyond the scope of this work. We start with an example that is motivated by the driven cavity flow problem.

Example 22. *We consider the following Dirichlet boundary conditions for the Navier-Stokes region ($\Omega_1 = (0, 1) \times (0, 1)$):*

$$\begin{aligned} \mathbf{u}_1 &= (\sin(\pi x), 0), \quad \text{on } (0, 1) \times \{2\}, \\ \mathbf{u}_1 &= (0, 0), \quad \text{on } (\{0\} \times (1, 2)) \cup (\{1\} \times (1, 2)) \end{aligned}$$

For the Darcy region ($\Omega_2 = (0, 1) \times (1, 2)$), we assume zero Neumann boundary condition for the vertical boundaries and zero Dirichlet boundary condition for the horizontal boundary. We use the CG-DG scheme of order one. The kinematic viscosity ν is chosen to be equal to one.

First we verify convergence of the numerical scheme for each model. Since the exact solution is unknown we compute the difference between solutions between successive refinements.

$1/h$	$\ P_1^{2h} - P_1^h\ _{L^2(\Omega_1)}$	$\ D(U_1^{2h} - U_1^h)\ _{L^2(\Omega_1)}$	$\ U_2^{2h} - U_2^h\ _{L^2(\Omega_2)}$
4	6.797×10^{-1}	9.397×10^{-1}	1.100×10^{-2}
8	2.071×10^{-1}	4.633×10^{-1}	2.866×10^{-3}
16	9.069×10^{-2}	2.392×10^{-1}	1.123×10^{-3}
32	4.024×10^{-2}	1.241×10^{-1}	5.290×10^{-4}
ratio	2.25	1.92	2.12

Table 5.9 : Relative numerical errors and ratios for model W_A^h with choice $k_2 = 1$.

$1/h$	$\ P_1^{2h} - P_1^h\ _{L^2(\Omega_1)}$	$\ D(U_1^{2h} - U_1^h)\ _{L^2(\Omega_1)}$	$\ U_2^{2h} - U_2^h\ _{L^2(\Omega_2)}$
4	6.797×10^{-1}	9.387×10^{-1}	1.234×10^{-2}
8	2.071×10^{-1}	4.633×10^{-1}	2.947×10^{-3}
16	9.067×10^{-2}	2.391×10^{-1}	1.066×10^{-3}
32	4.024×10^{-2}	1.241×10^{-1}	4.790×10^{-4}
ratio	2.25	1.92	2.22

Table 5.10 : Relative numerical errors and ratios for model W_B^h and the choice $k_2 = 1$.

From Tables (5.9) and (5.10) we observe the expected convergence rate of $\mathcal{O}(h)$ for the Navier-Stokes pressure, velocity and Darcy pressure.

Further, we analyze the solutions obtained from the two models on a uniform triangulation of the domain consisting of 16384 elements. In Fig. (5.12), we show the velocity streamlines obtained from the schemes W_A^h and W_B^h . They are almost identical to each other. The Euclidean norm of the velocity field is of order one. For a better comparison, we compute the difference between the two solutions. Fig. (5.13)(a) shows the contours of the difference between the two approximations of the x -component of the velocity field. We observe that the difference is very small, of the order 10^{-5} . A similar comment can be made about the difference between the two approximations of the y -component of the velocity field (see Fig. (5.13)(b)). The difference between the two approximations of the pressure is slightly larger, namely of the order 10^{-3} (see (5.15)).

Finally we repeat the same experiment but we set the fluid viscosity equal to 0.005. Fig. (5.15) shows the difference between the approximations of the two models. Overall the difference is small, of the order 10^{-5} . At some localized areas near the interface, the difference increases to 10^{-3} .

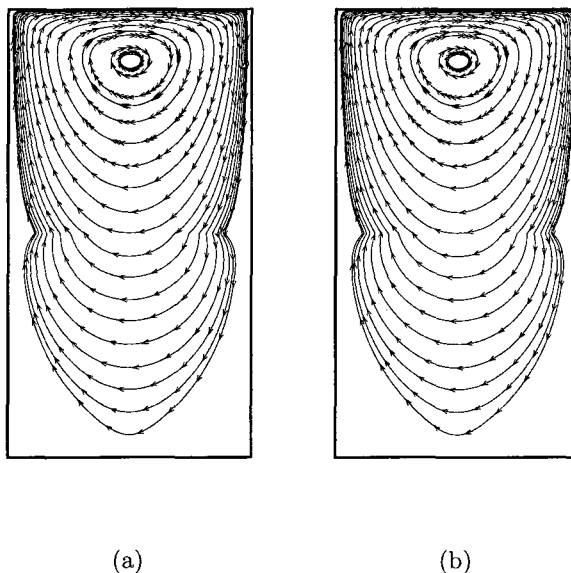


Figure 5.12 : Streamlines for the numerical velocity for the model without inertial forces (a) and with inertial forces (b) for viscosity equal to 1.

In Example (22) the magnitude of the inertial forces and the inflow through the interface are $\mathcal{O}(10^{-3})$ and $\mathcal{O}(10^{-2})$ respectively. In this case we have observed that the solutions obtained from the two models are the same. Next we consider an example in which the magnitude of the inertial forces and the inflow through the interface are $\mathcal{O}(1)$.

Example 23. *On the computational domain with $\Omega_1 = (0, 1) \times (0, 1)$ and $\Omega_2 = (0, 1) \times (1, 2)$, we impose the following boundary conditions:*

$$\mathbf{u}_1 = \left(0.0, -2\pi e^{-\left\{ \frac{r^2}{|r^2 - (x - \epsilon - 0.5)^2|} \right\}} \right) \text{ for } (0.2 \leq x \leq 0.8)$$

with the parameters $\epsilon = 10^{-6}$ and $r = 0.3 + \epsilon$ and a no-slip condition on the rest

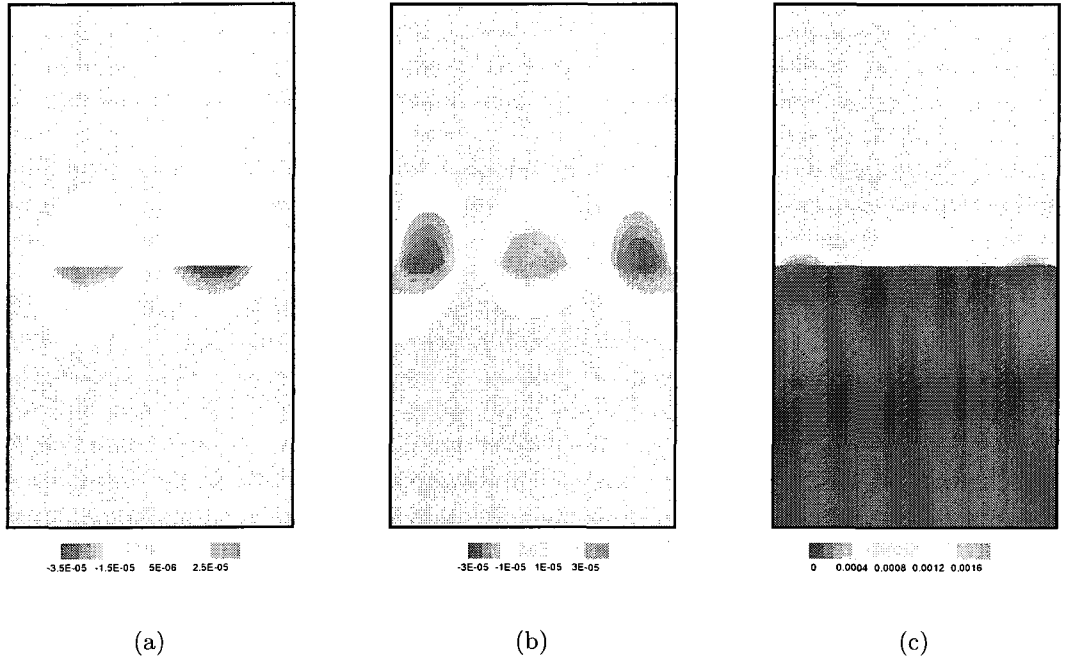


Figure 5.13 : Difference between the solutions obtained from the two models for viscosity equal to 1: (a) x -component of velocity, (b) y -component of velocity and (c) pressure.

of Γ_1 . We also impose Dirichlet and Neumann boundary conditions $g_D = 1.0$ and $g_N = 0.0$ on the bottom and lateral boundaries respectively. The external functions acting on the fluid in the Navier-Stokes and Darcy domains are set to $(0.0, 2.0)$ and zero respectively. The kinematic viscosity ν is equal to 1.0 and $\mathbf{K} = \mathbf{I}$.

First we verify convergence rates for the schemes W_A^h and W_B^h for the boundary conditions stated above. The NIPG method with a penalty parameter set equal to one is used for the discontinuous Galerkin method.

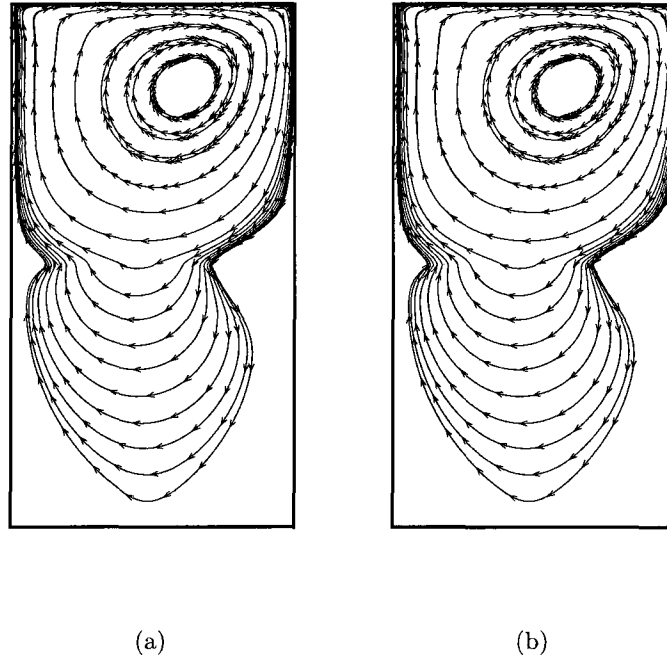


Figure 5.14 : Streamlines for the numerical velocity for the model without inertial forces (a) and with inertial forces for viscosity equal to 0.005.

$1/h$	$\ P_1^{2h} - P_1^h\ _{L^2(\Omega_1)}$	$\ D(U_1^{2h} - U_1^h)\ _{L^2(\Omega_1)}$	$\ U_2^{2h} - U_2^h\ _{L^2(\Omega_2)}$
4	1.391×10^0	1.890×10^0	1.335×10^{-1}
8	4.983×10^0	1.132×10^0	4.067×10^{-2}
16	2.413×10^{-1}	6.665×10^{-1}	1.888×10^{-2}
32	1.086×10^{-1}	3.643×10^{-1}	7.570×10^{-3}
ratio	2.22	1.82	2.00

Table 5.11 : Relative numerical errors and ratios for model W_A^h and the choice $k_2 = 1$.

In Tables (5.11) and (5.12) we list the norms of the differences in the solutions from successive refinements. From the ratios computed at each level we obtain the

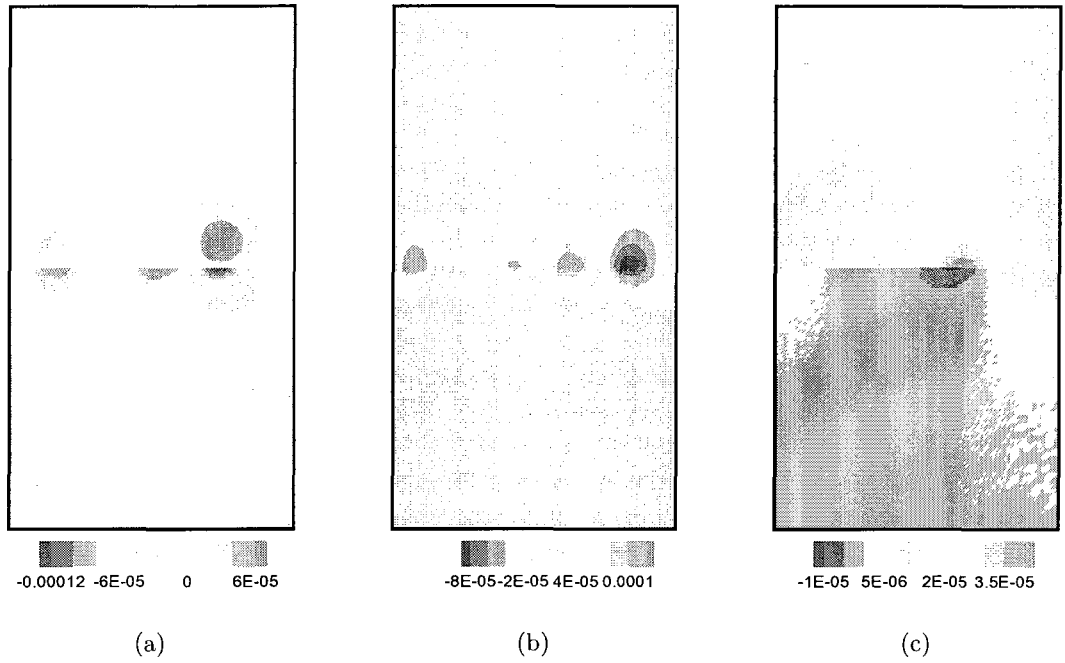


Figure 5.15 : Difference between the solutions obtained from the two models for viscosity equal to 0.005: (a) x -component of velocity, (b) y -component of velocity and (c) pressure.

$1/h$	$\ P_1^{\frac{h}{2}} - P_1^h\ _{L^2(\Omega_1)}$	$\ D(U_1^{\frac{h}{2}} - U_1^h)\ _{L^2(\Omega_1)}$	$\ U_2^{\frac{h}{2}} - U_2^h\ _{L^2(\Omega_2)}$
4	1.395×10^0	1.893×10^0	1.379×10^{-1}
8	4.985×10^{-1}	1.133×10^0	4.026×10^{-2}
16	2.417×10^{-1}	6.665×10^{-1}	1.756×10^{-2}
32	1.087×10^{-1}	3.641×10^{-1}	8.699×10^{-3}
ratio	2.22	1.83	2.00

Table 5.12 : Relative numerical errors and ratios for model W_B^h and the choice $k_2 = 1$.

expected convergence rate $\mathcal{O}(h)$ for the gradient norm of the Navier-Stokes velocity and Darcy pressure. Next we study the effect of the kinematic viscosity ν on the numerical schemes W_A^h and W_B^h . We fix the value of $\mathbf{K} = \mathbf{I}$.

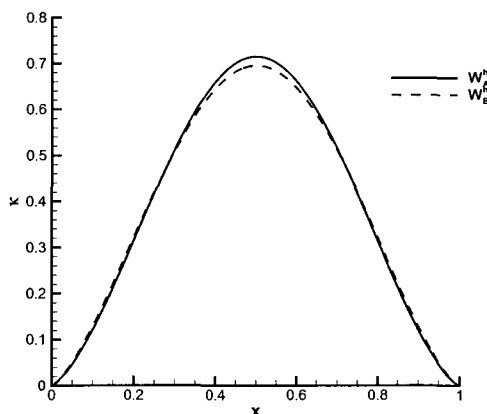


Figure 5.16 : Inertial forces (κ) for model W_A^h and W_B^h for $\nu = 1.0$ and $\mathbf{K} = \mathbf{I}$.

Fig. (5.16) is a plot of $\kappa = \frac{1}{2} \mathbf{u}_1 \cdot \mathbf{u}_1$, the inertial forces on the interface for both numerical schemes for the boundary conditions outlined above with $\nu = 0.1$. There is a very small difference in the value of the inertial forces obtained from the two numerical schemes. The numerical solutions obtained from the two models are the same as shown in Fig. (5.17).

Fig. (5.18) is a plot of the value of the inertial forces for the two models for $\nu = 0.1$. It is clear that that the scheme W_A^h produces larger values of the inertial forces on the interface. A further decrease in the kinematic viscosity results in a larger contrast in the value of the inertial forces on the interface from the two solutions (see Fig. (5.19)). Fig. (5.20)(a) shows that the solution from model W_A^h has flow patterns concentrated at the center due to large eddies that form near the boundary. On the

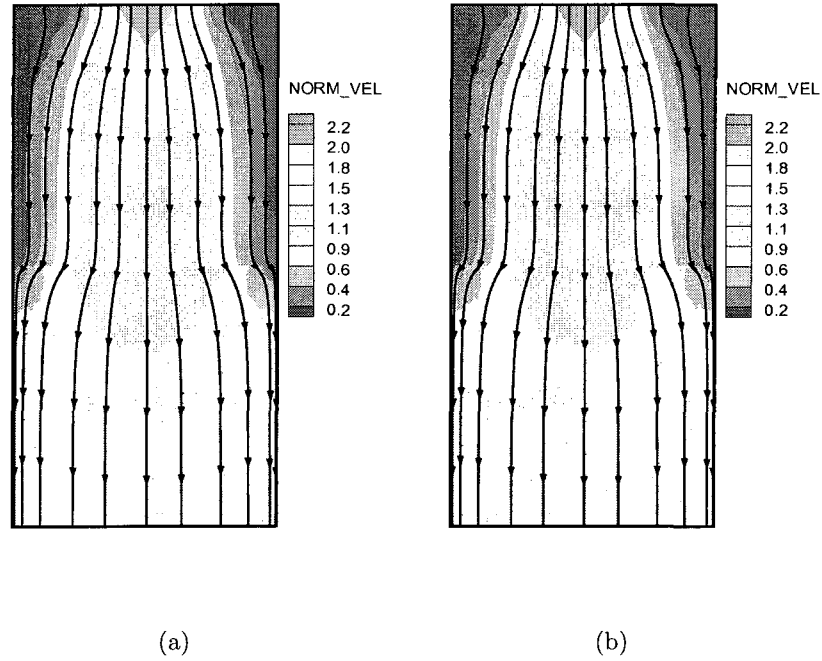


Figure 5.17 : Norm of velocity for model W_A^h (a) and W_B^h (b) for $\nu = 1.0$ and $\mathbf{K} = \mathbf{I}$.

other hand the solution from model W_B^h (see Fig. (5.20)(b)) appears less affected by the eddies and is less concentrated at the center. It is not clear which solution is correct or more physical, further clarification could be obtained through the help of physical experiments. Next we analyze the effect of the hydraulic conductivity \mathbf{K} on the numerical solutions obtained from the schemes. First we set the kinematic viscosity equal to 1.0 and then solve the coupled problem for different values of \mathbf{K} .

Fig. (5.21)(a) is a plot of the value of the inertial forces (κ) along the interface for decreasing hydraulic conductivity starting with a value of 10^{-2} for model W_A^h . Fig. (5.21)(b) is a plot of the flux $= (\mathbf{u}_1 \cdot \mathbf{n}_{12})$ which quantifies the amount of flow passing through the interface. As the permeability decreases we see that the flux

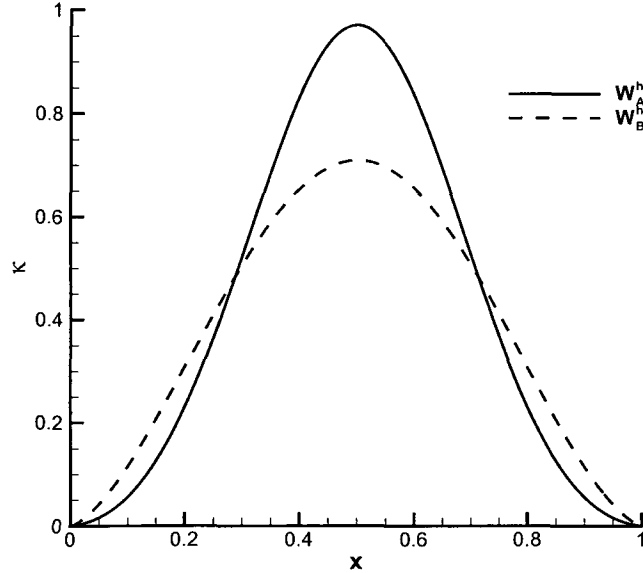


Figure 5.18 : Inertial forces (κ) for solution W_A^h and W_B^h for $\nu = 0.1$ and $\mathbf{K} = \mathbf{I}$.

through the interface decreases on the central part of the domain (see Fig. (5.21)(b)), the same pattern is observed for the inertial forces(κ) in Fig. (5.21)(a). The low permeability forces the flow towards boundary as a result the value of the inertial forces and flux is greater near the boundary. The same flow characteristics are observed in the solution from model W_B^h (see Fig. (5.22)). The solutions obtained from model W_A^h and W_B^h are the same (see for example Fig. (5.23) for the case $\mathbf{K} = 10^{-8}\mathbf{I}$). We conclude that for $\nu = 1.0$ the two models give comparable solutions. At low permeability, the numerical solutions obtained from the two schemes are comparable even at low kinematic viscosity. From Fig. (5.24) it is evident that the values of the inertial forces on both sides of the interface for the solutions from both models are identical for $\mathbf{K} = 10^{-8}$ and $\nu = 0.01$. The solutions obtained from model W_A^h and

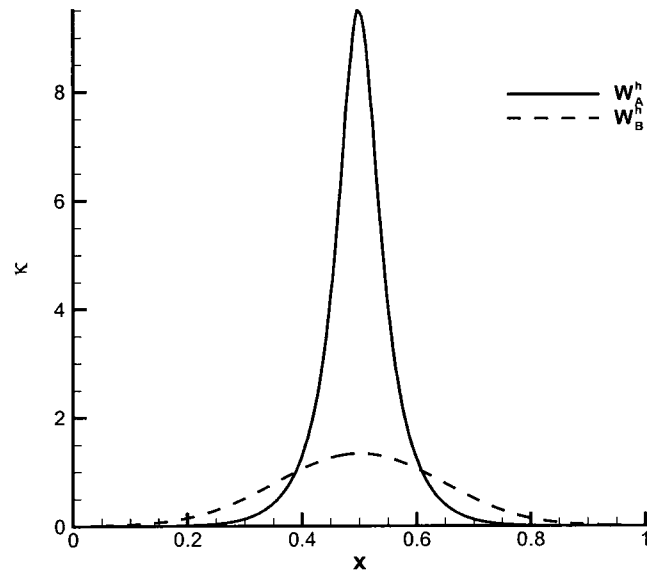


Figure 5.19 : Inertial forces (κ) for model W_A^h and W_B^h for $\nu = 0.01$ and $\mathbf{K} = \mathbf{I}$.

W_B^h are also the same (see Fig. (5.25)).

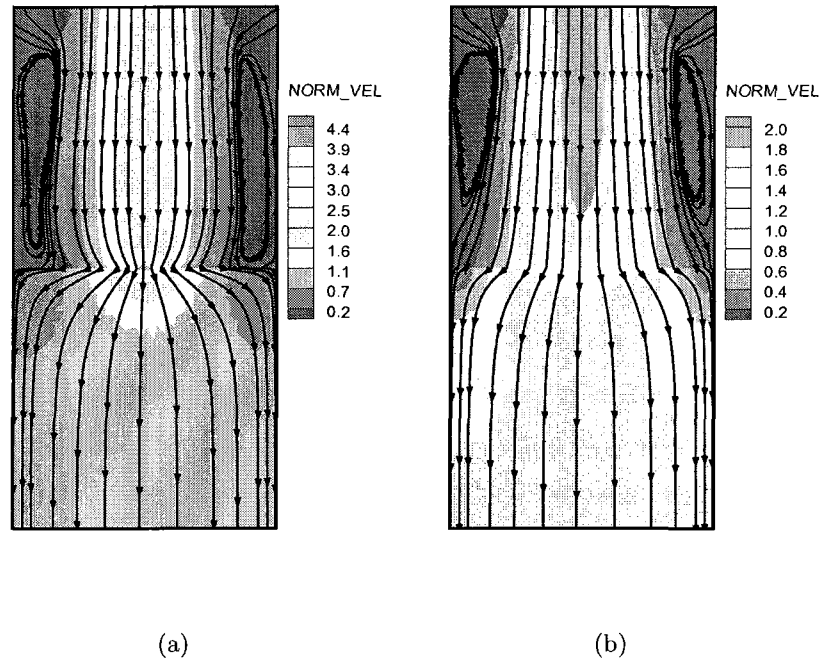


Figure 5.20 : Streamlines and norm velocity for the models W_A^h (a) and W_B^h (b) for $\nu = 0.01$ and $\mathbf{K} = \mathbf{I}$.

The next example will be used to compare conditions (5.5),(5.6) and (5.7). The condition (5.7) takes into account the normal component of the velocity into the inertial forces. As we would expect, a flow parallel to the surface of the interface should have lower inertial forces compared to the flow orthogonal to the surface. For simplicity the fluid density ρ is equal to one.

Example 24. *Polygonal Interface*

The domain is $\Omega = (0, 2) \times (0, 1.25)$ divided into the Navier-Stokes and Darcy region by a polygonal line Γ_{12} consisting of three forward steps of equal height equal to $1/4$

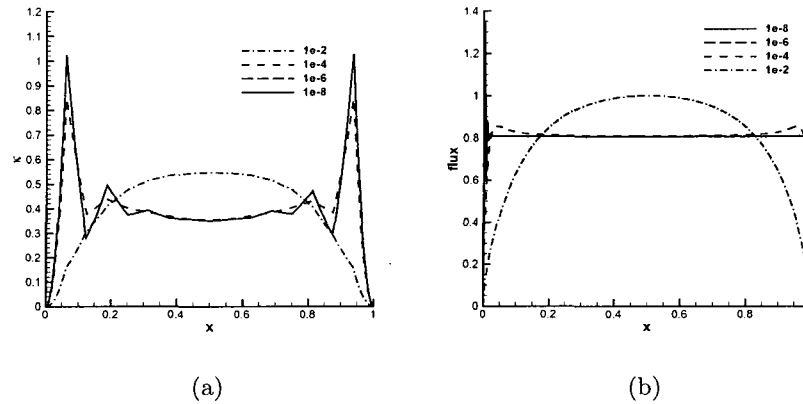


Figure 5.21 : Inertial forces κ (a) and flux (b) for model W_A^h for different values of K and $\nu = 1.0$.

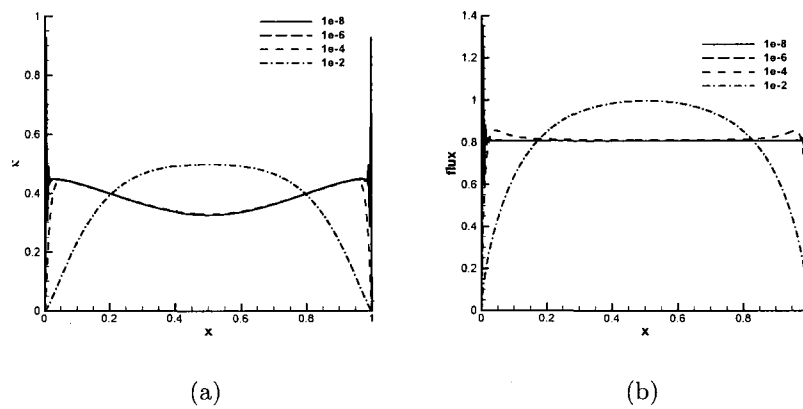


Figure 5.22 : Inertial forces (a) and flux (b) for model W_B^h for different values of K and $\nu = 1.0$.

(see Figure (5.26)). The porous medium has intrinsic permeability equal to $10^{-5}I$ and

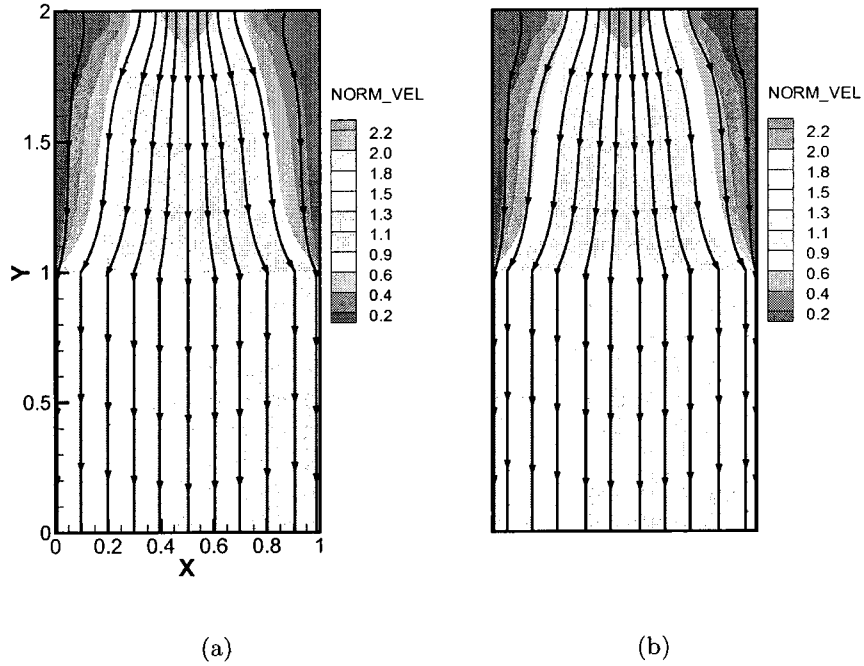


Figure 5.23 : Norm velocity for models W_A^h (a) and W_B^h (b) for $\mathbf{K} = 10^{-8}\mathbf{I}$ and $\nu = 1.0$.

is the subregion below the interface. The boundary conditions are set as follows:

$$\begin{aligned} \mathbf{u}_1 &= -3(y - 5/4)(y - 1/2) \text{ on } \Gamma_1 \\ g_D &= 0 \text{ on } \Gamma_{2D}, g_N = 0 \text{ on } \Gamma_{2N}, \mathbf{f}_1 = \mathbf{0}, f_2 = 0 \end{aligned}$$

The lateral boundary of the porous medium is Γ_{2D} , the rest of the domain in Γ_{2N} .

Figures (5.28) and (5.27) are plots of the norm of velocity profile for the solutions obtained from each scheme. In each plot the solution due to the condition (5.7) is plotted with a dotted line. It is clear that in this particular case and in other

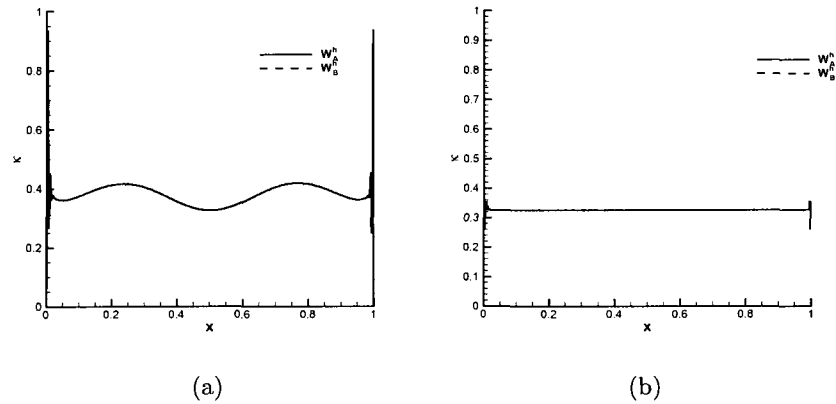


Figure 5.24 : Inertial forces on NSE (a) and Darcy (b) sides of interface for W_A^h and W_B^h for $\mathbf{K} = 10^{-8}\mathbf{I}$ and $\nu = 0.01$.

profiles extracted the norm of velocity is the same for each scheme. As expected the profile show a decrease associated with the interface between the free flow region and the porous medium as the fluid slows down. The addition of the normal velocity in balance of velocity component in this case does not seem to affect the solution. All solutions converge in 4 Picard Iterations with a tolerance set at 10^{-6} . Next we repeat the simulation with a smaller value of ν . For the same example above the kinematic viscosity ν is set equal to 0.01. The solutions from schemes W_A^h and W_B^h have been shown to differ under low viscosity. Figure (5.29) shows the norm velocity profiles of the solutions are compared along $y = 0.6$. From Figure (5.29) we note that for $0.0 \leq x \leq 0.5$, the solution with the condition (5.7) appears to be smaller than that due to (5.5), however along $x = 0.5$ the solution from scheme W_C^h has a slightly larger norm velocity. This small difference can possibly be explained by the fact that as expected the condition (5.7) will allow for more flow when the surface is

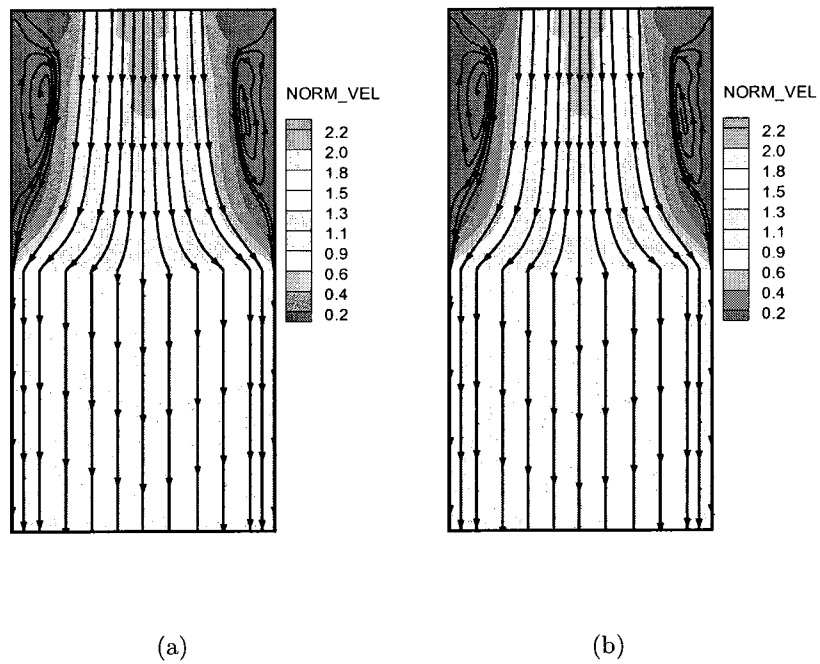


Figure 5.25 : Norm of velocity for models W_A^h (a) and W_B^h (b) for $\mathbf{K} = 10^{-8}\mathbf{I}$ and $\nu = 0.01$.

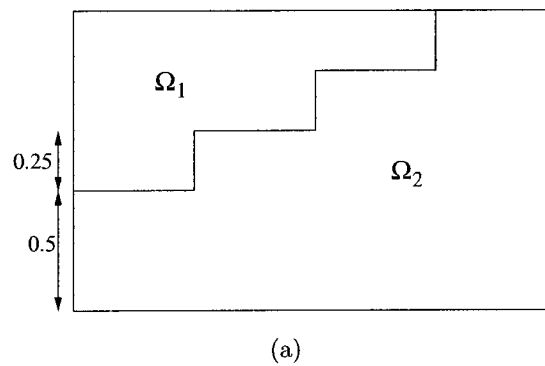
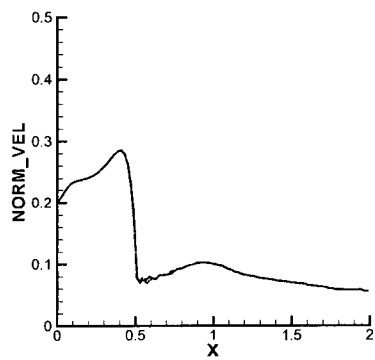
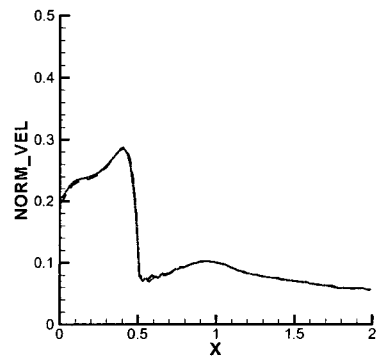
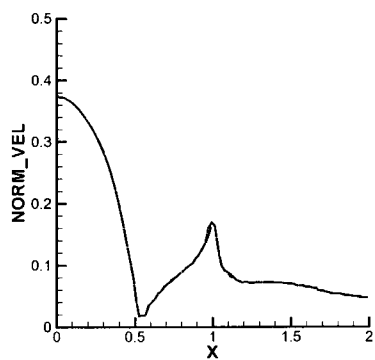
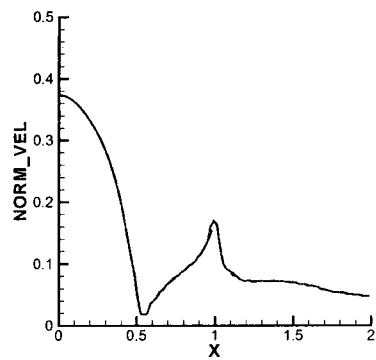


Figure 5.26 : Computational domain with polygonal interface

(a) W_A^h, W_C^h (b) W_B^h, W_C^h Figure 5.27 : Norm of velocity profiles along $y = 0.60$ for schemes W_A^h , W_B^h and W_C^h .(a) W_A^h, W_C^h (b) W_B^h, W_C^h Figure 5.28 : Norm of velocity profiles along $y = 0.75$ for schemes W_A^h , W_B^h and W_C^h .

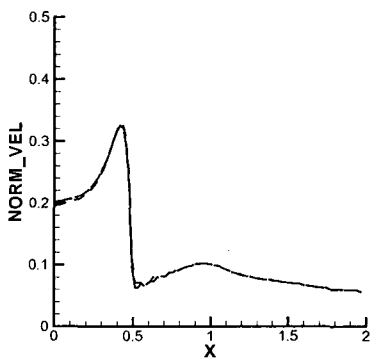
(a) W_A^h, W_C^h

Figure 5.29 : Norm of velocity profiles along $y = 0.60$ for schemes W_A^h and W_C^h for $\nu = 0.01$.

orthogonal to the direction of the flow. However, the differences are not significant enough to conclude that the condition (5.7) add new information to the solution of the coupled Navier-Stokes/Darcy problem. To conclude tests with this example we run the schemes under high permeability in the porous medium. The velocity profiles are shown in Figure (5.30) for $\mathbf{K} = \mathbf{I}$. The solution from scheme W_C^h is shown in the dashed line and the one due to W_A^h has a solid line. We note that there is not significant difference in the solutions.

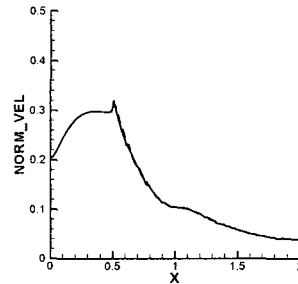
(a) W_A^h, W_C^h

Figure 5.30 : Norm of velocity profiles along $y = 0.6$ for schemes W_A^h and W_C^h for $K = I$.

Conclusion

Optimal convergence rates have been shown for the CG-CG and CG-DG scheme. The CG-CG scheme has a drawback in cases where higher order approximations might be needed to better capture the flow as significant modifications need to be made to the implementation. The CG-DG scheme is robust under all physical parameters that are crucial to the model. The CG-CG scheme exhibits unphysical behaviour under highly heterogeneous porous medium and requires a larger system to produce the expected result. The DG-DG scheme achieves higher order approximations but it is relatively computationally expensive. In view of the problems that the schemes have been tested on it is clear that solving the coupled Navier-Stokes and Darcy problem using the CG-DG scheme is more efficient than using the continuous Galerkin method. A numerical study of the interface conditions concludes that adding inertial forces to the model has an impact at low permeability, at this point it is not clear which

solution would be correct. The best way to determine the best interface condition is to perform physical experiments.

Chapter 6

Two Grid Method

The coupled Navier-Stokes and Darcy problem analyzed in this thesis results in large non-linear coupled systems which maybe time consuming to solve. This chapter improves the computational efficiency of the numerical schemes introduced in Chapter 5. We introduce a two-grid technique for both the Stokes/Darcy and Navier-Stokes/Darcy problems that naturally decouples the coupled model into two relatively smaller problems. The first will be a modified Navier-Stokes problem (or Stokes problem) to solve for the fluid velocity and pressure in the free flow domain. The second will be a modified Darcy problem to solve for the Darcy pressure in the porous medium. The two grid technique has several advantages. First it allows for parallelization of the code. Second, legacy codes exist that have been optimized to solve the Stokes, Navier-Stokes or Darcy problems separately. These codes can be used once the model has been decoupled. In this chapter we apply the two-grid decoupling method to both the coupled Stokes/Darcy and coupled Navier-Stokes/Darcy problems. We show that this method results in a more efficient scheme without compromising the accuracy of the solution.

6.1 Coupled Stokes/Darcy Model

First we briefly state the coupled Stokes/Darcy model. This model has been well studied for example in [14, 33, 7, 49, 45]. The work in this chapter is an extension of work in [4] and [36] in which the two-grid method is applied to the Navier-Stokes/Darcy

and Stokes/Darcy couplings respectively for the mixed finite element method. This chapter extends this work to the coupled problem with a multi-numeric scheme combining the classical finite element and the discontinuous Galerkin method. The flow in Ω_1 is modelled by the Stokes equations:

$$-\nabla \cdot (2\nu \mathbf{D}(\mathbf{u}_1) - p_1 \mathbf{I}) = \mathbf{f}_1, \quad \text{in } \Omega_1, \quad (6.1)$$

$$\nabla \cdot \mathbf{u}_1 = 0, \quad \text{in } \Omega_1, \quad (6.2)$$

$$\mathbf{u}_1 = 0, \quad \text{on } \partial\Omega_1 \setminus \Gamma_{12} = \Gamma_1. \quad (6.3)$$

The fluid velocity and pressure in Ω_1 are denoted by \mathbf{u}_1 and p_1 respectively. The coefficient $\nu > 0$ is the kinematic viscosity, the function \mathbf{f}_1 is an external force acting on the fluid, \mathbf{I} is the identity tensor and $\mathbf{D}(\mathbf{u}_1)$ is the strain rate:

$$\mathbf{D}(\mathbf{u}_1) = \frac{1}{2}(\nabla \mathbf{u}_1 + \nabla \mathbf{u}_1^T). \quad (6.4)$$

The flow in Ω_2 is modeled by Darcy's Law as described in Chapter 2:

$$-\nabla \cdot \mathbf{K} \nabla p_2 = f_2, \quad \text{in } \Omega_2, \quad (6.5)$$

$$-\mathbf{K} \nabla p_2 = \mathbf{u}_2, \quad \text{in } \Omega_2, \quad (6.6)$$

$$p_2 = g_D, \quad \text{on } \Gamma_{2D}, \quad (6.7)$$

$$\mathbf{K} \nabla p_2 \cdot \mathbf{n}_2 = g_N, \quad \text{on } \Gamma_{2N}. \quad (6.8)$$

The fluid velocity and pressure in Ω_2 are denoted by \mathbf{u}_2 and p_2 respectively. The function f_2 is an external force acting on the fluid, the functions g_D and g_N are the prescribed value and flux respectively. The vector \mathbf{n}_2 denotes the unit vector normal to Γ_2 and the coefficient \mathbf{K} is a symmetric positive definite tensor representing the hydraulic conductivity of the fluid. As in the case with the Navier-Stokes/Darcy coupling, the model is completed by specifying coupling conditions on the interface Γ_{12} with the omission of the condition including the inertial forces. The conditions are recalled below:

1. The continuity of the normal component of velocity arising from the incompressibility condition. Let \mathbf{n}_{12} be the unit normal vector to Γ_{12} directed from Ω_1 to Ω_2 then:

$$\mathbf{u}_1 \cdot \mathbf{n}_{12} = K \nabla p_2 \cdot \mathbf{n}_{12}. \quad (6.9)$$

2. The second condition is on the tangential component of the velocity in the free flow region. Let $\boldsymbol{\tau}_{12}$ be the unit tangent vector on the interface Γ_{12} then the Beavers-Joseph-Saffman law [3, 28, 50] will be written as:

$$\mathbf{u}_1 \cdot \boldsymbol{\tau}_{12} = -2\nu G(\mathbf{D}(\mathbf{u}_1)\mathbf{n}_{12}) \cdot \boldsymbol{\tau}_{12}. \quad (6.10)$$

3. The last condition relates to the balance of forces on the interface:

$$((-2\nu \mathbf{D}(\mathbf{u}_1) + p_1 \mathbf{I})\mathbf{n}_{12}) \cdot \mathbf{n}_{12} = p_2. \quad (6.11)$$

6.1.1 Variational Formulation for Stokes/Darcy Coupling

The function spaces for the Stokes velocity and pressure (\mathbf{u}_1, p_1) and Darcy pressure p_2 are the same as in Chapter 3 for the Navier-Stokes/ Darcy coupling. We briefly recall the function spaces. The Stokes velocity and pressure belong to the spaces:

$$\begin{aligned} \mathbf{X}_1 &= \{\mathbf{v}_1 \in (H^1(\Omega_1))^2 : \mathbf{v}_1 = 0 \text{ on } \Gamma_1\}, \\ M_1 &= L^2(\Omega_1), \end{aligned}$$

respectively. The Darcy pressure belongs to the function space

$$M_2 = \{q_2 \in H^1(\Omega_2) : q_2 = 0 \text{ on } \Gamma_{2D}\}.$$

We lift the Dirichlet boundary condition in 6.7. If $g_D \in H^{1/2}(\Gamma_{2D})$ there exists a function $p_D \in H^1(\Omega_2)$ satisfying

$$p_D = g_D, \text{ on } \Gamma_{2D}, \quad (6.12)$$

$$p_D = 0, \text{ on } \Gamma_{12}, \quad (6.13)$$

$$\|p_D\|_{H^1(\Omega_2)} \leq C_0 \|g_D\|_{H^{1/2}(\Gamma_{2D})}. \quad (6.14)$$

The variational form for the coupled Stokes/Darcy problem is (W_S) :

$$(W_S) \left\{ \begin{array}{l} \text{Find } \mathbf{u}_1 \in \mathbf{X}_1, p_1 \in M_1, p_2 = \varphi_2 + p_D, \text{ with } \varphi_2 \in M_2, \text{ s.t.} \\ \forall \mathbf{v}_1 \in \mathbf{X}_1, \forall q_2 \in M_2, \quad 2\nu(\mathbf{D}(\mathbf{u}_1), \mathbf{D}(\mathbf{v}_1))_{\Omega_1} - (p_1, \nabla \cdot \mathbf{v}_1)_{\Omega_1} \\ + (\varphi_2, \mathbf{v}_1 \cdot \mathbf{n}_{12})_{\Gamma_{12}} + \frac{1}{G}(\mathbf{u}_1 \cdot \boldsymbol{\tau}_{12}, \mathbf{v}_1 \cdot \boldsymbol{\tau}_{12})_{\Gamma_{12}} - (\mathbf{u}_1 \cdot \mathbf{n}_{12}, q_2)_{\Gamma_{12}} \\ + (\mathbf{K}\nabla\varphi_2, \nabla q_2)_{\Omega_2} = (\mathbf{f}_1, \mathbf{v}_1)_{\Omega_1} + (f_2, q_2)_{\Omega_2} - (\mathbf{K}\nabla p_D, \nabla q_2)_{\Omega_2} + (g_N, q_2)_{\Gamma_{2N}}, \\ \forall q_1 \in M_1, \quad (\nabla \cdot \mathbf{u}_1, q_1)_{\Omega_1} = 0. \end{array} \right.$$

6.1.2 Numerical Scheme: Stokes/Darcy coupling

As in Chapter 5, we consider a triangulation $(\mathcal{E}_h = \mathcal{E}_1^h \cup \mathcal{E}_2^h)$ of the computational domain with elements E . The Stokes velocity and pressure are approximated by conforming finite element spaces $\mathbf{X}_1^h \subset \mathbf{X}_1$ and $M_1^h \subset M_1$ defined in Section 4.2 of Chapter 4 satisfying the discrete inf-sup condition (4.1). The Discontinuous Galerkin method is used to approximate the Darcy pressure. The finite element space for the Darcy pressure is

$$M_2^h = \{q_2 \in L^2(\Omega_2) : \forall E \in \mathcal{E}_2^h, \quad q_2|_E \in \mathbb{P}_{k_2}(E)\}.$$

where \mathbb{P}_{k_2} denotes the space of polynomials of total degree less than or equal to k_2 . For the definition of the DG norm $||| \cdot |||$ and other DG notation, we refer the reader to Section 4.2 in Chapter 4. Recall the space of weakly divergence-free functions:

$$\mathbf{V}_1^h = \{\mathbf{v}_1 \in \mathbf{X}_1^h : \forall q_1 \in M_1^h, \quad b_S(\mathbf{v}_1, q_1) = 0\}.$$

Next, we recall the numerical scheme for the fully coupled Stokes/Darcy problem.

First we define the following bilinear forms:

$$\begin{aligned}
& \forall \mathbf{v}, \mathbf{w} \in \mathbf{X}_1^h, \quad a_S(\mathbf{v}, \mathbf{w}) = 2\nu(\mathbf{D}(\mathbf{v}), \mathbf{D}(\mathbf{w}))_{\Omega_1} \\
& \forall \mathbf{v} \in \mathbf{X}_1^h, \forall q_1 \in M_1^h, \quad b_S(\mathbf{v}, q_1) = -(q_1, \nabla \cdot \mathbf{v})_{\Omega_1}, \\
& \forall \mathbf{z}, \mathbf{v}, \mathbf{w} \in \forall q_2, t_2 \in M_2^h, \quad a_D(q_2, t_2) = \sum_{E \in \mathcal{E}_2^h} (\mathbf{K} \nabla q_2, \nabla t_2)_E + \sum_{e \in \Gamma_h^2} \frac{\sigma_e}{|e|} ([q_2], [t_2])_e \\
& \quad - \sum_{e \in \Gamma_2^h} (\{\mathbf{K} \nabla q_2 \cdot \mathbf{n}_e\} [t_2])_e + \epsilon_2 \sum_{e \in \Gamma_2^h} (\{\mathbf{K} \nabla t_2 \cdot \mathbf{n}_e\}, [q_2])_e. \\
& \forall \mathbf{v}, \mathbf{w} \in \mathbf{X}_1^h, \quad \forall q_2, t_2 \in M_2^h, \quad \gamma(\mathbf{v}, q_2; \mathbf{w}, t_2) = (q_2, \mathbf{w} \cdot \mathbf{n}_{12})_{\Gamma_{12}} - (\mathbf{v} \cdot \mathbf{n}_{12}, t_2)_{\Gamma_{12}} \\
& \quad + \frac{1}{G} (\mathbf{v} \cdot \boldsymbol{\tau}_{12}, \mathbf{w} \cdot \boldsymbol{\tau}_{12})_{\Gamma_{12}} \\
& \forall t_2 \in M_2^h, \forall \mathbf{v} \in \mathbf{X}_1^h, \quad L(\mathbf{v}, t_2) = (\mathbf{f}_1, \mathbf{v})_{\Omega_1} + (f_2, t_2)_{\Omega_2} \\
& \quad + \epsilon \sum_{e \in \Gamma_{2D}} (\mathbf{K} \nabla t_2 \cdot \mathbf{n}_e, g_D)_e + \sum_{e \in \Gamma_{2D}} \frac{\sigma_e}{|e|} (g_D, t_2)_e + \sum_{e \in \Gamma_{2N}} (g_N, t_2)_e
\end{aligned}$$

The parameters σ_e and ϵ_2 are the penalty and symmetrization parameters respectively. Having defined the bilinear forms, the numerical scheme to problem (W_S^h)

is:

$$(W_S^h) \left\{ \begin{array}{l} \text{Find } \mathbf{U}_1^h \in \mathbf{X}_1^h, P_1^h \in M_1^h, P_2^h \in M_2^h, \text{ s.t} \\ \forall \mathbf{v}_1 \in \mathbf{X}_1^h, q_2 \in M_2^h, a_S(\mathbf{U}_1^h, \mathbf{v}_1) + b_S(\mathbf{v}_1, P_1^h) + a_D(P_2^h, q_2) \\ + \gamma(\mathbf{U}_1^h, P_2^h; \mathbf{v}_1, q_2) = L(\mathbf{v}_1, q_2), \\ \forall q_1 \in M_1^h \quad b_S(\mathbf{U}_1^h, q_1) = 0. \end{array} \right.$$

The error analysis for the two-grid method applied to the Stokes/Darcy problem requires an L_2 error estimate on the Stokes velocity proved in the following section.

6.1.3 L_2 error estimate for Stokes/Darcy problem

First we recall the of weakly divergence free functions:

$$\mathbf{V}_1 = \{\mathbf{v}_1 \in \mathbf{X}_1, \nabla \cdot \mathbf{v}_1 = 0\}$$

In order to define the dual problem, we consider the following homogeneous Stokes and Darcy problems:

Find a pair (φ_1, ξ_1) in $H_0^1(\Omega_1) \times L_0^2(\Omega_1)$ such that for $\mathbf{g}_1 \in L^2(\Omega_1)^2$:

$$-\nabla \cdot (2\nu \mathbf{D}(\varphi_1) - \xi_1 \mathbf{I}) = \mathbf{g}_1 \text{ in } \Omega_1 \quad (6.15)$$

$$\nabla \cdot \varphi_1 = 0 \text{ in } \Omega_1 \quad (6.16)$$

$$\varphi_1 = \mathbf{0} \text{ on } \Gamma_1. \quad (6.17)$$

Find $\xi_2 \in H_{0,\Gamma_{2D}}^1(\Omega_2)$ such that for $g_2 \in L^2(\Omega_2)$.

$$-\nabla \cdot \mathbf{K} \nabla \xi_2 = g_2, \text{ in } \Omega_2, \quad (6.18)$$

$$\xi_2 = 0, \text{ on } \Gamma_{2D}, \quad (6.19)$$

$$\mathbf{K} \nabla \xi_2 \cdot \mathbf{n}_2 = 0, \text{ on } \Gamma_{2N}. \quad (6.20)$$

Following the Aubin-Nitsche duality technique, we define a dual problem W_S^* : given $(\mathbf{g}_1, g_2) \in (L^2(\Omega_1))^2 \times L^2(\Omega_2)$ we introduce the unique solution $(\varphi_1, \xi_1, \xi_2) \in (\mathbf{V}_1 \times M_1 \times M_2)$ such that:

$$(W_S^*) \begin{cases} \forall v_1 \in \mathbf{X}_1, q_2 \in M_2, a_S(v_1, \varphi_1) + b_S(v_1, \xi_1) + a_D(q_2, \xi_2) \\ + \gamma(v_1, q_2; \varphi_1, \xi_2) = (\mathbf{g}_1, v_1)_{\Omega_1} + (g_2, q_2)_{\Omega_2}, \\ \forall q_1 \in M_1 \quad b_S(\varphi_1, q_1) = 0. \end{cases},$$

The equivalence between the model problem and the form (W_S^*) is summarized in the following lemma. The proof is similar to Lemma 3.2 in Chapter 3.

Lemma 25. *If $(\varphi_1, \xi_1, \xi_2) \in (\mathbf{V}_1 \times M_1 \times M_2)$ satisfies (6.15) - (6.20) with interface conditions (6.9) - (6.11), then $(\varphi_1, \xi_1, \xi_2)$ is a solution to problem (W_S^*) . The converse is also true under some additional smoothness assumptions.*

6.1.4 Regularity for the Coupled Stokes/Darcy problem

Following the argument used in [23] the coupled Stokes-Darcy problem requires the following concept of regularity.

Definition 26. *We say the coupled problem (6.15) - (6.20) with interface conditions (6.9) - (6.11) is regular if the mapping*

$$(\varphi_1, \xi_1, \xi_2) \rightarrow \nu \Delta \varphi_1 + \nabla \xi_1 + \Delta \xi_2$$

is an isomorphism from $[H^2(\Omega_1)^2 \cap \mathbf{V}_1] \times [H^1(\Omega_1)] \times [H^2(\Omega_2)]$ onto $L^2(\Omega_1)^2 \times L^2(\Omega_2)$.

This definition implies that $\varphi_1 \in H^2(\Omega_1)$, $\xi_1 \in H^1(\Omega_1)$ and $\xi_2 \in H^2(\Omega_2)$ whenever $(\mathbf{g}_1, \mathbf{g}_2) \in (L^2(\Omega_1)^2 \times L^2(\Omega_2))$ and

$$\|\varphi_1\|_{H^2(\Omega_1)} + \|\xi_1\|_{H^1(\Omega_1)} + \|\xi_2\|_{H^2(\Omega_2)} \leq C(\|\mathbf{g}_1\|_{L^2(\Omega_1)} + \|\mathbf{g}_2\|_{L^2(\Omega_2)}) \quad (6.21)$$

6.1.5 Error estimates in L_2

Recalling the equations of the model in each domain, we have the following consistency lemma which can be proved in a manner similar to Lemma (10) in Chapter 4.

Lemma 27. *Let (\mathbf{u}_1, p_1, p_2) be the solution to the coupled Stokes and Darcy equations with interface conditions (6.9) - (6.11). Then, for $\mathbf{v}_1 \in \mathbf{X}_1^h$, $q_2 \in M_2^h$, $q_1 \in M_1^h$:*

$$a_{\text{NS}}(\mathbf{u}_1, \mathbf{v}_1) + b_{\text{NS}}(\mathbf{v}_1, p_1) + a_{\text{D}}(p_2, q_2) + \gamma(\mathbf{u}_1, p_2; \mathbf{v}_1, q_2) = L(\mathbf{v}_1, q_2), \quad (6.22)$$

$$b_{\text{NS}}(\mathbf{u}_1, q_1) = 0. \quad (6.23)$$

Theorem 28. *Assume that the solution (\mathbf{u}_1, p_1, p_2) to the problem W_S is such that $\mathbf{u}_1 \in (H^2(\Omega_1))^2$, $p_1 \in H^1(\Omega_1)$ and $p_2 \in H^2(\Omega_2)$. Then there exists a constant C independent of h such that:*

$$\begin{aligned} \|\mathbf{u}_1 - \mathbf{U}_1^h\|_{L^2(\Omega_1)} + \|p_2 - P_2^h\|_{L^2(\Omega_2)} &< Ch(\|\mathbf{D}(\mathbf{u}_1 - \mathbf{U}_1^h)\|_{L^2(\Omega_1)} + \|p_2 - P_2^h\| + \|p_1 - P_1^h\|_{L^2(\Omega_2)}) \\ &\leq Ch^2. \end{aligned}$$

Proof. Let $\mathbf{v}_1 = \mathbf{u}_1 - \mathbf{U}_1^h$ and $q_2 = p_2 - P_2^h$ in W_S^* then we have:

$$\begin{aligned} (\mathbf{g}_1, \mathbf{u}_1 - \mathbf{U}_1^h)_{\Omega_1} + (g_2, p_2 - P_2^h)_{\Omega_2} &= a_S(\mathbf{u}_1 - \mathbf{U}_1^h, \boldsymbol{\varphi}_1) + b_S(\mathbf{u}_1 - \mathbf{U}_1^h, \xi_1) \\ &+ \gamma(\mathbf{u}_1 - \mathbf{U}_1^h, p_2 - P_2^h; \boldsymbol{\varphi}_1, \xi_2) + a_D(p_2 - P_2^h, \xi_2) \end{aligned} \quad (6.24)$$

Then if we let $\mathbf{g}_1 = (\mathbf{u}_1 - \mathbf{U}_1^h)$ and $g_2 = (p_2 - P_2^h)$ in 6.24:

$$\begin{aligned} \|\mathbf{u}_1 - \mathbf{U}_1^h\|_{L^2(\Omega_1)}^2 + \|p_2 - P_2^h\|_{L^2(\Omega_2)}^2 &= a_S(\mathbf{u}_1 - \mathbf{U}_1^h, \boldsymbol{\varphi}_1) + b_S(\mathbf{u}_1 - \mathbf{U}_1^h, \xi_1) \\ &+ \gamma(\mathbf{u}_1 - \mathbf{U}_1^h, p_2 - P_2^h; \boldsymbol{\varphi}_1, \xi_2) + a_D(p_2 - P_2^h, \xi_2) \end{aligned} \quad (6.25)$$

Subtracting the discrete model (W_S^h) from (6.22) - (6.23) and using the definition of γ we have:

$$\begin{aligned} a_S(\mathbf{u}_1 - \mathbf{U}_1^h, \boldsymbol{\varphi}_h) + b_S(\boldsymbol{\varphi}_h, p_1 - P_1^h) + a_D(p_2 - P_2^h, q_h) + (p_2 - P_2^h, \boldsymbol{\varphi}_h \cdot \mathbf{n}_{12})_{\Gamma_{12}} \\ + \frac{1}{G}((\mathbf{u}_1 - \mathbf{U}_1^h) \cdot \boldsymbol{\tau}_{12}, \boldsymbol{\varphi}_h \cdot \boldsymbol{\tau}_{12})_{\Gamma_{12}} - ((\mathbf{u}_1 - \mathbf{U}_1^h) \cdot \mathbf{n}_{12}, q_h)_{\Gamma_{12}} = 0 \\ \forall \boldsymbol{\varphi}_h \in \mathbf{V}_1^h, \quad \forall q_h \in M_2^h \\ b_S(\mathbf{u}_1 - \mathbf{U}_1^h, \xi_h) = 0, \quad \forall \xi_h \in M_1^h \end{aligned} \quad (6.26)$$

Subtracting the left hand-side of 6.26 from the right-hand side of 6.25 and using the fact that $\boldsymbol{\varphi}_g \in \mathbf{V}_1$ we have $b_S(\boldsymbol{\varphi}_g, p_1 - P_1^h) = 0$ thus we obtain:

$$\begin{aligned} \|\mathbf{u}_1 - \mathbf{U}_1^h\|_{L^2(\Omega_1)}^2 + \|p_2 - P_2^h\|_{L^2(\Omega_2)}^2 &= T_{\Omega_1} + T_{\Omega_2} + T_{\Gamma_{12}} \\ \forall \boldsymbol{\varphi}_h \in \mathbf{V}_1^h, \quad \forall \xi_h \in M_h^1, \quad \forall q_h \in M_h^2 \end{aligned} \quad (6.27)$$

with the terms defined as:

$$\begin{aligned} T_{\Omega_1} &= a_S(\mathbf{u}_1 - \mathbf{U}_1^h, \boldsymbol{\varphi}_1 - \boldsymbol{\varphi}_h) + b_S(\boldsymbol{\varphi}_1 - \boldsymbol{\varphi}_h, p_1 - P_1^h) + b_S(\mathbf{u}_1 - \mathbf{U}_1^h, \xi_1 - \xi_h) \\ T_{\Omega_2} &= a_D(p_2 - P_2^h, \xi_2 - q_h) \\ T_{\Gamma_{12}} &= \frac{1}{G}((\mathbf{u}_1 - \mathbf{U}_1^h) \cdot \boldsymbol{\tau}_{12}, (\boldsymbol{\varphi}_1 - \boldsymbol{\varphi}_h) \cdot \boldsymbol{\tau}_{12})_{\Gamma_{12}} - ((\mathbf{u}_1 - \mathbf{U}_1^h) \cdot \mathbf{n}_{12}, \xi_2 - q_h)_{\Gamma_{12}} \\ &+ (p_2 - P_2^h, (\boldsymbol{\varphi}_h - \boldsymbol{\varphi}_1) \cdot \mathbf{n}_{12})_{\Gamma_{12}} \end{aligned}$$

Next we use approximation properties (4.6) - (4.9) of the discrete spaces \mathbf{X}_1, M_1 and M_2 defined in Chapter 4. Assume that $(\varphi_1, \xi_1, \xi_2) \in \mathbf{X}_1 \times M_1 \times M_2$ is smooth enough, i.e. $\varphi_1 \in H^2(\Omega_1)$, $\xi_1 \in H^1(\Omega_1)$ and $\xi_2 \in H^2(\Omega_2)$, we can take $(\varphi_h, \xi_h, q_h) = (\tilde{\varphi}_h, \tilde{\xi}_h, \tilde{q}_h)$ such that:

$$\|\nabla(\varphi_1 - \tilde{\varphi}_h)\|_{L^2(\Omega_1)} \leq Ch\|\varphi_1\|_{H^2(\Omega_1)}, \quad (6.28)$$

$$\|\xi_1 - \tilde{\xi}_h\|_{L^2(\Omega_1)} \leq Ch\|\xi_1\|_{H^1(\Omega_1)}, \quad (6.29)$$

$$\|\xi_2 - \tilde{q}_h\| \leq Ch\|\xi_2\|_{H^2(\Omega_2)}. \quad (6.30)$$

Bounding the terms in T_{Ω_1} :

$$a_S(\mathbf{u}_1 - \mathbf{U}_1^h, \varphi_1 - \varphi_h) \leq 2\nu\|\mathbf{D}(\mathbf{u}_1 - \mathbf{U}_1^h)\|_{L^2(\Omega_1)}\|\mathbf{D}(\varphi_1 - \varphi_h)\|_{L^2(\Omega_1)},$$

$$b_S(\varphi_1 - \varphi_h, p_1 - P_1^h) \leq C_1\|\mathbf{D}(\varphi_1 - \varphi_h)\|_{L^2(\Omega_1)}\|p_1 - P_1^h\|_{L^2(\Omega_1)},$$

$$b_S(\mathbf{u}_1 - \mathbf{U}_1^h, \xi_1 - \xi_h) \leq C_1\|\mathbf{D}(\mathbf{u}_1 - \mathbf{U}_1^h)\|_{L^2(\Omega_1)}\|\xi_1 - \xi_h\|_{L^2(\Omega_1)}.$$

Bounding the term T_{Ω_2} we obtain:

$$T_{\Omega_2} \leq C_{DG}\|p_2 - P_2^h\|\|p_2 - q_h\|_{L^2(\Omega_2)}.$$

The interface terms can be bounded as follows:

$$\left| \frac{1}{G} ((\mathbf{u}_1 - \mathbf{U}_1^h) \cdot \boldsymbol{\tau}_{12}, (\varphi_1 - \varphi_h) \cdot \boldsymbol{\tau}_{12})_{\Gamma_{12}} \right| \leq \frac{(C_1 C_2)^2}{G} \|\mathbf{D}(\mathbf{u}_1 - \mathbf{U}_1^h)\|_{L^2(\Omega_1)} \|\nabla(\varphi_1 - \varphi_h)\|_{L^2(\Omega_1)}$$

$$|(\mathbf{u}_1 - \mathbf{U}_1^h) \cdot \mathbf{n}_{12}, \xi_2 - q_h)_{\Gamma_{12}}| \leq C_2 C_1 \|\mathbf{D}(\mathbf{u}_1 - \mathbf{U}_1^h)\|_{L^2(\Omega_1)} \|\xi_2 - q_h\|$$

$$|(p_2 - P_2^h, (\varphi_1 - \varphi_h) \cdot \mathbf{n}_{12})_{\Gamma_{12}}| \leq C_6 C_2 \|\varphi_2 - P_2^h\| \|\nabla(\varphi_1 - \varphi_h)\|_{L^2(\Omega_1)}$$

The error analysis performed in [15, 45] shows that

$$\|\mathbf{D}(\mathbf{u}_1 - \mathbf{U}_1^h)\|_{L^2(\Omega_1)} \leq Ch \quad (6.31)$$

$$\|p_1 - P_1^h\|_{L^2(\Omega_1)} \leq Ch \quad (6.32)$$

$$\|p_2 - P_2^h\| \leq Ch \quad (6.33)$$

From the approximation properties (6.28) - (6.30) we obtain:

$$\begin{aligned} \|\mathbf{u}_1 - \mathbf{U}_1^h\|_{L^2(\Omega_1)}^2 + \|\varphi - P_2^h\|_{L^2(\Omega_2)}^2 \leq Ch\{ & \|\mathbf{D}(\mathbf{u}_1 - \mathbf{U}_1^h)\|_{L^2(\Omega_1)}(\|\varphi_g\|_{H^2(\Omega_1)} + \|\xi_s\|_{H^2(\Omega_1)} \\ & + \|\rho_2\|_{H^2(\Omega_2)}) + \|p_1 - P_1^h\|_{L^2(\Omega_1)}\|\xi_s\|_{H^1(\Omega_1)} + \|\varphi_2 - P_2^h\|_{L^2(\Omega_2)}\|\varphi_g\|_{H^1(\Omega_1)}\}. \end{aligned}$$

Using 6.21 and recalling that $g_1 = \mathbf{u}_1 - \mathbf{U}_1^h$ and $g_2 = \varphi_2 - P_2^h$ gives:

$$\begin{aligned} \|\mathbf{u}_1 - \mathbf{U}_1^h\|_{L^2(\Omega_1)} + \|\varphi_2 - P_2^h\|_{L^2(\Omega_2)} \leq Ch\{ & \|\mathbf{D}(\mathbf{u}_1 - \mathbf{U}_1^h)\|_{L^2(\Omega_1)} \\ & + \|p_1 - P_1^h\|_{L^2(\Omega_1)} + \|\varphi_2 - P_2^h\|_{L^2(\Omega_2)}\}. \end{aligned}$$

The constant C depends on constants C_1 through C_6 defined in Chapter 3 which depend on the domains Ω_1 and Ω_2 . \square

6.1.6 Two Grid Algorithm: Coupled Stokes/Darcy Model

In this section we present the two-grid algorithm applied to the coupled Stokes/Darcy problem. The two-grid method algorithm solves the more expensive fully coupled problem on a coarse grid of size H which is assumed to be much bigger than the fine grid of size h . We then use the solution from the coarse grid to approximate unknowns on the fine grid to solve modified Stokes and Darcy problems. The algorithm is summarized in the following steps:

1. First we solve a coarse grid problem on a grid of size H :

$$(W^H) \left\{ \begin{array}{l} \text{Find } \mathbf{U}_1^H \in \mathbf{X}_1^H, P_1^H \in M_1^H, P_2^H \in M_2^H, \text{ s.t.} \\ \forall \mathbf{v}_1 \in \mathbf{X}_1^H, \forall q_2 \in M_2^H, \quad a_S(\mathbf{U}_1^H, \mathbf{v}_1) + b_S(\mathbf{v}_1, P_1^H) + a_D(P_2^H, q_2) \\ \quad + \gamma(\mathbf{U}_1^H, P_2^H; \mathbf{v}_1, q_2) = L(\mathbf{v}_1, q_2), \\ \forall q_1 \in M_1^H, \quad b_S(\mathbf{U}_1^H, q_1) = 0. \end{array} \right.$$

2. We then solve a modified fine grid problem on a grid of size h :

$$(W_h) \begin{cases} \text{Find } \mathbf{U}_{h,1} \in \mathbf{X}_1^h, P_{h,1} \in M_1^h, P_{h,2} \in M_2^h, \text{ s.t.} \\ \forall \mathbf{v}_1 \in \mathbf{X}_1^h, \forall q_2 \in M_2^h, a_S(\mathbf{U}_{h,1}, \mathbf{v}_1) + \frac{1}{G}(\mathbf{U}_{h,1} \cdot \boldsymbol{\tau}_{12}, \mathbf{v}_1 \cdot \boldsymbol{\tau}_{12}) + b_S(\mathbf{v}_1, P_{h,1}) \\ + a_D(P_{h,2}, q_2) = L(\mathbf{v}_1, q_2) - (P_2^H, \mathbf{v}_1 \cdot \mathbf{n}_{12})_{\Gamma_{12}} + (\mathbf{U}_1^H \cdot \mathbf{n}_{12}, q_2)_{\Gamma_{12}}, \\ \forall q_1 \in M_1^h, b_S(\mathbf{U}_{h,1}, q_1) = 0. \end{cases}$$

The modified fine grid problem is equivalent to solving modified Stokes and Darcy problems in Ω_1 and Ω_2 respectively. The modified problems can be stated as follows: in Ω_1 ,

$$(W_{h,S}) \begin{cases} \text{Find } \mathbf{U}_{h,1} \in \mathbf{X}_1^h, P_{h,1} \in M_1^h, \text{ s.t.} \\ \forall \mathbf{v}_1 \in \mathbf{X}_1^h, \forall q_2 \in M_2^h, a_S(\mathbf{U}_{h,1}, \mathbf{v}_1) + b_S(\mathbf{v}_1, P_{h,1}) + \frac{1}{G}(\mathbf{U}_{h,1} \cdot \boldsymbol{\tau}_{12}, \mathbf{v}_1 \cdot \boldsymbol{\tau}_{12})_{\Gamma_{12}} \\ = (\mathbf{f}_1, \mathbf{v}_1)_{\Omega_1} - (P_2^H, \mathbf{v}_1 \cdot \mathbf{n}_{12})_{\Gamma_{12}}, \\ \forall q_1 \in M_1^h, b_S(\mathbf{U}_{h,1}, q_1) = 0, \end{cases}$$

and in Ω_2 ,

$$(W_{h,D}) \begin{cases} \text{Find } P_{h,2} \in M_2^h, \text{ s.t.} \\ \forall q_2 \in M_2^h, a_D(P_{h,2}, q_2) = (f_1, q_2)_{\Omega_2} + (\mathbf{U}^H \cdot \mathbf{n}_{12}, q_2)_{\Gamma_{12}} + (g_N, q_2)_{\Gamma_{2N}} \\ + \epsilon \sum_{e \in \Gamma_{2D}} (\mathbf{K} \nabla q_2 \cdot \mathbf{n}_e, g_D)_e + \sum_{e \in \Gamma_{2D}} \frac{\sigma_e}{|e|} (g_D, q_2)_e \end{cases}$$

The next section presents the error analysis for the Two grid algorithm defined above.

6.1.7 Error Analysis: Two Grid Stokes/Darcy Algorithm

The objective of this section is to show that the modified two-grid algorithm results in a solution that is an approximation of the solution from the coupled problem.

Theorem 29. *Let $\mathbf{U}_{h,1}, P_{h,1}, P_{2,h}$ be the solution to the two-grid coupled Stokes-Darcy problem and $\mathbf{U}_1^h, P_1^h, P_2^h$ be the solution to the fully coupled Stokes-Darcy problem.*

Then we have the following error estimates:

$$\|P_2^h - P_{h,2}\| \leq CH^2 \quad (6.34)$$

$$\|D(\mathbf{U}_1^h - \mathbf{U}_{h,1})\|_{L^2(\Omega_1)} \leq CH^{3/2} \quad (6.35)$$

$$\|P_1^h - P_{h,1}\|_{L^2(\Omega_1)} \leq CH^{3/2} \quad (6.36)$$

Proof. On the fine grid \mathcal{E}_h taking the difference between (W_S^h) (the fully coupled scheme) and $(W_{h,S})$ (the modified two-grid scheme) gives:

$$\begin{cases} \forall \mathbf{v}_1 \in \mathbf{X}_1^h, \forall q_2 \in M_2^h, a_S(\mathbf{U}_1^h - \mathbf{U}_{h,1}, \mathbf{v}_1) + b_S(\mathbf{v}_1, P_1^h - P_{h,1}) + a_D(P_2^h - P_{h,2}, q_2) \\ + \frac{1}{G}((\mathbf{U}_1^h - \mathbf{U}_{h,1}) \cdot \boldsymbol{\tau}_{12}, \mathbf{v}_1)_{\Gamma_{12}} + (P_2^h - P_2^H, \mathbf{v}_1 \cdot \mathbf{n}_{12})_{\Gamma_{12}} - ((\mathbf{U}_1^h - \mathbf{U}_1^H) \cdot \mathbf{n}_{12}, q_2)_{\Gamma_{12}} = 0, \\ \forall q_1 \in M_1^h, b_S(\mathbf{U}_1^h - \mathbf{U}_{h,1}, q_1) = 0. \end{cases} \quad (6.37)$$

In 6.37 if we pick $\mathbf{v}_1 = \mathbf{0}$, $q_2 = P_2^h - P_{h,2}$ and using the definition of γ we obtain

$$a_D(P_2^h - P_{h,2}, P_2^h - P_{h,2}) = \int_{\Gamma_{12}} (P_2^h - P_{h,2})(\mathbf{U}_1^h - \mathbf{U}_1^H) \cdot \mathbf{n}_{12}.$$

Following the argument in [4, 36] for the mixed Stokes-Darcy case we define θ a harmonic extension of $P_2^h - P_{h,2}$ into the fluid flow region such that:

$$\begin{cases} -\Delta\theta = 0 \text{ in } \Omega_f, \\ \theta = P_2^h - P_{h,2} \text{ on } \Gamma_{12} \\ \theta = 0 \text{ on } \Gamma_1 \end{cases}$$

The harmonic extension has the property [36]

$$\|\theta\|_{H^1(\Omega_f)} \leq \|P_2^h - P_{h,2}\|_{H_{00}^{1/2}(\Gamma_{12})} \leq \|P_2^h - P_{h,2}\|$$

$$\begin{aligned}
\int_{\Gamma_{12}} (P_2^h - P_{h,2})(\mathbf{U}_1^h - \mathbf{U}_1^H) \cdot \mathbf{n}_{12} &= \int_{\partial\Omega_1} \theta(\mathbf{U}_1^h - \mathbf{U}_1^H) \mathbf{n}_{12} \\
&= \int_{\Omega_1} \nabla \cdot (\mathbf{U}_1^h - \mathbf{U}_1^H) \theta + \int_{\Omega_1} (\mathbf{U}_1^h - \mathbf{U}_1^H) \cdot \nabla \theta \\
&= \int_{\Omega_1} (\theta - q_1^H) \nabla \cdot (\mathbf{U}_1^h - \mathbf{U}_1^H) + \int_{\Omega_1} (\mathbf{U}_1^h - \mathbf{U}_1^H) \cdot \nabla \theta
\end{aligned}$$

The last equality follows from the weakly divergence-free property for \mathbf{U}_1^h and \mathbf{U}_1^H .

$$b_S(\mathbf{U}_1^h - \mathbf{U}_1^H, q_1^H) = 0 \quad \forall q_1^H \in M_1^H$$

Using the coercivity property of the bilinear form a_D

$$\begin{aligned}
\kappa \| \|P_2^h - P_{h,2}\| \|^2 &\leq a_D(P_2^h - P_{h,2}, P_2^h - P_{h,2}) \\
&\leq \inf_{q_1^H \in M_1^H} \left| \int_{\Omega_f} (\theta - q_1^H) \nabla \cdot (\mathbf{U}_1^h - \mathbf{U}_1^H) \right| + \left| \int_{\Omega_1} (\mathbf{U}_1^h - \mathbf{U}_1^H) \cdot \nabla \theta \right| \\
&\leq C \| \mathbf{U}_1^h - \mathbf{U}_1^H \|_{H^1(\Omega_1)} \inf_{q_1^H \in M_1^H} \| \theta - q_1^H \|_{L^2(\Omega_1)} + \| \mathbf{U}_1^h - \mathbf{U}_1^H \|_{L^2(\Omega_1)} \| \theta \|_{H^1(\Omega_1)} \\
&\leq CH^2 \| P_2^h - P_{h,2} \|_{H_0^{1/2}(\Gamma_{12})} \\
&\leq CH^2 \| \|P_2^h - P_{h,2}\| \|.
\end{aligned}$$

This proves the result 6.41. Next we pick $q_2 = 0$ in 6.37 we obtain

$$\begin{aligned}
a_S(\mathbf{U}_1^h - \mathbf{U}_{h,1}, \mathbf{v}_1) + b_S(\mathbf{v}_1, P_1^h - P_{h,1}) + \frac{1}{G} ((\mathbf{U}_1^h - \mathbf{U}_{h,1}) \cdot \boldsymbol{\tau}_{12}, \mathbf{v}_1 \cdot \boldsymbol{\tau}_{12})_{\Gamma_{12}} \\
+ (P_2^h - P_2^H, \mathbf{v}_1 \cdot \mathbf{n}_{12})_{\Gamma_{12}} = 0
\end{aligned}$$

For the choice $\mathbf{v}_1 = \mathbf{U}_1^h - \mathbf{U}_{h,1}$ we obtain

$$b_S(\mathbf{U}_1^h - \mathbf{U}_{h,1}, P_1^h - P_{h,1}) = 0$$

due to the divergence-free property of \mathbf{U}_1^h and $\mathbf{U}_{h,1}$. This leads to

$$a_S(\mathbf{U}_1^h - \mathbf{U}_{h,1}, \mathbf{U}_1^h - \mathbf{U}_{h,1}) + \frac{1}{G} ((\mathbf{U}_1^h - \mathbf{U}_{h,1}) \cdot \boldsymbol{\tau}_{12}, (\mathbf{U}_1^h - \mathbf{U}_{h,1}) \cdot \boldsymbol{\tau}_{12})_{\Gamma_{12}} \quad (6.38)$$

$$= (P_2^H - P_2^h, (\mathbf{U}_1^h - \mathbf{U}_{h,1}) \cdot \mathbf{n}_{12})_{\Gamma_{12}} \quad (6.39)$$

$$\begin{aligned}
\frac{1}{G}((\mathbf{U}_1^h - \mathbf{U}_{h,1}) \cdot \boldsymbol{\tau}_{12}, (\mathbf{U}_{h,1} - \mathbf{U}_1^h) \cdot \boldsymbol{\tau}_{12})_{\Gamma_{12}} &= \frac{1}{G} \|(\mathbf{U}_1^h - \mathbf{U}_{h,1}) \cdot \boldsymbol{\tau}_{12}\|_{L^2(\Gamma_{12})}^2 \\
(P_2^h - P_2^H, (\mathbf{U}_1^h - \mathbf{U}_1^H) \cdot \mathbf{n}_{12})_{\Gamma_{12}} &\leq \|P_2^h - P_2^H\|_{L^2(\Gamma_{12})} \|(\mathbf{U}_1^h - \mathbf{U}_{h,1})\|_{L^2(\Gamma_{12})} \\
&\leq C_6 \|P_2^h - P_2^H\| \|C_1 C_2\| \|\mathbf{D}(\mathbf{U}_1^h - \mathbf{U}_{h,1})\|_{L^2(\Omega_1)}
\end{aligned}$$

Using the above bounds we have

$$2\nu \|\mathbf{D}(\mathbf{U}_1^h - \mathbf{U}_{h,1})\|_{L^2(\Omega_1)}^2 \leq C_6 \|P_2^h - P_2^H\| \|C_1 C_2\| \|\mathbf{D}(\mathbf{U}_1^h - \mathbf{U}_{h,1})\|_{L^2(\Omega_1)}$$

Using the trace inequality due to J.Xu in [36],

$$\|P_2^h - P_2^H\|_{L^2(\Omega_2)} \leq C \|P_2^h - P_2^H\|_{L^2(\Omega_2)} + H^{1/2} \|P_2^h - P_2^H\| < CH^{3/2},$$

gives 6.42. Finally we prove an error estimate on the Stokes pressure. In 6.37 for the choice $q_2 = 0$ we obtain

$$\begin{aligned}
a_S(\mathbf{U}_1^h - \mathbf{U}_{h,1}, \mathbf{v}_1) + b_S(\mathbf{v}_1, P_1^h - P_{h,1}) + \frac{1}{G}((\mathbf{U}_1^h - \mathbf{U}_{h,1}) \cdot \boldsymbol{\tau}_{12}, \mathbf{v}_1 \cdot \boldsymbol{\tau}_{12})_{\Gamma_{12}} \\
+ (P_2^h - P_2^H, \mathbf{v}_1 \cdot \mathbf{n}_{12})_{\Gamma_{12}} = 0
\end{aligned}$$

$$\begin{aligned}
|a_S(\mathbf{U}_1^h - \mathbf{U}_{h,1}, \mathbf{v}_1)| &\leq 2\nu \|\mathbf{D}(\mathbf{U}_1^h - \mathbf{U}_{h,1})\|_{L^2(\Omega_1)} \|\mathbf{D}(\mathbf{v}_1)\|_{L^2(\Omega_1)} \\
\left| \frac{1}{G}((\mathbf{U}_1^h - \mathbf{U}_{h,1}) \cdot \boldsymbol{\tau}_{12}, \mathbf{v}_1 \cdot \boldsymbol{\tau}_{12})_{\Gamma_{12}} \right| &\leq \frac{1}{G} \|\mathbf{U}_1^h - \mathbf{U}_{h,1}\|_{L^2(\Gamma_{12})} \|\mathbf{v}_1\|_{L^2(\Omega_2)} \\
&\leq \frac{(C_1 C_2)^2}{G} \|\mathbf{D}(\mathbf{U}_1^h - \mathbf{U}_{h,1})\|_{L^2(\Omega_1)} \|\mathbf{D}(\mathbf{v}_1)\|_{L^2(\Omega_1)} \\
|(P_2^h - P_{h,2}, \mathbf{v}_1 \cdot \mathbf{n}_{12})_{\Gamma_{12}}|_{L^2(\Gamma_{12})} &\leq \|P_2^h - P_{h,2}\|_{L^2(\Gamma_{12})} C_1 C_2 \|\mathbf{D}(\mathbf{v}_1)\|_{L^2(\Gamma_{12})}
\end{aligned} \tag{6.40}$$

Using the bounds in 6.40 and the inf-sup condition on Ω_1 :

$$\|P_1^h - P_{h,1}\|_{L^2(\Omega_1)} \leq \frac{b_S(\mathbf{v}_1, P_1^h - P_{h,1})}{\|\mathbf{D}(\mathbf{v}_1)\|_{L^2(\Omega_1)}},$$

we obtain

$$\begin{aligned}
\|P_1^h - P_{h,1}\|_{L^2(\Omega_1)} &\leq \frac{|a_S(\mathbf{U}_1^h - \mathbf{U}_{h,1}, \mathbf{v}_1)| + |T_{\Gamma_{12}}|}{\|\mathbf{D}(\mathbf{v}_1)\|_{L^2(\Omega_1)}} \\
&\leq C\|\mathbf{D}(\mathbf{U}_1^h - \mathbf{U}_{h,1})\|_{L^2(\Omega_1)} + \|P_2^h - P_{h,1}\|_{L^2(\Gamma_{12})} \\
&\leq Ch^{3/2}
\end{aligned}$$

where $T_{\Gamma_{12}} = \frac{1}{G}((\mathbf{U}_1^h - \mathbf{U}_{h,1}) \cdot \boldsymbol{\tau}_{12}, \mathbf{v}_1 \cdot \boldsymbol{\tau}_{12}) + (P_2^h - P_{h,2}, \mathbf{v}_1 \cdot \mathbf{n}_{12})_{\Gamma_{12}}$. We conclude the proof. \square

In the numerical results section that follows we pick $h = H^2$, the expected convergence rates are summarized in the following corollary.

Corollary 30. *Let $\mathbf{U}_{h,1}, P_{h,1}, P_{h,2}$ be solutions of the two-grid problem applied to the coupled Stokes/Darcy model with $H = \sqrt{h}$. Then we have*

$$\|p_2 - P_{h,2}\| \leq Ch$$

and

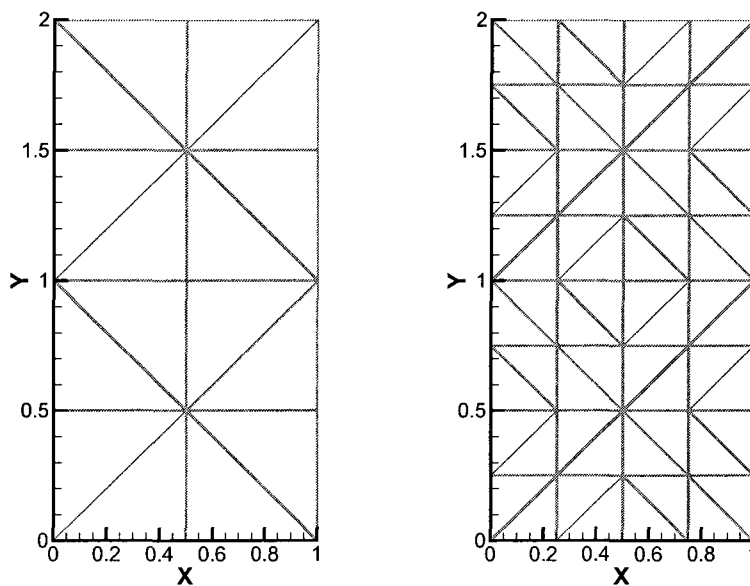
$$\|\mathbf{D}(\mathbf{u}_1 - \mathbf{U}_{h,1})\|_{L^2(\Omega_1)} + \|p_1 - p_{1,h}\|_{L^2(\Omega_1)} \leq Ch^{3/4}$$

In order to theoretically obtain an $O(h)$ convergence rate we have to pick $h = H^{3/2}$, this is not practical for the mesh refinement technique used in this chapter.

6.1.8 Numerical Results: Two Grid Stokes/Darcy problem

We present examples to verify convergence rates for the two-grid algorithm applied to the Stokes/Darcy problem proposed in the previous section. For a given mesh size we also compare the accuracy of the two grid method to solving the fully coupled problem and the CPU time to solve each problem. The coarse and fine mesh sizes

will be denoted by H and h respectively. The mesh parameters are chosen such that $H = \sqrt{h}$. Let \mathcal{E}_h and \mathcal{E}_H be regular triangulations [11] of the domain, \mathcal{E}_h is obtained from \mathcal{E}_H through mesh refinement (see Fig. 6.1). This condition may be relaxed for the Stokes-Darcy case. Let \mathbf{X}_1^H, M_1^H and M_2^H be the velocity and pressure discrete spaces defined on \mathcal{E}_H . Similarly we define \mathbf{X}_1^h, M_1^h and M_2^h on the fine mesh \mathcal{E}_h . The spaces are defined in such a way that $\mathbf{X}_1^H \subset \mathbf{X}_1^h, M_1^H \subset M_1^h$ and $M_2^H \subset M_2^h$. We use the continuous finite element method in Ω_1 and the discontinuous Galerkin method in Ω_2 . The finite element spaces are defined in Section 5.2.3 in Section 6.1.2.

(a) Coarse Mesh (\mathcal{E}_H)(b) Fine Mesh (\mathcal{E}_h)Figure 6.1 : Computational meshes $H = 0.5, h = 0.25$.

Convergence Study: Stokes/Darcy Model

Example 31. *The boundary conditions are chosen in such a way that the exact solution to the coupled Stokes/Darcy problem is:*

$$\begin{aligned} \mathbf{u}_1 &= (y^2 - 2y + 2x, x^2 - x - 2y), \quad p_1 = x^2y + xy + y^2 - 4.0 \\ p_2 &= -x^2y + xy + y^2. \end{aligned}$$

For simplicity we set

$$\mathbf{K} = \mathbf{I} \text{ and } \nu = 1.0.$$

The computational domain $\Omega_1 = (0, 1) \times (0, 1)$ and $\Omega_2 = (0, 1) \times (1, 2)$.

Table 6.1 shows the errors and convergence rates for the fully coupled problem on the fine mesh \mathcal{E}_h . We use the NIPG method with penalty $\sigma = 1$ with order of approximation $k_2 = 1$ in the Darcy region. As expected from the theory we observe the expected $O(h)$ convergence rate in the Stokes and Darcy velocities. The Stokes pressure has a slightly higher convergence rate than the expected $O(h)$. Subsequent tables show the errors and convergence rates obtained from solving the coupled problem on \mathcal{E}_h using the modified two-grid algorithm. We will compare the order of convergence and the errors obtained to judge the effectiveness of the two-grid method.

h	$\ \mathbf{U}_1^h - \mathbf{u}_1\ _0$	$\ P_1^h - p_1\ _0$	$\ D(\mathbf{U}_1^h - \mathbf{u}_1)\ _0$	$\ P_2^h - p_2\ _0$	$\ \nabla(P_2^h - p_2)\ _0$
$\frac{1}{4}$	1.591×10^{-2}	6.346×10^{-2}	1.365×10^{-1}	1.341×10^{-2}	1.637×10^{-1}
$\frac{1}{16}$	9.984×10^{-4}	6.645×10^{-3}	3.390×10^{-2}	8.210×10^{-4}	3.856×10^{-2}
$\frac{1}{64}$	6.227×10^{-5}	7.363×10^{-4}	8.469×10^{-3}	5.150×10^{-5}	9.552×10^{-3}
rate(h)	2.00	1.58	1.00	2.00	1.00

Table 6.1 : Errors and rates for (W^h) ($k_1 = 1$, NIPG $\sigma = 1$, $k_2 = 1$).

The two grid algorithm is done in two steps. First we solve the fully coupled problem on a coarse mesh \mathcal{E}_H and then solve the modified Stokes and Darcy problem

on the fine mesh \mathcal{E}_h . Tables 6.2 and 6.3 show the errors and convergence rates for the modified two grid algorithm using the NIPG and SIPG methods in Ω_2 respectively. First we note that the errors obtained from the NIPG and SIPG are comparable. For the SIPG method the expected convergence rate is obtained by making the penalty parameter large enough. This is expected because the coercivity of the bilinear form a_D for the SIPG method is obtained by making the penalty parameter large enough. We obtain order one convergence in the parameter h for both methods. The errors are comparable to solving the fully coupled problem (Table 6.1) for both methods, however the Stokes pressure error is relatively larger for the two-grid problem compared to the fully coupled problem.

h	H	$\ U_{h,1} - u_1\ _0$	$\ P_{h,1} - p_1\ _0$	$\ D(U_{h,1} - u_1)\ _0$	$\ P_{h,2} - p_2\ _0$	$\ \nabla(P_{h,2} - p_2)\ _0$
$\frac{1}{4}$	$\frac{1}{2}$	1.599×10^{-2}	6.647×10^{-2}	1.364×10^{-1}	1.235×10^{-2}	1.657×10^{-1}
$\frac{1}{16}$	$\frac{1}{4}$	9.984×10^{-4}	1.571×10^{-2}	3.397×10^{-2}	1.018×10^{-3}	3.923×10^{-2}
$\frac{1}{64}$	$\frac{1}{8}$	6.073×10^{-5}	4.349×10^{-3}	8.473×10^{-3}	2.699×10^{-4}	9.638×10^{-3}
rate(H)	-	4.00	1.85	2.00	1.92	2.00
rate(h)	-	2.00	0.92	1.00	0.95	1.00

Table 6.2 : Errors and rates for $(W_{h,\alpha}, \alpha = S, D)$ ($k_1 = 1$, NIPG $\sigma = 1$, $k_2 = 1$).

h	H	$\ U_{h,1} - u_1\ _0$	$\ P_{h,1} - p_1\ _0$	$\ D(U_{h,1} - u_1)\ _0$	$\ P_{h,2} - p_2\ _0$	$\ \nabla(P_{h,2} - p_2)\ _0$
$\frac{1}{4}$	$\frac{1}{2}$	1.594×10^{-2}	7.383×10^{-2}	1.363×10^{-1}	8.788×10^{-3}	1.703×10^{-1}
$\frac{1}{16}$	$\frac{1}{4}$	1.002×10^{-3}	1.489×10^{-2}	3.397×10^{-2}	1.471×10^{-3}	4.137×10^{-2}
$\frac{1}{64}$	$\frac{1}{8}$	6.616×10^{-5}	4.166×10^{-3}	8.473×10^{-3}	3.115×10^{-4}	1.011×10^{-2}
rate(H)	-	4.00	1.84	2.00	2.24	2.00
rate(h)	-	2.00	0.92	1.00	1.12	1.00

Table 6.3 : Errors and rates for $(W_{h,\alpha}, \alpha = S, D)$ ($k_1 = 1$, SIPG $\sigma = 3$, $k_2 = 1$).

We increase the degree of approximation in Ω_2 to two. Table 6.4 and 6.5 show

the errors and convergence rates for the two grid algorithm of the NIPG method with $\sigma = 0$ and SIPG with $\sigma = 18$ respectively. On a mesh of size $\frac{1}{64}$ the error in the Darcy velocity is almost ten times smaller compared to Tables 6.2 and 6.3. The Stokes velocity error is unchanged from the case $k_2 = 1$ to $k_2 = 2$. The Stokes pressure error decreases by a factor of four.

h	H	$\ U_{h,1} - u_1\ _0$	$\ P_{h,1} - p_1\ _0$	$\ D(U_{h,1} - u_1)\ _0$	$\ P_{h,2} - p_2\ _0$	$\ \nabla(P_{h,2} - p_2)\ _0$
$\frac{1}{4}$	$\frac{1}{2}$	1.599×10^{-2}	6.577×10^{-2}	1.363×10^{-1}	5.134×10^{-3}	2.556×10^{-2}
$\frac{1}{16}$	$\frac{1}{4}$	9.928×10^{-4}	7.708×10^{-3}	3.396×10^{-2}	1.213×10^{-3}	5.654×10^{-3}
$\frac{1}{64}$	$\frac{1}{8}$	6.258×10^{-5}	1.304×10^{-3}	8.470×10^{-3}	2.981×10^{-4}	1.378×10^{-3}
rate(H)	-	4.00	2.56	2.00	2.00	2.00
rate(h)	-	2.00	1.28	1.00	1.00	1.00

Table 6.4 : Errors and rates for $(W_{h,\alpha}, \alpha = S, D)$ ($k_1 = 1$, NIPG $\sigma = 0$, $k_2 = 2$).

h	H	$\ U_{h,1} - u_1\ _0$	$\ P_{h,1} - p_1\ _0$	$\ D(U_{h,1} - u_1)\ _0$	$\ P_{h,2} - p_2\ _0$	$\ \nabla(P_{h,2} - p_2)\ _0$
$\frac{1}{4}$	$\frac{1}{2}$	1.599×10^{-2}	6.470×10^{-2}	1.364×10^{-1}	4.965×10^{-3}	2.470×10^{-2}
$\frac{1}{16}$	$\frac{1}{4}$	9.927×10^{-4}	7.253×10^{-3}	3.395×10^{-2}	1.192×10^{-3}	5.585×10^{-3}
$\frac{1}{64}$	$\frac{1}{8}$	6.236×10^{-5}	1.124×10^{-3}	8.473×10^{-3}	2.968×10^{-4}	1.374×10^{-3}
rate(H)	-	4.00	2.68	2.00	2.00	2.00
rate(h)	-	2.00	1.34	1.00	1.00	1.00

Table 6.5 : Errors and rates for $(W_{h,\alpha}, \alpha = S, D)$ ($k_1 = 1$, SIPG $\sigma = 18$, $k_2 = 2$).

However, since the order of approximation remains one in the Stokes domain increasing the order to 3 does not have any further improvement in the accuracy of the solution in both domains(see Table 6.6).

The next step is to apply the two-grid method to the fully coupled Navier-Stokes/Darcy model. This method is particularly attractive for this case because it results in a linear system on the fine mesh.

h	H	$\ U_{h,1} - u_1\ _0$	$\ P_{h,1} - p_1\ _0$	$\ D(U_{h,1} - u_1)\ _0$	$\ P_{h,2} - p_2\ _0$	$\ \nabla(P_{h,2} - p_2)\ _0$
$\frac{1}{4}$	$\frac{1}{2}$	1.599×10^{-2}	6.417×10^{-2}	1.363×10^{-1}	4.942×10^{-3}	2.328×10^{-2}
$\frac{1}{16}$	$\frac{1}{4}$	9.926×10^{-4}	7.196×10^{-3}	3.395×10^{-2}	1.191×10^{-3}	5.579×10^{-3}
$\frac{1}{64}$	$\frac{1}{8}$	6.233×10^{-5}	1.119×10^{-3}	8.470×10^{-3}	2.967×10^{-4}	1.375×10^{-3}
rate(H)	-	4.00	2.68	2.00	2.00	2.00
rate(h)	-	2.00	1.34	1.00	1.00	1.00

Table 6.6 : Errors and rates for $(W_{h,\alpha}, \alpha = S, D)$ ($k_1 = 1$, NIPG $\sigma = 0$, $k_2 = 3$).

6.2 Coupled Navier-Stokes/Darcy Model

The two grid approach is applied to the non-linear coupled Navier-Stokes/Darcy coupling. This approach leads to greater computational efficiency in this case because we linearize the modified Navier-Stokes problem.

6.2.1 Two Grid Algorithm: Coupled Navier-Stokes/Darcy

We present the two-grid algorithm applied to the coupled Navier-Stokes-Darcy problem: The bilinear forms are the same as defined in the Stokes-Darcy section. We recall an additional bilinear form for the discretization of the non-linear term:

$$c_{NS}(z, v, w) = \frac{1}{2}(z \cdot \nabla v, w)_{\Omega_1} - \frac{1}{2}(z \cdot \nabla w, v)_{\Omega_1} + \frac{1}{2}(z \cdot n_{12}, v \cdot w)_{\Gamma_{12}}$$

The scheme used for the fully coupled Navier-Stokes/Darcy model is W_B^h defined in Chapter 4 without inertial forces.

1. First we solve a coarse grid problem on a grid of size H :

$$(W^H) \left\{ \begin{array}{l} \text{Find } U_1^H \in X_1^h, P_1^H \in M_1^H, P_2^H \in M_2^H, \text{ s.t.} \\ \forall v_1 \in X_1^H, \forall q_2 \in M_2^H, a_S(U_1^H, v_1) + b_S(v_1, P_1^H) + c_{NS}(U_1^H; U_1^H; v_1) \\ + a_D(P_2^H, q_2) + \gamma(U_1^H, P_2^H; v_1, q_2) = L(v_1, q_2), \\ \forall q_1 \in M_1^h, b_S(U_1^H, q_1) = 0. \end{array} \right.$$

The solution $(\mathbf{U}_1^H, P_1^H, P_2^H)$ is obtained using a Picard iteration as described in Chapter 5.

2. We then solve a modified fine grid problem on a grid of size h :

$$(W_h) \left\{ \begin{array}{l} \text{Find } \mathbf{U}_{h,1} \in \mathbf{X}_1^h, P_{h,1} \in M_1^h, P_{h,2} \in M_2^h, \text{ s.t.} \\ \forall \mathbf{v}_1 \in \mathbf{X}_1^h, \forall q_2 \in M_2^h, \quad a_S(\mathbf{U}_{h,1}, \mathbf{v}_1) + b_S(\mathbf{v}_1, P_{h,1}) + c_{NS}(\mathbf{U}_1^H; \mathbf{U}_1^h, \mathbf{v}_1) \\ + \frac{1}{G}(\mathbf{U}_{h,1} \cdot \boldsymbol{\tau}_{12}, \mathbf{v}_1 \cdot \boldsymbol{\tau}_{12})_{\Gamma_{12}} + a_D(P_{h,2}, q_2) \\ = L(\mathbf{v}_1, q_2) - (P_2^H, \mathbf{v}_1 \cdot \mathbf{n})_{\Gamma_{12}} + (\mathbf{U}_1^H \cdot \mathbf{n}_{12}, q_2)_{\Gamma_{12}}, \\ \forall q_1 \in M_1^h, \quad b_S(\mathbf{U}_{h,1}, q_1) = 0. \end{array} \right.$$

Remark 32. *The modified problem does not require a Picard iteration because the non-linear term (c_{NS}) has been linearized.*

The modified fine grid problem is equivalent to solving modified Navier-Stokes and Darcy problems in Ω_1 and Ω_2 respectively. The modified problems can be stated as follows: in Ω_1 ,

$$(W_{h,NS}) \left\{ \begin{array}{l} \text{Find } \mathbf{U}_{h,1} \in \mathbf{X}_1^h, P_{h,1} \in M_1^h, \text{ s.t.} \\ \forall \mathbf{v}_1 \in \mathbf{X}_1^h, \forall q_2 \in M_2^h, \quad a_S(\mathbf{U}_{h,1}, \mathbf{v}_1) + b_S(\mathbf{v}_1, P_{h,1}) + c_{NS}(\mathbf{U}_1^H; \mathbf{U}_1^h, \mathbf{v}_1) \\ + \frac{1}{G}(\mathbf{U}_{h,1} \cdot \boldsymbol{\tau}_{12}, \mathbf{v}_1 \cdot \boldsymbol{\tau}_{12})_{\Gamma_{12}} = (\mathbf{f}_1, \mathbf{v}_1)_{\Omega_1} - (P_2^H, \mathbf{v}_1 \cdot \mathbf{n})_{\Gamma_{12}}, \\ \forall q_1 \in M_1^h, \quad b_S(\mathbf{U}_{h,1}, q_1) = 0, \end{array} \right.$$

and in Ω_2 ,

$$(W_{h,D}) \left\{ \begin{array}{l} \text{Find } P_{h,2} = P_{h,2} + g_D, P_{h,2} \in M_2^h, \text{ s.t.} \\ \forall q_2 \in M_2^h, \quad a_D(P_{h,2}, q_2) = (f_1, q_2)_{\Omega_2} + (\mathbf{U}_1^H \cdot \mathbf{n}_{12}, q_2)_{\Gamma_{12}} + (g_N, q_2)_{\Gamma_{2N}} \\ + \epsilon \sum_{\Gamma_2^h} (\mathbf{K} \nabla q_2 \cdot \mathbf{n}_e, g_D)_e + \sum_{e \in \Gamma_{2D}} \frac{\sigma_e}{|e|} (q_2, g_D)_e \end{array} \right.$$

6.2.2 Error Analysis: Two-grid Navier-Stokes/Darcy Model

The theory of the two-grid algorithm applied to the Coupled Navier-Stokes/Darcy model has been recently published in [4] for the mixed finite element method applied to Navier-Stokes/Darcy coupling. In the case of the multi-numeric coupled Navier-Stokes/Darcy model studied in this work the proofs are similar. As a result, in this section we state the results without proof and present numerical results from the implementation of this algorithm on the coupling presented in this work.

Theorem 33. *Let $\mathbf{U}_{h,1}, P_{h,1}, P_{2,h}$ be the solution to the two-grid coupled Navier-Stokes-Darcy problem and $\mathbf{U}_1^h, P_1^h, P_2^h$ be the solution to the fully coupled Stokes-Darcy problem. Then under certain regularity conditions [4] and for sufficiently large ν we have the following error estimates:*

$$\|P_2^h - P_{h,2}\| \leq CH^2 \quad (6.41)$$

$$\|\mathbf{D}(\mathbf{U}_2^h - \mathbf{U}_{h,1})\|_{L^2(\Omega_1)} \leq CH^{3/2} \quad (6.42)$$

$$\|P_1^h - P_{h,1}\|_{L^2(\Omega_1)} \leq CH^{3/2} \quad (6.43)$$

Corollary 34. *Let $\mathbf{U}_{h,1}, P_{h,1}, P_{h,2}$ be solutions of the two-grid problem applied to the coupled Navier-Stokes/Darcy model with $H = \sqrt{h}$. Then we have*

$$\|p_2 - P_{h,2}\| \leq Ch$$

and

$$\|\mathbf{D}(\mathbf{u}_1 - \mathbf{U}_{h,1})\|_{L^2(\Omega_1)} + \|p_1 - p_{1,h}\|_{L^2(\Omega_1)} \leq Ch^{3/4}$$

6.2.3 Convergence Study: Two-grid Navier-Stokes/Darcy Model

We present a numerical example with a known solution to verify theoretical convergence rates and to compare the effectiveness of the two-grid method to the fully coupled Navier-Stokes/Darcy model.

Example 35. *The boundary conditions are chosen in such a way that the exact solution to the coupled Stokes/Darcy problem is:*

$$\mathbf{u}_1 = (y^2 - 2y + 2x, x^2 - x - 2y), p_1 = x^2y + xy + y^2 - 4.0$$

$$p_2 = -x^2y + xy + y^2.$$

For simplicity we set

$$\mathbf{K} = \mathbf{I} \text{ and } \nu = 1.0.$$

The computational domain $\Omega_1 = (0, 1) \times (0, 1)$ and $\Omega_2 = (0, 1) \times (1, 2)$.

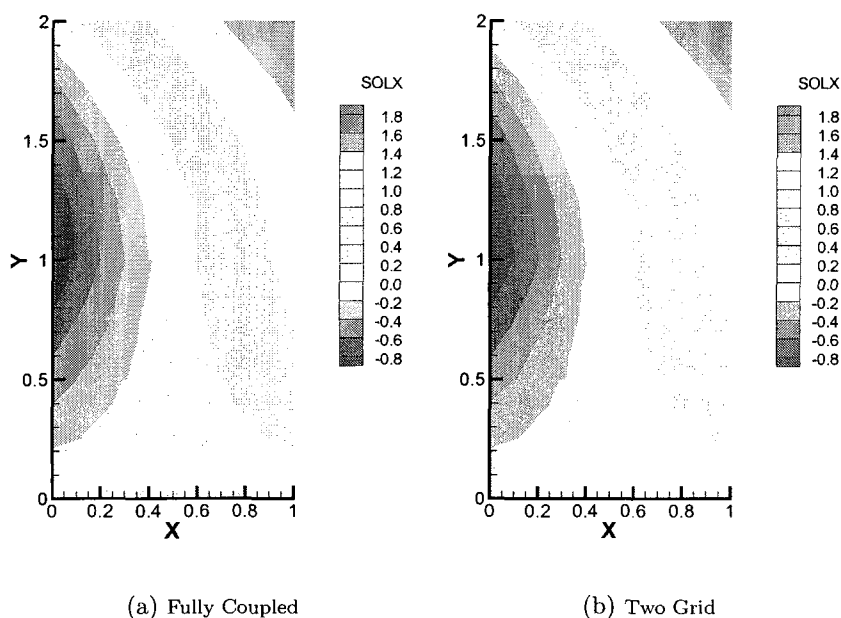
First we solve the fully coupled problem (W_{NS}^h) on the fine mesh \mathcal{E}_h .

h	$\ \mathbf{U}_1^h - \mathbf{u}_1\ _0$	$\ P_1^h - p_1\ _0$	$\ D(\mathbf{U}_1^h - \mathbf{u}_1)\ _0$	$\ P_2^h - p_2\ _0$	$\ \nabla(P_2^h - p_2)\ _0$
$\frac{1}{4}$	1.598×10^{-2}	6.889×10^{-2}	1.366×10^{-1}	2.598×10^{-2}	1.625×10^{-1}
$\frac{1}{16}$	9.988×10^{-4}	6.754×10^{-3}	3.390×10^{-2}	1.592×10^{-3}	3.841×10^{-2}
$\frac{1}{64}$	6.232×10^{-5}	7.403×10^{-4}	8.467×10^{-3}	9.948×10^{-5}	9.541×10^{-3}
rate(h)	2.00	1.59	1.00	2.00	1.00

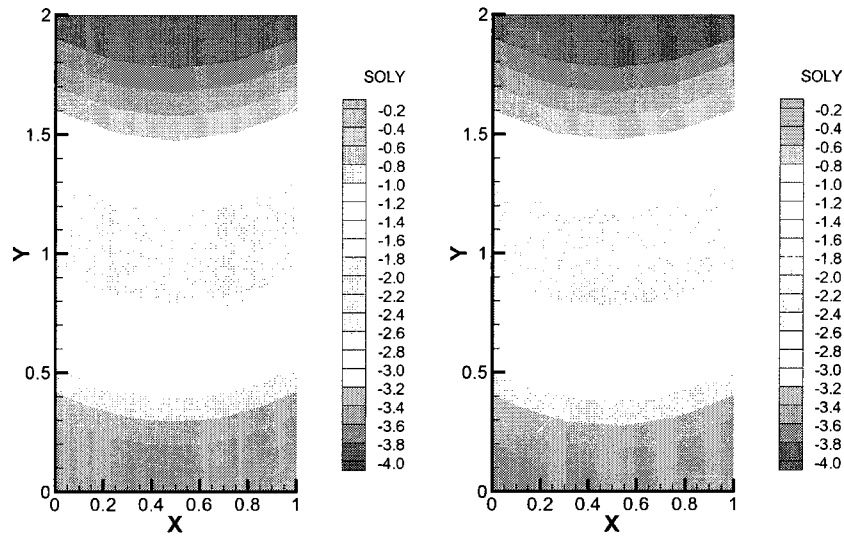
Table 6.7 : Errors and rates for ($W_{h,\text{NS}}$) ($k_1 = 1$, NIPG $\sigma = 1$, $k_2 = 1$).

Table 6.7 shows the errors and convergence rates for the solution from the fully coupled Navier-Stokes/Darcy model solved using a Picard iteration with a tolerance set at 10^{-7} . We observe $O(h)$ convergence rate in the energy norm for the Navier-Stokes and Darcy velocities. Next we compare the solution from the fully coupled problem to the two-grid algorithm. From Table 6.8 we note that the errors from the two-grid method are comparable to the fully coupled problem for the Navier-Stokes and Darcy velocities. The convergence rates are $O(h)$ for the velocity and pressure in both domains. This is better than the theoretical result $O(h^{3/4})$ for the case $H = \sqrt{h}$. The objective of this method is to obtain a solution in a quick manner

h	H	$\ U_{h,1} - u_1\ _0$	$\ P_{h,1} - p_1\ _0$	$\ D(U_{h,1} - u_1)\ _0$	$\ P_{h,2} - p_2\ _0$	$\ \nabla(P_{h,2} - p_2)\ _0$
$\frac{1}{4}$	$\frac{1}{2}$	1.594×10^{-2}	9.7277×10^{-2}	1.365×10^{-1}	4.258×10^{-2}	1.708×10^{-1}
$\frac{1}{16}$	$\frac{1}{4}$	9.696×10^{-4}	1.728×10^{-2}	3.399×10^{-2}	7.068×10^{-3}	4.029×10^{-2}
$\frac{1}{64}$	$\frac{1}{8}$	7.137×10^{-5}	3.961×10^{-3}	8.477×10^{-3}	1.5671×10^{-3}	9.896×10^{-3}
$r(h)$	-	2.00	1.00	1.00	1.20	1.20
$r(H)$	-	4.00	2.00	2.00	2.41	2.40

Table 6.8 : Errors and rates for $(W_{h,\alpha}, \alpha = NS, D)$ ($k_1 = 1$, NIPG $\sigma = 1$, $k_2 = 1$).Figure 6.2 : x- component of velocity $H = 0.5$, $h = 0.25$, NIPG, $k_2 = 2$, $\sigma = 0$.

that gives enough information about the flow. Figures 6.2 and 6.3 are plots of the x and y components of the velocity solutions respectively for the fully coupled Navier-Stokes/Darcy scheme and the two-grid schemes. It is clear that even for the coarse mesh $H = 0.5$ the two-grid solution from $h = 0.25$ gives the same information for the



(a) Fully Coupled

(b) Two Grid

Figure 6.3 : y - component of velocity $H = 0.5, h = 0.25, NIPG, k_2 = 2, \sigma = 0$.

velocity as in the case for the fully coupled problem. We note for the application of this work in tracking contaminants the velocity field for the coupled problem is the input we seek to couple with the Transport equation [8]. Next, we increase the order of approximation in Ω_2 to $k_2 = 2$. From Tables 6.9 as expected the Darcy solution is

h	$\ U_1^h - u_1\ _0$	$\ P_1^h - p_1\ _0$	$\ D(U_1^h - u_1)\ _0$	$\ P_2^h - p_2\ _0$	$\ \nabla(P_2^h - p_2)\ _0$
$\frac{1}{4}$	1.599×10^{-2}	6.687×10^{-2}	1.366×10^{-1}	7.449×10^{-3}	1.463×10^{-2}
$\frac{1}{16}$	9.994×10^{-4}	6.685×10^{-3}	3.390×10^{-2}	4.953×10^{-4}	9.275×10^{-4}
$\frac{1}{64}$	6.232×10^{-5}	7.379×10^{-4}	8.467×10^{-3}	3.1225×10^{-5}	5.812×10^{-5}
rate(h)	2.00	1.59	1.00	2.00	2.00

Table 6.9 : Errors and rates for $(W_{h,NS})$ ($k_1 = 1, NIPG \sigma = 0, k_2 = 2$).

h	H	$\ U_{h,1} - u_1\ _0$	$\ P_{h,1} - p_1\ _0$	$\ D(U_{h,1} - u_1)\ _0$	$\ P_{h,2} - p_2\ _0$	$\ \nabla(P_{h,2} - p_2)\ _0$
$\frac{1}{4}$	$\frac{1}{2}$	1.594×10^{-2}	7.758×10^{-2}	1.364×10^{-1}	2.562×10^{-2}	1.708×10^{-1}
$\frac{1}{16}$	$\frac{1}{4}$	9.674×10^{-4}	1.278×10^{-2}	3.397×10^{-2}	6.1307×10^{-3}	1.057×10^{-2}
$\frac{1}{64}$	$\frac{1}{8}$	6.698×10^{-5}	2.882×10^{-3}	8.474×10^{-3}	1.511×10^{-5}	2.616×10^{-3}
$r(h)$	-	2.00	1.00	1.00	1.20	1.20
$r(H)$	-	4.00	2.00	2.00	2.41	2.40

Table 6.10 : Errors and rates for $(W_{h,\alpha}, \alpha = \text{NS}, D)$ ($k_1 = 1$, NIPG $\sigma = 0$, $k_2 = 2$).

more accurate compared to the order one approximation, the convergence rate in the velocity increases to two. In Table 6.10 we observe that the two grid solution with $k_2 = 2$ is more accurate compared to the one with $k_2 = 1$ in Table 6.8. The Darcy velocity error decreases by a factor of almost 4, this in-turn results in an improvement in the Navier-Stokes velocity and pressure solutions in Ω_1 . However, due to the fact that the order of approximation in Ω_1 remains at $k_1 = 1$ the errors in Table 6.10 are larger compared to the coupled problem in Table 6.9. The convergence rate for the Navier-Stokes velocity and pressure in Ω_1 is $O(h)$, the same holds true for the Darcy velocity in Ω_2 . We also present results for the SIPG method below. As in the case with the Stokes/Darcy, coupling the parameter σ has to be chosen to be large enough in order to observe the expected convergence rate. Table 6.11 shows the errors and

h	$\ U_1^h - u_1\ _0$	$\ P_1^h - p_1\ _0$	$\ D(U_1^h - u_1)\ _0$	$\ P_2^h - p_2\ _0$	$\ \nabla(P_2^h - p_2)\ _0$
$\frac{1}{4}$	1.600×10^{-2}	6.681×10^{-2}	1.366×10^{-1}	5.060×10^{-2}	1.612×10^{-1}
$\frac{1}{16}$	1.000×10^{-3}	6.682×10^{-3}	3.390×10^{-2}	4.000×10^{-4}	3.9791×10^{-2}
$\frac{1}{64}$	6.232×10^{-5}	7.378×10^{-4}	8.467×10^{-3}	2.618×10^{-5}	9.974×10^{-3}
rate(h)	2.00	1.59	1.00	2.00	1.00

Table 6.11 : Errors and rates for $(W_{h,\text{NS}})$ ($k_1 = 1$, SIPG $\sigma = 6$, $k_2 = 1$).

convergence rate for the fully coupled problem with $k_2 = 1$ using the SIPG method in

h	H	$\ U_{h,1} - u_1\ _0$	$\ P_{h,1} - p_1\ _0$	$\ D(U_{h,1} - u_1)\ _0$	$\ P_{h,2} - p_2\ _0$	$\ \nabla(P_{h,2} - p_2)\ _0$
$\frac{1}{4}$	$\frac{1}{2}$	1.594×10^{-2}	7.931×10^{-2}	1.364×10^{-1}	5.289×10^{-2}	1.661×10^{-1}
$\frac{1}{16}$	$\frac{1}{4}$	9.747×10^{-4}	1.278×10^{-2}	3.397×10^{-2}	5.714×10^{-3}	4.153×10^{-2}
$\frac{1}{64}$	$\frac{1}{8}$	6.350×10^{-5}	2.842×10^{-3}	8.474×10^{-3}	1.482×10^{-3}	1.029×10^{-2}
$r(H)$	-	4.00	2.00	2.00	2.41	2.40
$r(h)$	-	2.00	1.00	1.00	1.20	1.20

Table 6.12 : Errors and rates for $(W_{h,\alpha}, \alpha = \text{NS}, D)$ ($k_1 = 1$, SIPG $\sigma = 6$, $k_2 = 1$).

Ω_2 . In Table 6.12 shows the errors and convergence rate from the two grid method on the same meshes. We observe the same trend as in the case with the NIPG method above. The errors for the two-grid method algorithm converge with order h and are comparable to the fully coupled problem.

h	$\ U_1^h - u_1\ _0$	$\ P_1^h - p_1\ _0$	$\ D(U^h - u_1)\ _0$	$\ P_2^h - p_2\ _0$	$\ \nabla(P_2^h - p_2)\ _0$
$\frac{1}{4}$	1.599×10^{-2}	6.604×10^{-2}	1.366×10^{-1}	6.021×10^{-3}	1.301×10^{-2}
$\frac{1}{16}$	9.993×10^{-4}	6.668×10^{-3}	3.390×10^{-2}	3.759×10^{-4}	8.183×10^{-4}
$\frac{1}{64}$	6.233×10^{-5}	7.373×10^{-4}	8.469×10^{-3}	2.349×10^{-5}	5.123×10^{-5}
rate(h)	2.00	1.59	1.00	2.00	1.00

Table 6.13 : Errors and rates for $(W_{h,\text{NS}})$ ($k_1 = 1$, SIPG $\sigma = 18$, $k_2 = 2$).

h	H	$\ U_{h,1} - u_1\ _0$	$\ P_{h,1} - p_1\ _0$	$\ D(U_{h,1} - u_1)\ _0$	$\ P_{h,1} - p_2\ _0$	$\ \nabla(P_{h,2} - p_2)\ _0$
$\frac{1}{4}$	$\frac{1}{2}$	1.594×10^{-2}	7.722×10^{-2}	1.364×10^{-1}	2.4063×10^{-2}	4.206×10^{-2}
$\frac{1}{16}$	$\frac{1}{4}$	9.671×10^{-4}	1.249×10^{-2}	3.397×10^{-2}	6.014×10^{-3}	1.042×10^{-2}
$\frac{1}{64}$	$\frac{1}{8}$	6.764×10^{-5}	2.784×10^{-3}	8.477×10^{-3}	1.503×10^{-3}	2.606×10^{-3}
$r(h)$	-	2.00	1.00	1.00	1.20	1.20
$r(H)$	-	4.00	2.00	2.00	2.41	2.40

Table 6.14 : Errors and rates for $(W_{h,\alpha}, \alpha = \text{NS}, D)$ ($k_1 = 1$, SIPG $\sigma = 18$, $k_2 = 2$).

Tables 6.13 and 6.14 show the errors and convergence rates for the fully coupled

Navier-Stokes/Darcy model and the two-grid method respectively. Increasing the order of approximation in Ω_2 improves the quality of the solution in both domains.

6.2.4 CPU Times: Two-grid Coupled Navier-Stokes/Darcy Model

The advantage of the two-grid method for the Navier-Stokes/Darcy coupling is that it linearizes the problem. This means that on the fine grid we only solve the linear system resulting from the modified Navier-Stokes problem in Ω_1 once. This results in gains in computational time and efficiency of the solver. We first present the CPU times for the time it takes to solve the resulting linear systems.

h	H	Fully Coupled ($t_{W_{NS}^h}$)	Navier-Stokes ($t_{W_{h,NS}}$)	Darcy ($t_{W_{h,D}}$)
$\frac{1}{16}$	$\frac{1}{4}$	1.29×10^0	6.00×10^{-2}	1.20×10^{-1}
$\frac{1}{64}$	$\frac{1}{8}$	$8.731 \times 10^{+1}$	1.69×10^0	7.36×10^0

Table 6.15 : Direct Solver CPU times (s): $W_{NS}^h, W_{h,NS}, W_{h,D}$, (*NIPG* $\sigma = 0, k_2 = 2$).

Table 6.15 shows the CPU times for the fully coupled Navier-Stokes/Darcy model and the two-grid method. Note that for the times $t_{W_{h,NS}}$ and $t_{W_{h,D}}$ includes the time taken to solve for solution of the coupled problem on the coarse mesh. It is very clear that decoupling the problem makes the resulting linear systems much easier to solve as seen by the significant decrease in the time taken to solve them. In most finite element computations the bulk of the time is spent during the assembly of the matrices for the linear system. We also present the total time taken to assemble and solve the system.

From Table 6.16 it is clear that the decoupling technique cuts down the computational time significantly. In the example shown in Table 6.16 the fully coupled

h	H	Fully Coupled ($t_{W_{NS}^h}$)	Navier-Stokes ($t_{W_{h,NS}}$)	Darcy ($t_{W_{h,D}}$)
$\frac{1}{16}$	$\frac{1}{4}$	9.430×10^0	6.800×10^{-1}	6.900×10^{-1}
$\frac{1}{64}$	$\frac{1}{8}$	$1.042 \times 10^{+3}$	2.443×10^2	1.198×10^1

Table 6.16 : Assembly and Solve CPU times (s): W_{NS}^h , $W_{h,NS}$, $W_{h,D}$, (*NIPG* $\sigma = 0$, $k_2 = 2$).

problem has a linear system of size (77825×77825) . The two-grid method results in two problems of sizes (28673×28673) and (49152×49152) for the Navier-Stokes and Darcy domains respectively. The amount of time it takes to solve the problem is cut by a factor of 4.

6.3 Conclusion

The two-grid method has been applied to the Stokes/Darcy and Navier-Stokes/Darcy coupled models. Theoretically we have shown that the solution obtained from the two-grid model converges to the true solution with order $h^{3/4}$ in the case when $h = \sqrt{H}$. However, numerical simulations show an order h convergence rate. A finer analysis will be needed to achieve this convergence rate. The two-grid algorithm achieves the goal of obtaining a solution which gives the essential features of the flow in a fraction of the time. One can further improve on the gains shown in this chapter by the use solvers that have been optimized for each problem in each domain.

Chapter 7

Coupled Discontinuous Galerkin Method with Finite Volume Method

7.1 Introduction

In previous chapters the Discontinuous Galerkin method has been used to approximate the flow in the porous medium. We have shown that this method captures the flow well for example in heterogeneous media and faults. In practice, these areas are a small subset of the computational domain. In the rest of the domain the permeability is well behaved. This means that we could cut down the size of the problem by using the Discontinuous Galerkin method only in the problem areas and using a low order method in the rest of the domain. In this chapter we propose to couple the Discontinuous Galerkin method with the finite volume method on Voronoi cells. We show that we are able to obtain an accurate solution by solving relatively smaller linear systems.

7.2 Model Problem And Scheme

Let $\Omega \in \mathbb{R}^d$, $d = 2, 3$, be a bounded polygonal domain subdivided into non overlapping subdomains Ω_F^i and Ω_D^i and let $\Omega_F = \cup_i \Omega_F^i$ and $\Omega_D = \cup_i \Omega_D^i$. The numerical method discussed in this chapter uses a finite volume method on Ω_F and a discontinuous Galerkin method on Ω_D . Let $f \in L^2(\Omega)$ and $g \in H^{1/2}(\partial\Omega)$. The solution u of the

elliptic problem satisfies

$$-\nabla \cdot (K \nabla u) = f, \quad \text{in } \Omega, \quad (7.1)$$

$$u = g, \quad \text{on } \partial\Omega. \quad (7.2)$$

The coefficient K is bounded above and below by positive constants k_1 and k_0 respectively. Let \mathcal{E}_D^h (resp. \mathcal{E}_F^h) be a subdivision of Ω_D (resp. Ω_F), made of cells V (Voronoi cells in Ω_F and either triangles/tetrahedra/hexahedra or Voronoi cells in Ω_D). We also denote by h_F (resp. h_D) the maximum diameter over all cells in Ω_F (resp. Ω_D) and we let $h = \max(h_F, h_D)$. We assume that the meshes match at the interface $\Gamma_{DF} = \partial\Omega_D \cap \partial\Omega_F$.

The definition of the mesh \mathcal{E}_F^h requires further notation. We assume that \mathcal{E}_F^h is an admissible finite volume mesh, in the following sense:

1. There is a family of nodes $\{x_V\}_{V \in \mathcal{E}_F^h}$ such that $x_V \in \overline{V}$ and if an edge γ is such that $\gamma = \partial V \cap \partial W$ with $W \neq V$, it is assumed that $x_W \neq x_V$ and that the straight line going through x_V and x_W is orthogonal to γ .
2. For any boundary edge $\gamma = \partial V \cap \partial\Omega$ with $V \in \mathcal{E}_F^h$, it is assumed that $x_V \notin \gamma$. However this condition can be relaxed (see Remark 1 in Section 7.3). Let y_γ be the (non-empty) intersection between the straight line going through x_V and orthogonal to γ .

We denote by $\Gamma_F^{h,\mathcal{I}}$ the set of edges that belong to the interior of Ω_F and by $\Gamma_F^{h,\partial}$ the set of boundary edges that belong to $\partial\Omega_F \cap \partial\Omega$. Similarly, the sets of edges that belong to the interior of Ω_D and boundary edges that belong to $\partial\Omega_D \cap \partial\Omega$ are denoted by $\Gamma_D^{h,\mathcal{I}}$ and $\Gamma_D^{h,\partial}$ respectively. We also define

$$\Gamma_F^h = \Gamma_F^{h,\mathcal{I}} \cup \Gamma_F^{h,\partial}, \quad \Gamma_D^h = \Gamma_D^{h,\mathcal{I}} \cup \Gamma_D^{h,\partial}.$$

There remains the set of edges that belong to the interface Γ_{DF} ; this particular set is denoted by Γ_{DF}^h .

We now define a parameter d_γ that is associated to each edge in the FV mesh. Let V and W be two cells in the FV region such that $\gamma = \partial V \cap \partial W$ is an interior edge. We define the parameter d_γ to be the Euclidean distance between the nodes x_V and x_W .

$$d_\gamma = d(x_V, x_W).$$

If the edge γ is a boundary edge (i.e. belongs to $\partial V \cap \partial\Omega$) the parameter d_γ is the distance between the node x_V and the edge γ .

$$d_\gamma = d(x_V, \gamma) = d(x_V, y_\gamma).$$

Next, assume that an edge γ is the intersection of a FV cell V and a DG cell W . The parameter d_γ is defined to be the distance between the node x_V and the point y_γ , which is (as in the boundary case) the intersection between the straight line going through x_V and orthogonal to γ . Here, we have made the assumption that x_V does not lie on the interface γ . Assume there is some $\theta > 0$ such that

$$\forall \gamma \in \Gamma_F^{h,\mathcal{I}}, \quad \gamma = \partial V \cap \partial W, \quad d_\gamma \geq \theta \max(h_V, h_W),$$

$$\forall \gamma \in \Gamma_F^{h,\partial}, \quad \gamma = \partial V \cap \partial\Omega, \quad d_\gamma \geq \theta h_V,$$

$$\forall \gamma \in \Gamma_{DF}^h, \quad \gamma = \partial V \cap \partial W, \quad V \in \mathcal{E}_F^h, \quad W \in \mathcal{E}_D^h, \quad d_\gamma \geq \theta h_V.$$

Finally, we define the harmonic average of the diffusion coefficient:

$$\forall \gamma \in \Gamma_F^{h,\mathcal{I}}, \quad \gamma = \partial V \cap \partial W, \quad K_\gamma = d_\gamma \left| \int_{x_V}^{x_W} \frac{ds}{K(s)} \right|^{-1},$$

$$\forall \gamma \in \Gamma_F^{h,\partial}, \quad \gamma = \partial V \cap \partial\Omega, \quad K_\gamma = d_\gamma \left| \int_{x_V}^{y_\gamma} \frac{ds}{K(s)} \right|^{-1},$$

$$\forall \gamma \in \Gamma_{DF}^h, \quad \gamma = \partial V \cap \partial W, \quad V \in \mathcal{E}_F^h, \quad W \in \mathcal{E}_D^h, \quad K_\gamma = d_\gamma \left| \int_{x_V}^{y_\gamma} \frac{ds}{K(s)} \right|^{-1}.$$

It is easy to see that K_γ is also bounded above and below by k_1 and k_0 respectively.

We denote by $|\gamma|$ the length of an edge γ . The finite dimensional space consists of piecewise polynomials of degree less than or equal to r in the DG region and of degree equal to zero in the FV region.

$$X^h = \{v \in L^2(\Omega) : v|_V \in \mathbb{P}_r(V) \quad \forall V \in \mathcal{E}_D^h, \quad v|_V \in \mathbb{P}_0(V) \quad \forall V \in \mathcal{E}_F^h\}.$$

Define the jump of a function in X^h . For any edge γ we fix a unit normal vector \mathbf{n}_γ to γ . We assume that if γ is a boundary edge (belongs to $\partial\Omega$), then \mathbf{n}_γ points outward of $\partial\Omega$. If γ belongs to the interface Γ_{DF}^h , then we assume that \mathbf{n}_γ points from the DG region into the FV region. Let us denote by V and W the mesh elements so that the vector \mathbf{n}_γ points from ∂V into ∂W . We define the jump of a function $u \in X^h$.

$$\gamma \in \Gamma_F^{h,\mathcal{I}}, \quad [u]|_\gamma = u(x_V) - u(x_W),$$

$$\gamma \in \Gamma_D^{h,\mathcal{I}}, \quad [u]|_\gamma = u|_V - u|_W,$$

$$\gamma \in \Gamma_{DF}^h, \quad [u]|_\gamma = u|_{\Omega_D}(y_\gamma) - u|_{\Omega_F}(x_W),$$

$$\gamma \in \Gamma_F^{h,\partial}, \quad [u]|_\gamma = u(x_V),$$

$$\gamma \in \Gamma_D^{h,\partial}, \quad [u]|_\gamma = u|_V.$$

We remark that the quantity $[u]|_\gamma$ is a number except for the edges $\gamma \in \Gamma_D^h$. The DG method requires additional notation. Let $\{u\}$ denote the average of a function $u \in X^h$.

$$\gamma \in \Gamma_D^{h,\mathcal{I}}, \quad \gamma = \partial V \cap \partial W, \quad \{u\}_\gamma = 0.5(u|_V + u|_W),$$

$$\gamma \in \Gamma_D^{h,\partial}, \quad \gamma \in \partial V, \quad \{u\}_\gamma = u.$$

Let $\sigma > 0$ denote the penalty parameter and $\epsilon \in \{-1, 1\}$ be the symmetrization parameter. For a given edge γ shared by two mesh elements V and W , let $h_\gamma =$

$\max(\text{diam}(V), \text{diam}(W))$. The DG bilinear form is for all $u, v \in X^h$

$$\begin{aligned} a_D(u, v) &= \sum_{V \in \mathcal{E}_D^h} \int_V K \nabla u \cdot \nabla v - \sum_{\gamma \in \Gamma_D^h} \int_\gamma \{K \nabla u \cdot \mathbf{n}_\gamma\} [v] \\ &+ \epsilon \sum_{\gamma \in \Gamma_D^h} \int_\gamma \{K \nabla v \cdot \mathbf{n}_\gamma\} [u] + \sum_{\gamma \in \Gamma_D^h} \frac{\sigma}{h_\gamma} \int_\gamma [u][v]. \end{aligned} \quad (7.3)$$

The cell-centered finite volume method is defined by the following bilinear form for all $u, v \in X^h$

$$a_F(u, v) = \sum_{\gamma \in \Gamma_F^h} \frac{|\gamma|}{d_\gamma} K_\gamma [u][v]. \quad (7.4)$$

Our scheme uses the overall bilinear form for all $u, v \in X^h$

$$a(u, v) = a_D(u, v) + a_F(u, v) + a_{DF}(u, v), \quad (7.5)$$

where a_{DF} is the coupling form at the interface Γ_{FD}^h :

$$a_{DF}(u, v) = \sum_{\gamma \in \Gamma_{FD}^h} \frac{|\gamma|}{d_\gamma} K_\gamma [u][v]. \quad (7.6)$$

The source functions and boundary conditions are taken into account in the form

$$\forall v \in X^h, \quad \ell(v) = \int_\Omega f v + \epsilon \sum_{\gamma \in \Gamma_D^{h,\partial}} \int_\gamma (K \nabla v \cdot \mathbf{n}_\gamma + \frac{\sigma}{h_\gamma} v) g + \sum_{\gamma \in \Gamma_F^{h,\partial}} K_\gamma \frac{|\gamma|}{d_\gamma} g(y_\gamma) v. \quad (7.7)$$

The numerical scheme is: to find $U \in X^h$ satisfying

$$\forall v \in X^h, \quad a(U, v) = \ell(v) \quad (7.8)$$

We next define some norms, that naturally arise from the bilinear forms above:

$$\|v\|_{DG} = \left(\sum_{V \in \mathcal{E}_D^h} \|K^{1/2} \nabla v\|_{L^2(V)}^2 + \sum_{\gamma \in \Gamma_D^h} h_\gamma^{-1/2} \|[v]\|_{L^2(\gamma)}^2 \right)^{1/2}, \quad (7.9)$$

$$\|v\|_{FV} = \left(\sum_{\gamma \in \Gamma_F^h} \frac{|\gamma|}{d_\gamma} K_\gamma [v]^2 \right)^{1/2}, \quad (7.10)$$

$$\|v\|_{\mathcal{E}} = \left(\|v\|_{DG}^2 + \|v\|_{FV}^2 + \sum_{\gamma \in \Gamma_{FD}^h} \frac{K_\gamma}{d_\gamma} [v]^2 \right)^{1/2}. \quad (7.11)$$

We now give some important properties of the bilinear forms.

Lemma 36. *There exist α, β positive constants independent of h such that*

$$\forall v \in X^h, \quad a_D(v, v) \geq \alpha \|v\|_{DG}^2, \quad (7.12)$$

$$\forall v \in X^h, \quad a_F(v, v) = \|v\|_{FV}^2, \quad (7.13)$$

$$\forall v \in X^h, \quad a(v, v) \geq \beta \|v\|_{\mathcal{E}}^2. \quad (7.14)$$

Proof. Inequality (7.12) is well known and requires the penalty parameter σ to be large enough if $\epsilon = -1$ [47]. Inequality (7.13) is trivial and the third inequality is a straightforward consequence of the first two and the definition (7.5). \square

Lemma 37. *There exists a unique solution $U \in X^h$ satisfying (7.8).*

Proof. It suffices to show uniqueness of U satisfying (7.8) with $f = g = 0$. Take $v = U$ in (7.8), and use coercivity of a . This implies that $\|U\|_{\mathcal{E}} = 0$ and thus $U = 0$ in X^h . \square

7.3 Error Analysis

For simplicity proofs are given in the case where there are only one DG region and one FV region, but the proofs for the general case are similar. For each edge γ we define a subdomain \mathcal{V}_γ as follows. Assume that $\gamma \in \Gamma_F^{h, \mathcal{I}}$ with $\gamma = \partial V \cap \partial W$. Define

$$\mathcal{V}_{W, \gamma} = \{tx_V + (1-t)x, \quad x \in \gamma, \quad t \in [0, 1]\},$$

and let

$$\mathcal{V}_\gamma = \mathcal{V}_{W, \gamma} \cap \mathcal{V}_{V, \gamma}.$$

Assume now that $\gamma \in \Gamma_F^{h, \partial}$ with $\gamma \subset \partial W$, then $\mathcal{V}_\gamma = \mathcal{V}_{W, \gamma}$. Finally if $\gamma \in \Gamma_{DF}^h$ with $\gamma = \partial V \cap \partial W$, and $W \in \mathcal{E}_F^h$, then $\mathcal{V}_\gamma = \mathcal{V}_{W, \gamma}$.

Lemma 38. Define the residuals for any $u \in H^2(\Omega)$.

$$\gamma \in \Gamma_F^{h,\mathcal{I}} \quad R_\gamma(u) = -\frac{|\gamma|}{d_\gamma} K_\gamma[u] - \int_\gamma K \nabla u \cdot n_\gamma, \quad (7.15)$$

$$\gamma \in \Gamma_F^{h,\partial}, \quad \gamma = \partial V \cap \partial \Omega \quad R_\gamma(u) = -\frac{|\gamma|}{d_\gamma} K_\gamma(u(x_V) - g(y_\gamma)) - \int_\gamma K \nabla u \cdot n_\gamma, \quad (7.16)$$

$$\forall \gamma \in \Gamma_{DF}^h, \quad R_\gamma(u) = -K \nabla u \cdot n_\gamma - \frac{K_\gamma}{d_\gamma} [u]. \quad (7.17)$$

Let $H(u)$ denote the Hessian matrix of u . Assume K is a positive constant. Then, there exists a constant C independent of h and u , but dependent on θ , such that

$$\gamma \in \Gamma_F^h, \quad |R_\gamma(u)|^2 \leq C \frac{h_F^2 |\gamma|}{d_\gamma} \int_{\mathcal{V}_\gamma} |H(u)|^2, \quad (7.18)$$

$$\gamma \in \Gamma_{DF}^h, \quad \left(\int_\gamma |R_\gamma(u)| \right)^2 \leq C \frac{h_F^2 |\gamma|}{d_\gamma} \int_{\mathcal{V}_\gamma} |H(u)|^2. \quad (7.19)$$

Proof. Inequalities (7.18) and (7.19) can be found in [18]. \square

The following result shows that there is a consistency error only due to the FV discretization. In the DG region, there is no consistency error.

Lemma 39. Let $u \in H^1(\Omega) \cap H^2(\mathcal{E}^h)$ be the solution to problem (7.1)-(7.2). Then u satisfies

$$\begin{aligned} \forall v \in X^h, \quad a(u, v) &= \ell(v) - \sum_{\gamma \in \Gamma_F^h} R_\gamma(u)[v] - \sum_{\gamma \in \Gamma_{DF}^h} [v] \int_\gamma R_\gamma(u) \\ &- \sum_{\gamma \in \Gamma_{DF}^h} \int_\gamma R_\gamma(u) (v|_{\Omega_D} - v|_{\Omega_D}(y_\gamma)) + \sum_{\gamma \in \Gamma_{DF}^h} \frac{|\gamma| K_\gamma}{d_\gamma} [u] \left(v|_{\Omega_D}(y_\gamma) - |\gamma|^{-1} \int_\gamma v|_{\Omega_D} \right). \end{aligned} \quad (7.20)$$

Proof. Let $V \in \mathcal{E}_F^h$ and let $v \in X^h$ such that $v|_V = 1$ and $v = 0$ elsewhere. Denote by n_V the outward unit normal to V . Multiply (7.1) by v and integrate on V by parts:

$$- \int_{\partial V} K \nabla u \cdot n_V v = \int_V f v,$$

or

$$- \sum_{\gamma \in \partial V} \int_\gamma K \nabla u \cdot n_V v = \int_V f v. \quad (7.21)$$

Summing (7.21) over all FV cells, and using the residual definitions, we obtain for all $v \in X^h$:

$$a_F(u, v) + \sum_{\gamma \in \Gamma_{DF}^h} \int_{\gamma} K \nabla u \cdot \mathbf{n}_{\gamma} v_{FV} + \sum_{\gamma \in \Gamma_F^h} R_{\gamma}(u)[v] - \sum_{\gamma \in \Gamma_F^{h,\theta}} \frac{|\gamma|}{d_{\gamma}} K_{\gamma} g(y_{\gamma}) v = \int_{\Omega_F} f v. \quad (7.22)$$

For readability, we denote by v_{DG} the restriction of v to the DG region and by v_{FV} its restriction to the FV region. Next, we consider $V \in \mathcal{E}_D^h$, multiply (7.1) by $v \in X^h$ and integrate by parts:

$$\int_V K \nabla u \cdot \nabla v - \int_{\partial V} K \nabla u \cdot \mathbf{n}_V v = \int_V f v.$$

Sum over all V in the DG region, add the stabilization terms to obtain

$$a_D(u, v) - \sum_{\gamma \in \Gamma_{DF}^h} \int_{\gamma} K \nabla u \cdot \mathbf{n}_{\gamma} v_{DG} = \int_{\Omega_D} f v + \epsilon \sum_{\gamma \in \Gamma_D^{h,\theta}} \int_{\gamma} (K \nabla v \cdot \mathbf{n}_{\gamma} + \frac{\sigma}{h_{\gamma}} v) g. \quad (7.23)$$

We now add (7.22) and (7.23):

$$a_F(u, v) + a_D(u, v) + T = \ell(v) - \sum_{\gamma \in \Gamma_F^h} R_{\gamma}(u)[v],$$

where T corresponds to the terms involving integrals on the interface Γ_{DF} . We can write using the regularity of the solution u (namely the fact that $u \in H^2(\Omega)$):

$$\begin{aligned} T &= - \sum_{\gamma \in \Gamma_{DF}^h} \int_{\gamma} K \nabla u \cdot \mathbf{n}_{\gamma} (v_{DG} - v_{FV}) = - \sum_{\gamma \in \Gamma_{DF}^h} \int_{\gamma} K \nabla u \cdot \mathbf{n}_{\gamma} (v_{DG} - v_{DG}(y_{\gamma})) \\ &\quad - \sum_{\gamma \in \Gamma_{DF}^h} [v] \int_{\gamma} K \nabla u \cdot \mathbf{n}_{\gamma}. \end{aligned}$$

Using the definition of the residual in Lemma 38, we obtain

$$T = \sum_{\gamma \in \Gamma_{DF}^h} \int_{\gamma} (R_{\gamma}(u) + \frac{K_{\gamma}}{d_{\gamma}} [u]) (v_{DG} - v_{DG}(y_{\gamma})) + \sum_{\gamma \in \Gamma_{DF}^h} [v] \int_{\gamma} (R_{\gamma}(u) + \frac{K_{\gamma}}{d_{\gamma}} [u]),$$

or

$$T = a_{DF}(u, v) + \sum_{\gamma \in \Gamma_{DF}^h} [v] \int_{\gamma} R_{\gamma}(u) + \sum_{\gamma \in \Gamma_{DF}^h} \int_{\gamma} R_{\gamma}(u) (v_{DG} - v_{DG}(y_{\gamma})) - \sum_{\gamma \in \Gamma_{DF}^h} \frac{|\gamma| K_{\gamma}}{d_{\gamma}} [u] E(v_{DG}),$$

with

$$E(v_{DG}) = v_{DG}(y_\gamma) - \frac{1}{|\gamma|} \int_\gamma v_{DG}.$$

Thus we can conclude. \square

Theorem 40. *Assume that $u \in H^2(\Omega)$ and that $u|_{\Omega_D} \in H^{r+1}(\mathcal{E}_D^h)$ for $r \geq 1$. Under the assumptions of Lemma 38, there exists a constant C independent of h_D and h_F such that*

$$\|U - u\|_{\mathcal{E}} \leq C(h_D^r + h_F).$$

Proof. We can write

$$U - u = \chi - \xi, \quad \chi = U - \tilde{u}, \quad \xi = u - \tilde{u}.$$

The function $\tilde{u} \in X^h$ is chosen so that

$$\forall V \in \mathcal{E}_F^h, \quad \tilde{u}|_V = u(x_V). \tag{7.24}$$

On the DG region \tilde{u} is assumed to satisfy the usual approximation properties. Using the definition of the scheme (7.8) and Lemma 39, we obtain an error equation:

$$\begin{aligned} a(\chi, \chi) &= a(\xi, \chi) + \sum_{\gamma \in \Gamma_F^h} R_\gamma(u)[\chi] + \sum_{\gamma \in \Gamma_{DF}^h} [\chi] \int_\gamma R_\gamma(u) + \sum_{\gamma \in \Gamma_{DF}^h} \int_\gamma R_\gamma(u)(\chi|_{\Omega_D} - \chi|_{\Omega_D}(y_\gamma)) \\ &\quad + \sum_{\gamma \in \Gamma_{DF}^h} \frac{|\gamma|K_\gamma}{d_\gamma} [u] \left(\chi|_{\Omega_D}(y_\gamma) - |\gamma|^{-1} \int_\gamma \chi|_{\Omega_D} \right). \end{aligned}$$

Let us estimate the terms in the right hand side. Since $\xi(x_V) = 0$ for all nodes x_V in Ω_F , we have

$$a(\xi, \chi) = a_D(\xi, \chi) + a_F(\xi, \chi) + a_{DF}(\xi, \chi) = a_D(\xi, \chi) + a_{DF}(\xi, \chi).$$

We can use standard techniques to bound $a_D(\xi, \chi)$. The other term reduces to

$$a_{DF}(\xi, \chi) = \sum_{\gamma \in \Gamma_{DF}^h} \frac{|\gamma|K_\gamma}{d_\gamma} [\chi] \xi|_{\Omega_D}(y_\gamma).$$

We claim that we can choose the approximation \tilde{u} such that $\xi|_{\Omega_D}(y_\gamma) = 0$. In that case we have $a_{DF}(\xi, \chi) = 0$. The first consistency error term is bounded as follows:

$$\sum_{\gamma \in \Gamma_F^h} R_\gamma(u)[\chi] \leq \frac{1}{16} \sum_{\gamma \in \Gamma_F^h} \frac{|\gamma| K_\gamma}{d_\gamma} [\chi]^2 + 4 \sum_{\gamma \in \Gamma_F^h} \frac{d_\gamma}{|\gamma|} (R_\gamma(u))^2.$$

Using the bound (7.18) and denoting by $H(u)$ the Hessian matrix of u , we have

$$\sum_{\gamma \in \Gamma_F^h} R_\gamma(u)[\chi] \leq \frac{1}{16} \sum_{\gamma \in \Gamma_F^h} \frac{|\gamma| K_\gamma}{d_\gamma} [\chi]^2 + Ch_F^2 \int_{\Omega_F} |H(u)|^2.$$

The second consistency error term is as:

$$\sum_{\gamma \in \Gamma_{DF}^h} [\chi] \int_\gamma R_\gamma(u) \leq \frac{1}{16} \sum_{\gamma \in \Gamma_{DF}^h} \frac{|\gamma| K_\gamma}{d_\gamma} [\chi]^2 + 4 \sum_{\gamma \in \Gamma_{DF}^h} \frac{d_\gamma}{|\gamma|} \left(\int_\gamma R_\gamma(u) \right)^2.$$

which with the bound (7.19) gives:

$$\sum_{\gamma \in \Gamma_{DF}^h} [\chi] \int_\gamma R_\gamma(u) \leq \frac{1}{16} \sum_{\gamma \in \Gamma_{DF}^h} \frac{|\gamma| K_\gamma}{d_\gamma} [\chi]^2 + Ch_F^2 \int_{\Omega_F} |H(u)|^2.$$

Finally we have

$$\sum_{\gamma \in \Gamma_{DF}^h} \int_\gamma R_\gamma(u) (\chi|_{\Omega_D} - \chi|_{\Omega_D}(y_\gamma)) \leq \sum_{\gamma \in \Gamma_{DF}^h} \int_\gamma |R_\gamma(u)| |\chi|_{\Omega_D} - \chi|_{\Omega_D}(y_\gamma)|.$$

Let us fix an edge $\gamma \in \Gamma_{DG}^h$ with $\gamma = \partial V \cap \partial W$, and $V \in \mathcal{E}_D^h$. Let us denote by $\eta = \chi|_V - \chi|_V(y_\gamma)$. Then we have by trace and inverse inequalities:

$$\|\eta\|_{L^\infty(\gamma)} \leq Ch_D^{-1/2} \|\eta\|_{L^2(\gamma)} \leq C \|\nabla \eta\|_{L^2(V)}.$$

Therefore we obtain

$$\begin{aligned} \sum_{\gamma \in \Gamma_{DF}^h} \int_\gamma R_\gamma(u) (\chi|_{\Omega_D} - \chi|_{\Omega_D}(y_\gamma)) &\leq \frac{1}{16} \|\chi\|_{DG}^2 + C \sum_{\gamma \in \Gamma_{DF}^h} \left(\int_\gamma |R_\gamma(u)| \right)^2 \\ &\leq \frac{1}{16} \|\chi\|_{DG}^2 + Ch_F^2 \int_{\Omega_F} |H(u)|^2. \end{aligned}$$

The last consistency error term is bounded as follows. Fix an edge in Γ_{DF}^h such that $\gamma = \partial V \cap \partial W$ with $V \in \mathcal{E}_D^h$:

$$\frac{|\gamma| K_\gamma}{d_\gamma} [u] \left(\chi|_{\Omega_D}(y_\gamma) - |\gamma|^{-1} \int_\gamma \chi|_{\Omega_D} \right) \leq C \|\nabla \chi\|_{L^2(V)} \frac{|\gamma| K_\gamma}{d_\gamma} |[u]|.$$

Using the density of C^1 into H^2 and a Taylor expansion, we can prove that:

$$|[u]|_\gamma \leq d_\gamma |\gamma|^{1/2} \|\nabla u \cdot \mathbf{n}\|_{L^2(\gamma)}.$$

So we have

$$\begin{aligned} \sum_{\gamma \in \Gamma_{DF}^h} \frac{|\gamma| K_\gamma}{d_\gamma} [u] \left(\chi|_{\Omega_D}(y_\gamma) - |\gamma|^{-1} \int_\gamma \chi|_{\Omega_D} \right) &\leq \frac{1}{16} \|\chi\|_{DG}^2 + Ch_F^3 \|\nabla u \cdot \mathbf{n}\|_{L^2(\Gamma_{DF}^h)}^2 \\ &\leq \frac{1}{16} \|\chi\|_{DG}^2 + Ch_F^2 \|u\|_{H^2(\Omega_F)}^2. \end{aligned}$$

We can then conclude. \square

Remark 1: The results of Theorem 40 are still valid if there are some nodes x_V located on boundary edges $\gamma \in \Gamma_F^{h,\partial}$. Let denote by $\Gamma_F^{h,0}$ the set of such edges. The coupled scheme is slightly modified. The discrete space is the set Y^h of functions $v \in X^h$ such that $v(x_V) = 0$ for all $x_V \in \Gamma_F^{h,0}$. The bilinear form a_F and linear form ℓ become

$$\begin{aligned} a_F(u, v) &= \sum_{\gamma \in \Gamma_F^h \setminus \Gamma_F^{h,0}} \frac{|\gamma|}{d_\gamma} K_\gamma [u][v] \\ \ell(v) &= \int_\Omega f v + \epsilon \sum_{\gamma \in \Gamma_D^{h,\partial}} \int_\gamma (K \nabla v \cdot \mathbf{n}_\gamma + \frac{\sigma}{h_\gamma} v) g + \sum_{\gamma \in \Gamma_F^{h,\partial} \setminus \Gamma_F^{h,0}} K_\gamma \frac{|\gamma|}{d_\gamma} g(y_\gamma) v. \end{aligned}$$

The solution $U \in X^h$ is such that $U(x_V) = g(x_V)$ for all $x_V \in \Gamma_F^{h,0}$, and satisfies

$$\forall v \in Y^h, \quad a(U, v) = \ell(v)$$

7.4 Numerical Examples

In the following section we present examples that verify the convergence rates for the proposed FV-DG coupling and illustrate cases in which the coupled scheme yields a more accurate solution.

Example 41. Convergence Study

First we consider the unit square domain Ω partitioned into two subdomains Ω_D and Ω_F (see Fig. 7.1). The boundary conditions are chosen so that the exact solution $u(x, y) = (x^2 - x)(y^2 - y)$ and the coefficient K is equal to one.

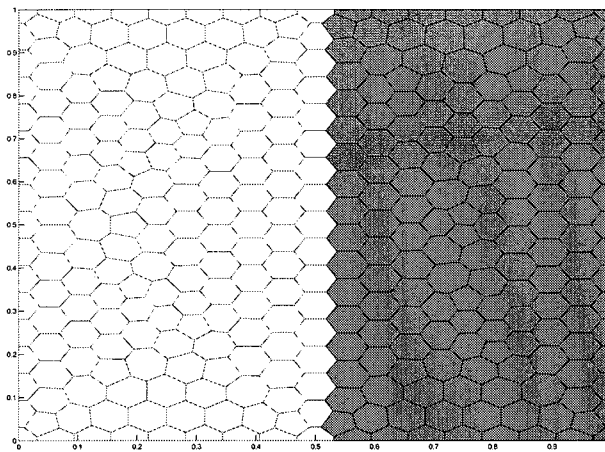
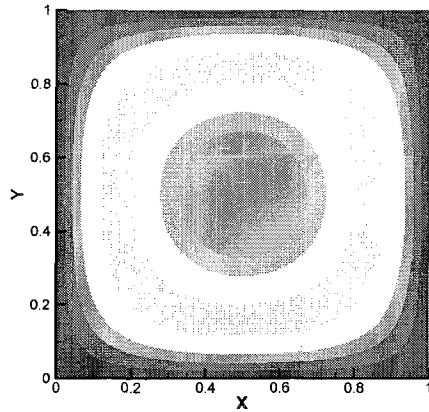


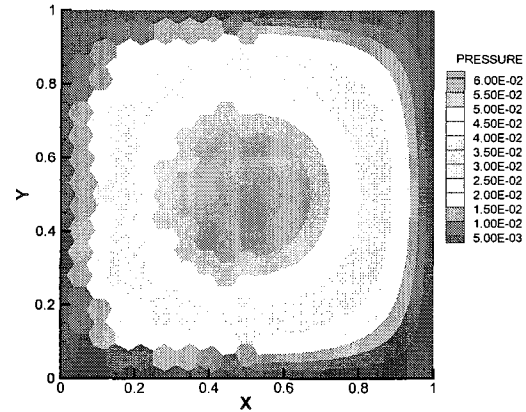
Figure 7.1 : Computational mesh with 340 Voronoi cells: Ω_F is the white region and Ω_D is the grey region.

In order to perform the convergence tests we generate four Delaunay triangulations using the software EasyMesh developed by Bojan Niceno [37]. At each level of refinement we ensure that the maximum area of each triangle decreases by a factor of 4. We then generate the dual Voronoi mesh for each Delaunay triangulation. This technique has been used in [35]. Fig. 7.1 shows an example of the mesh for the convergence test with 340 Voronoi cells. The shaded subdomain is Ω_D on which the solution is approximated using the discontinuous Galerkin method and the rest of the domain is Ω_{FV} , on which the finite volume method is used. The DG parameters are

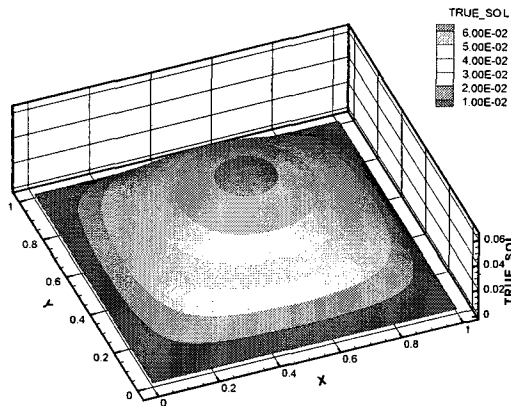
chosen as: $\sigma = 1, \epsilon = 1$.



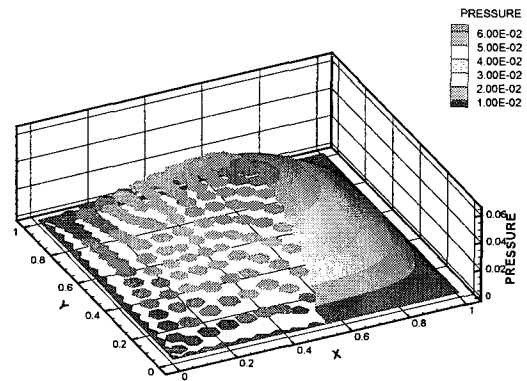
(a) Exact Pressure



(b) Approximate Pressure



(c) Exact Pressure



(d) Approximate Pressure

Figure 7.2 : Contours of exact and numerical solutions for example 1.

Fig. 7.2 shows the exact solution and the numerical solution obtained on the mesh shown in Fig. 7.1. We observe the expected clear distinction between the piecewise constant solution on Ω_F and the smoother solution on Ω_D on which the solution is

approximated by discontinuous quadratic polynomials. Tables 7.1 and 7.2 show the

N	$\ U - u\ _{0,FV}$	$\ U - u\ _{FV}$	$\ U - u\ _{L^2(\Omega_D)}$	$\ U - u\ _{DG}$	$\ U - u\ _{\mathcal{E}}$
31	1.489×10^{-3}	1.034×10^{-2}	1.147×10^{-3}	3.049×10^{-2}	3.872×10^{-3}
102	4.010×10^{-4}	2.748×10^{-3}	3.034×10^{-4}	1.503×10^{-2}	1.781×10^{-3}
340	1.033×10^{-4}	8.143×10^{-4}	8.386×10^{-5}	8.031×10^{-3}	9.276×10^{-4}
1272	2.609×10^{-5}	2.722×10^{-4}	2.112×10^{-5}	4.039×10^{-3}	4.653×10^{-4}
4895	6.496×10^{-6}	1.016×10^{-4}	5.322×10^{-6}	2.039×10^{-3}	2.313×10^{-4}
rate	2.00	1.40	2.00	1.00	1.00

Table 7.1 : Numerical errors and convergence rates for DG scheme of order one coupled with FV.

N	$\ U - u\ _{0,FV}$	$\ U - u\ _{FV}$	$\ U - u\ _{L^2(\Omega_D)}$	$\ U - u\ _{DG}$	$\ U - u\ _{\mathcal{E}}$
31	9.479×10^{-4}	6.592×10^{-3}	4.881×10^{-4}	4.298×10^{-3}	2.172×10^{-3}
102	2.593×10^{-4}	1.872×10^{-3}	1.176×10^{-4}	1.598×10^{-3}	9.009×10^{-4}
340	6.578×10^{-5}	6.148×10^{-4}	4.028×10^{-5}	7.550×10^{-4}	4.415×10^{-4}
1272	1.744×10^{-5}	2.389×10^{-4}	9.198×10^{-6}	4.328×10^{-4}	2.397×10^{-4}
4895	4.766×10^{-6}	1.012×10^{-4}	2.487×10^{-6}	1.120×10^{-4}	1.198×10^{-4}
rate	1.88	1.23	1.89	1.95	1.00

Table 7.2 : Numerical errors and convergence rates for DG scheme of order two coupled with FV.

expected convergence rate of $O(h)$ in the energy norm. The error in the L^2 norm for the DG solution are also given; they are $O(h^2)$ as expected. A discrete L^2 error is computed for the FV region:

$$\|U - u\|_{0,FV} = \left(\sum_{V \in \mathcal{E}_F^h} |V| (U(x_V) - u(x_V))^2 \right)^{1/2}.$$

The rates for the discrete L^2 errors are also $O(h^2)$.

The variable N is the total number of Voronoi cells in the domain Ω . When we increase the degree of approximation in Ω_D to two, the pressure solution is more accurate and the local convergence rate increases to two. This feature is important because it allows for one to use the Discontinuous Galerkin method to obtain accurate solutions on parts of the domain of interest.

Example 42. *Discontinuity in Porous Medium*

In the next example we consider a square domain $\Omega = (0, 2) \times (0, 2)$ with an enclosed triangular domain (see Fig. 7.3 left). The diffusion coefficient K is equal to 0.01 in the triangular subdomain and 1.0 in the rest of the domain. We impose zero Dirichlet boundary conditions and the source function

$$f(x, y) = -2.0(x^2 - 2x) + (y^2 - 2y).$$

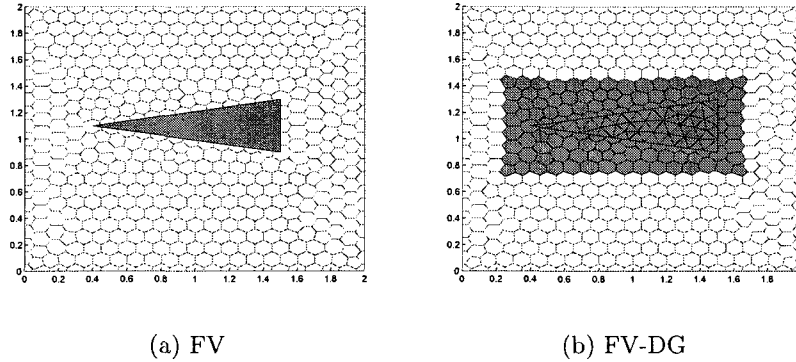
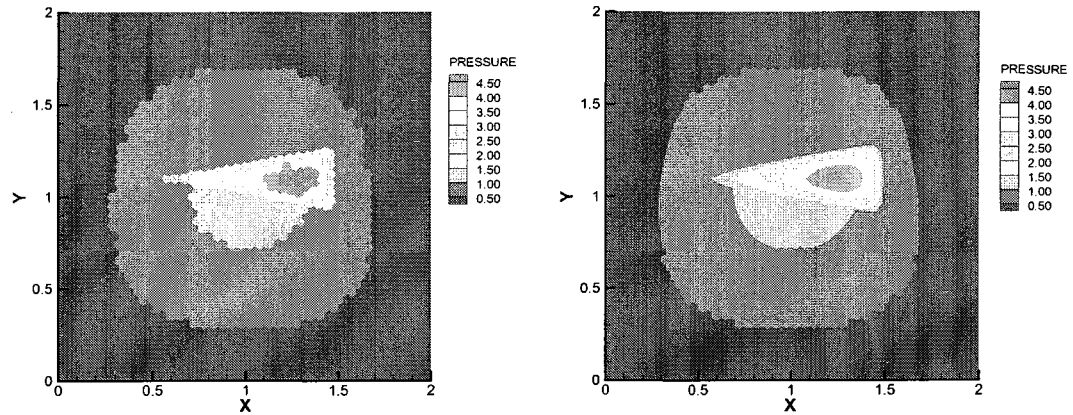


Figure 7.3 : Computational meshes in the case of triangular inclusion (grey region in left figure). The DG region is a larger rectangular region that contains the triangular inclusion (grey region in right figure).

The challenge for the finite volume method in this case arises from the discontinuity in the permeability of the porous medium that changes rapidly over a small part

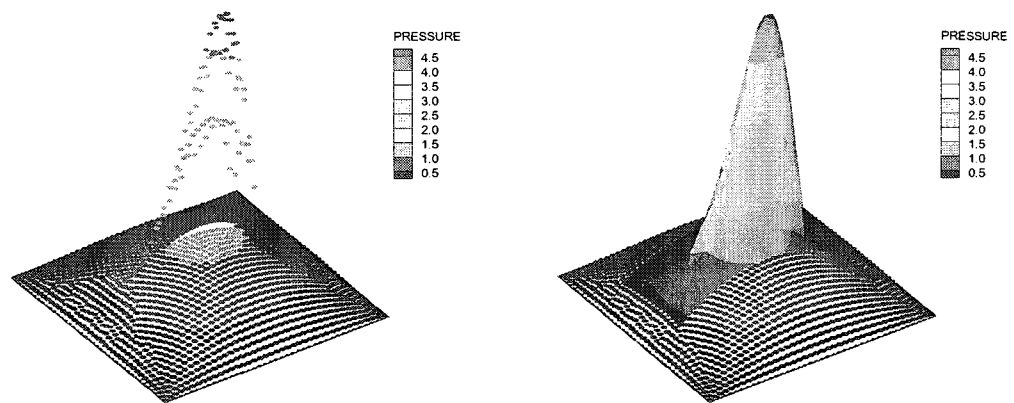
of the domain. We want to compare the FV solution with the FV-DG solution on the domains shown in Fig. 7.3. We first solve the problem on a mesh with 1985 Voronoi cells using the finite volume method on the mesh shown in Fig. 7.3(a). The solution is shown in Fig. 7.4 (a) and (c). It is clear the the finite volume solution captures the low permeability in the triangular domain, however it is difficult to obtain an accurate solution as indicated by the three-dimensional plot. Next we solve the problem by using the DG method with parameters $\epsilon = \sigma = 1$ and $r = 2$ in the rectangular shaded region that includes the triangular region as shown in Fig. 7.3(b). The mesh is a combination of Voronoi cells and triangular elements. The flexibility of DG easily allows the use of hybrid meshes, that can capture the discontinuity interface. The solution is shown in Fig. 7.4 (b) and (d). We observe that we are able to obtain a more accurate representation of the solution in contrast to the case when the finite volume method is used throughout the domain. This is explained partially by the fact that we have a higher order approximation in the DG region. The FV-DG solution is obtained by solving a problem of size 6509 which as expected is larger than the problem size from the FV solution. We note that solving this problem using the discontinuous Galerkin method on the whole domain yields a problem of size 13734. In this case we have shown that with prior knowledge of the domain, the proposed coupling can be useful to obtain an accurate solution of a subdomain of interest and still keep the size of the problem small when compared to using the discontinuous Galerkin method on the whole domain. We believe that this feature works well for applications to porous media flow. Fractures and pinches are often areas of interest in the flow problem. Since they occupy often small portions of the domain, the proposed coupling can lead to more accurate solutions in these areas at a relatively low computational cost.

Example 43. *Anisotropic Diffusion Problem*



(a) FV: 2D view

(b) FV-DG: 2D view



(c) FV: 3D view

(d) FV-DG: 3D view

Figure 7.4 : Contours of pressure solution for example 2

In the following example we consider a domain $\Omega = (0, 2) \times (0, 2)$ that contains a rectangular subdomain with an anisotropic diffusion matrix (see Fig. 7.5), instead of a simple diffusion scalar. This example is motivated by a benchmark problem described

in [44]. The diffusion matrix is defined by

$$\mathbf{K} = \mathbf{R}_\phi \begin{pmatrix} 1 & 0 \\ 0 & \delta \end{pmatrix} \mathbf{R}_\phi^{-1},$$

where \mathbf{R}_ϕ is the rotation matrix (with $\phi = 30$ degrees) and $\delta = 10^{-3}$ in the shaded triangulated region of the domain (see Fig. 7.5) and $\delta = 1$ on the rest of the domain.

We solve the problem using the discontinuous Galerkin method in the shaded region in Fig. 7.5 with parameters $\sigma = \epsilon = 1$ and $r = 2$. We note that other types of finite volume methods can be used to solve problems with anisotropic diffusion coefficients for example [42, 43]. These methods are relatively more complicated to implement because they involve the construction of a discrete gradient. In practice for the finite volume method discussed in this chapter one can align the computational grid to the principal directions the flow. This approach is strenuous and easily gets complicated in cases involving changes in the direction of the flow. Fig. 7.6 shows

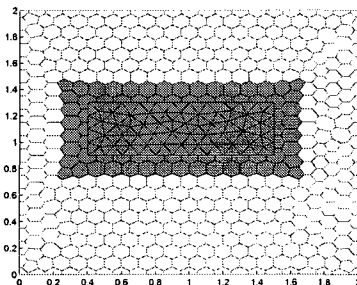


Figure 7.5 : Computational mesh for example 3: $\delta = 10^{-3}$ in the triangulated grey region and $\delta = 1$ in region partitioned into Voronoi cells.

the pressure contours obtained from the proposed FV-DG scheme. We also plot some

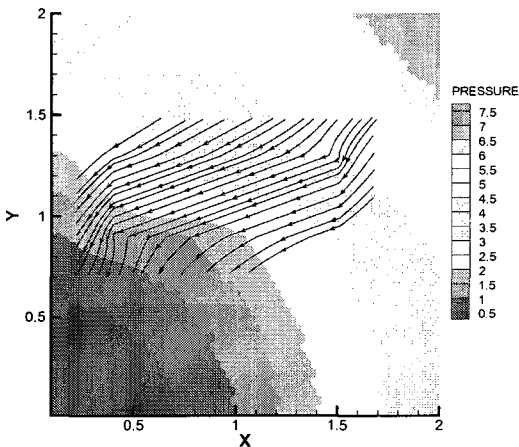


Figure 7.6 : Contours of pressure solution for example 3. Streamlines are only shown in the DG region.

of the streamlines located in the DG region only. We can clearly see the oblique flow in the rectangular subdomain due to the anisotropic diffusion tensor.

7.5 Conclusions

The coupling of discontinuous Galerkin and finite volume methods seems natural for the porous medium. As we have seen the finite volume method works well in parts of the domain where the permeability varies gradually. The Discontinuous Galerkin method on the other hand works in all cases but is more expensive. Thus combining these two methods allows one to obtain an accurate solution at a lower computational cost in the porous medium. This chapter presents both theoretical and numerical results that confirm the convergence of the multi-numeric algorithm in the porous medium. The multi-numeric scheme in the Darcy domain can easily be coupled with the Navier-Stokes flow as shown in previous chapters. The resulting solution is gives

us a good solution to the flow problem at a lower cost because we use a lower order method on most of the porous medium.

Chapter 8

Conclusion

8.1 Coupled Navier-Stokes/Darcy Model

The coupling of Navier-Stokes and Darcy equations remains an interesting problem due to its applications in science and engineering. In this thesis we have shown existence and uniqueness results for a weak solution to the coupled Navier-Stokes Darcy system for two sets of interface conditions. The first case includes inertial forces on the balance of forces condition and requires extra restrictions on the data. The second condition does not include inertial forces and does not require restrictions on the data. There is no consensus in the scientific community on the correct interface conditions to incorporate for this problem. We have also done a numerical comparison of a third interface condition that includes the normal component on the inertial forces. For the particular examples considered in this work there is no significant difference in the numerical solutions. In this work we have shown that these two conditions differ under low viscosity. On the issue of interface conditions, comparing numerical simulations to experimental results may provide better insight as to which condition is better.

Optimal a priori error estimates for numerical schemes for using both continuous and Discontinuous Galerkin methods have been shown. The convergence rates for the numerical scheme have been thoroughly verified by grid studies for known continuous solutions. This work is motivated by applications to geo-sciences, as a result we have

tested the numerical scheme on a wide range of cases that show the robustness of the numerical scheme under the parameters of the model.

The choice of coupling the continuous finite element method with the Discontinuous Galerkin (DG) is due to the fact that the finite element method provides a fairly efficient and proven capability of solving free flow problems. The DG method on the other hand is more robust to handle the difficulties that arise in porous media flow. While we have shown the advantages of using the DG method in the porous medium, it is also clear that computationally it leads to large systems which are time consuming to solve. Another important characteristic of porous media flow problems is that the areas (for example kinks, faults) which cause difficulties are often a small subset of the computational domain. In view of these two problems this work proposes two ways of making computations leaner and more efficient.

8.2 Computational Efficiency

Improving the coupled Navier-Stokes/Darcy code has been the objective of the second half of the thesis. This has been done in two ways. The first approach is a two-grid algorithm that involves solving the fully coupled problem on a coarse grid and then decoupling the problem on a finer grid. We have shown that this method produces a fairly accurate solution in about a quarter of the time it takes the fully coupled problem. This is very important especially in the case of large domains and in the case of the time dependent problem where a fully non-linear problem would have to be solved on each time step. Another way of improving computation comes out of the realization that the problem areas are small subsets of the domain. This has led to the idea of coupling the finite volume method with the Discontinuous Galerkin method. The Finite Volume method is relatively cheap compared to the DG method

and gives accurate solutions in cases where the permeability is well behaved. In view of this, it is a natural choice to use this method in parts of the domain where the permeability does not change much and the Discontinuous Galerkin method in problem areas. We have shown convergence of the coupled scheme and illustrated its potential through numerical examples.

8.3 Future Work

In practice the permeability field in the porous medium has a wide range of scales. The small scale effects often have profound effects of the nature of the flow as a result it is important to incorporate them into the model. However due to the size of the domain it is computationally expensive to do this without some kind of approximation. Incorporating multi-scale techniques into the Darcy region would improve the model's capability to solve more realistic problems that arise in porous media flow.

Extending the model to three dimensions will allow for a more extensive numerical study of the model. The theory shown in this work extends to three dimensions already. Parallelization of the code will also help speed up computations on larger domains in three dimensions. In the numerical results section the fracture example demonstrated the potential advantage of adaptive mesh refinement. This will require error estimators for the coupled problem. Developing error estimators will be a very interesting mathematical problem. This will also improve the computational aspects of the model.

Bibliography

- [1] R. Adams. *Sobolev Spaces*. Academic Press, New York, 1975.
- [2] D.N Arnold, F. Brezzi, and M. Fortin. A stable finite element for the Stokes equations. *Estratto da Calcolo*, XXI, 1984.
- [3] G.S. Beavers and D.D. Joseph. Boundary conditions at a naturally permeable wall. *Journal of Fluid Mechanics*, 30:197–207, 1967.
- [4] M. Cai, M. Mu, and J. Xu. Numerical solution to a mixed navierstokes/darcy model by the two-grid approach. *SIAM Journal on Numerical Analysis*, 47(5):3325–3338, 2009.
- [5] Z. Cai. On the finite volume element method. *Numer. Math.*, 58:713–735, 1991.
- [6] Z. Cai, J. Mandel, and S.Mc Cormick. The finite volume element method for diffusion equations on general triangulations. *SIAM J. Numer. Anal.*, 28:392–402, 1991.
- [7] Y. Cao, M. Gunzburger, and X. Wang. Coupled stokes-darcy model with beavers-joseph interface boundary condition. *Communications in Mathematical*, 8(1):1–25, 2010.
- [8] A. Cesmelioglu, P.Chidyagwai, and B. Rivière. Continuous and Discontinuous Finite Element Methods for Coupled Surface-Subsurface Flow and Transport Problems. *Applied Numerical Mathematics*, submitted.

- [9] A. Cesmelioglu and B. Rivière. Analysis of time-dependent Navier-Stokes flow coupled with Darcy flow. *Journal of Numerical Mathematics*, 16:249–280, 2008.
- [10] A. Cesmelioglu and B. Rivière. Primal Discontinuous Galerkin Methods for Time-Dependent Coupled Surface flow and Subsurface Flow. *Journal of Scientific Computing*, To appear.
- [11] P. Ciarlet. *The finite element method for elliptic problems*. North-Holland, Amsterdam, 1978.
- [12] C. Taylor and P. Hood. A numerical solution of the Navier-Stokes equations using the finite element technique. *Computers & Fluids*, 1:73–100, 1973.
- [13] C. Dawson, S. Sun, and M.F. Wheeler. Compatible algorithms for coupled flow and transport. *Comput Meth. Appl. Mech. Eng.*, 193:2565–2580, 2004.
- [14] M. Discacciati, E. Migliorini, and A. Quarteroni. Mathematical and numerical models for coupling surface and groundwater flows. *Applied Numerical Mathematics*, 43:57–74, 2002.
- [15] M. Discacciati and A. Quarteroni. Convergence analysis of a subdomain iterative method for the finite element approximation of the coupling of stokes darcy equations. *Computing and Visualization Science*, 6(2-3):93–103, 2004.
- [16] Y. Epshteyn and B. Rivière. Estimation of penalty parameters for symmetric interior penalty Galerkin methods. *Journal of Computational and Applied Mathematics*, Published online:doi:10.1016/j.cam.2006.08.029, 2006.
- [17] N.S. Hanspal et al. Numerical analysis of coupled Stokes/Darcy flows in industrial filtrations. *Transport in Porous Media*, 64:73–101, 2006.

- [18] R. Eymard, T. Gallouët, and R. Herbin. *Handbook for Numerical Analysis Spaces*. North Holland, 2000.
- [19] P.A. Forsyth. A control volume finite element approach to NAPL groundwater contamination. *SIAM J. Sci. Statist. Comput.*, 12:1029–1057, 1991.
- [20] D.K. Gartling, C.E. Hickox, and R.C. Givoler. Simulation of viscous and porous flow problems. *International Journal for Computational Fluid Dynamics*, 7:23–48, 1996.
- [21] V. Girault and J. Lions. Two grid finite element schemes for the transient Navier-Stokes problem. *Mathematical Modelling and Numerical Analysis*, 45:1801–1813, 2007.
- [22] V. Girault and J.L. Lions. Two-grid finite element schemes for the steady Navier-Stokes problem in polyhedra. *Port. Math(N.S)*, 1:25–57, 2001.
- [23] V. Girault and P. Raviart. *Finite Element Methods for Navier-Stokes Equations*. Springer-Verlag, 1986. First Edition.
- [24] V. Girault and B. Rivière. DG approximation of coupled Navier-Stokes and Darcy equations by Beaver-Joseph Saffman interface condition. *SIAM Journal of Numerical Analysis and Modeling*, to appear.
- [25] V. Girault, B. Rivière, and M. Wheeler. A discontinuous Galerkin method with non-overlapping domain decomposition for the Stokes and Navier-Stokes problems. *Mathematics of Computation*, 74:53–84, 2004.
- [26] V. Girault, B. Rivière, and M. Wheeler. A Discontinuous Galerkin Method with

Non-Overlapping Domain Decomposition for Stokes and Navier-Stokes Problems. *Mathematics of Computation*, 74:53–84, 2005.

- [27] R. Herbin. An error estimate for a finite volume scheme for a diffusion-convection problem on a triangular mesh. *Numer. Meth. Partial Diff. Equations*, 11:165–173, 1995.
- [28] W. Jager and A. Mikelic. On the boundary conditions at the contact interface between a porous medium and a free fluid. *Ann. Scuola Norm. Sup. Pisa Cl.Sci.*, 23:403–465, 1996.
- [29] W. Jager, A. Mikelic, and N. Neuss. Asymptotic analysis of the laminar viscous flow over a porous bed. *SIAM Journal on Scientific Computing*, 22(6):2006–2028, 2001.
- [30] E.F Kaasshieter. Mixed finite elements for accurate particle tracking in saturated groundwater flow. *Advances in Water Resources*, 18(5):277–294, 1995.
- [31] H. Kardestuncer. *Finite Element Handbook*. McGraw-Hill Inc, 1987.
- [32] William Layton. *Introduction to the Numerical Analysis of Incompressible Viscous Flows*. Society for Industrial and Applied Mathematics, 2008.
- [33] W.J. Layton, F. Schieweck, and I.Yotov. Coupling fluid flow with porous media flow. *SIAM J. Numer. Anal.*, 40:2195–2218, 2003.
- [34] M. Marion and J. Xu. Error estimate on a new nonlinear galerkin method based on two-grid finite elements. *SIAM Journal on Numerical Analysis*, 32(4):1170–1184, 1995.

- [35] I.D. Mishev. Finite Volume methods on Voronoi meshes. *Numerical methods for Partial Differential equations*, 14:193–212, 1998.
- [36] M. Mu and J. Xu. A Two grid method of a mixed Stokes-Darcy model for coupling fluid flow with porous media flow. *SIAM J. Numerical Analysis*, 45:1801–1813, 2007.
- [37] B. Niceno. Easymesh. <http://www-dinma.units.it/nirftc/research/easymesh/easymesh.html>.
- [38] P.G Nutting. Physical analysis of oil sands. *Bull. Am. Ass. petrol. Geol.*, 14:1337–1349, 1930.
- [39] L.E Payne and B. Straughan. Analysis of the boundary condition at the interface between a viscous fluid and a porous medium and related modelling questions. *J. Math. Pures Appl*, 4:317–354, 1998.
- [40] P.Chidyagwai and B. Rivire. On the solution of the coupled navier-stokes and darcy equations. *Computer Methods in Applied Mechanics and Engineering*, 198(47-48):3806 – 3820, 2009.
- [41] A. Quarteroni and A. Valli. *Numerical Approximation of Partial Differential Equations*. Springer-Verlag, Berlin Heidelberg, 1994.
- [42] R.Eymard, T.Gallout, and R. Herbin. A cell-centered finite volume approximation for anisotropic operators on unstructured meshes in any space dimension. *IMA Journal of Numerical Analysis*, 26(2):326–353, 2006.
- [43] R.Eymard, T.Gallout, and R. Herbin. A new finite volume scheme for anisotropic diffusion problems on general grids: convergence analysis. *Comptes Rendus Mathematique*, 344(6):403 – 406, 2007.

- [44] R. Herbin and F. Hubert. Benchmark on discretization schemes for anisotropic diffusion problems on general grids. *Finite Volumes for Complex Applications V*, R. Eymard and J-M Herard eds, pages 659–692, 2008.
- [45] B. Rivière. Analysis of a discontinuous finite element method for coupled stokes darcy problems. *Journal of Scientific Computing*, 22-23(1-3):479–500, 2005.
- [46] B. Rivière. *Discontinuous galerkin method for solving elliptic and parabolic equations*. Society for Industrial and Applied Mathematics, 2008.
- [47] B. Riviere. *Discontinuous Galerkin Methods for Solving Elliptic and Parabolic Equations: Theory and Implementation*. SIAM, 2008.
- [48] B. Rivière, M. Wheeler, and V. Girault. Improved energy estimates for interior penalty, constrained and discontinuous Galerkin methods for elliptic problems. *Part 1, Computational Geosciences*, 3:337–360, 1999.
- [49] B. Rivière and I. Yotov. Coupled stokes-darcy model with beavers-joseph interface boundary condition. *Siam Journal on Numerical Analysis*, 42(5):1959–1977, 2004.
- [50] P.G. Saffman. On the boundary condition at the surface of a porous medium. *Journal of Fluid Mechanics*, 2:93–101, 1971.
- [51] A.G Salinger, R. Aris, and J.J. Derby. Finite element formulations for large-scale coupled flows in adjacent porous and open fluid domains. *International Journal for Numerical Methods in Fluids*, 18:1185–1209, 1994.
- [52] M.F. Wheeler. An elliptic collocation-finite element method with interior penalties. *SIAM Journal on Numerical Analysis*, 15(1):152–161, 1978.

- [53] J. Xu. A new class of iterative methods for nonselfadjoint or indefinite problems. *SIAM Journal on Numerical Analysis*, 29(2):303–319, 1992.
- [54] J. Xu. A novel two-grid method for semilinear elliptic equations. *SIAM Journal on Scientific Computing*, 15(1):231–237, 1994.
- [55] J. Xu. Two-grid discretization techniques for linear and nonlinear pdes. *SIAM Journal on Numerical Analysis*, 33(5):1759–1777, 1996.